



**HAL**  
open science

## New $H(\text{div})$ -conforming multiscale hybrid-mixed methods for the elasticity problem on polygonal meshes

Philippe R B Devloo, Agnaldo M Farias, Sonia M. Gomes, Wesley S Pereira, Antonio J B dos Santos, Frédéric Valentin

► **To cite this version:**

Philippe R B Devloo, Agnaldo M Farias, Sonia M. Gomes, Wesley S Pereira, Antonio J B dos Santos, et al.. New  $H(\text{div})$ -conforming multiscale hybrid-mixed methods for the elasticity problem on polygonal meshes. 2019. hal-02415020v1

**HAL Id: hal-02415020**

**<https://hal.science/hal-02415020v1>**

Preprint submitted on 16 Dec 2019 (v1), last revised 17 Sep 2020 (v2)

**HAL** is a multi-disciplinary open access archive for the deposit and dissemination of scientific research documents, whether they are published or not. The documents may come from teaching and research institutions in France or abroad, or from public or private research centers.

L'archive ouverte pluridisciplinaire **HAL**, est destinée au dépôt et à la diffusion de documents scientifiques de niveau recherche, publiés ou non, émanant des établissements d'enseignement et de recherche français ou étrangers, des laboratoires publics ou privés.

## New $H(\text{div})$ -conforming multiscale hybrid-mixed methods for the elasticity problem on polygonal meshes

Philippe R. B. Devloo<sup>‡</sup>, Agnaldo M. Farias<sup>†</sup>, Sônia M. Gomes<sup>\*</sup>,  
Wesley S. Pereira<sup>§</sup>, Antonio J. B. dos Santos<sup>¶</sup>, Frédéric Valentin<sup>||</sup>

<sup>‡</sup>*Faculdade de Engenharia Civil, Arquitetura e Urbanismo, Universidade Estadual de Campinas, Rua Josiah Willard Gibbs, 85, Campinas, São Paulo, 13083-839 - Brazil.*

<sup>†</sup>*Instituto Federal do Norte de Minas Gerais, Fazenda Varginha, km 02 Rodovia MG-404, Salinas, Minas Gerais, 39560-000 Brazil.*

<sup>\*</sup>*Instituto de Matemática, Estatística e Computação Científica, Universidade Estadual de Campinas, Rua Sérgio Buarque de Holanda, 651, Campinas, São Paulo, 13083-859, Brazil.*

<sup>§</sup>*Laboratório Nacional de Computação Científica, Petrópolis, Rio de Janeiro, 25651-075, Brazil.*

<sup>¶</sup>*Centro de Informática, Universidade Federal da Paraíba, R. dos Escoteiros, s/n - Mangabeira, João Pessoa - PB, João Pessoa, Paraíba, 58055-000, Brazil.*

<sup>||</sup>*Laboratório Nacional de Computação Científica, Petrópolis, Rio de Janeiro, 25651-075, Brazil.*

<sup>‡</sup>*phil@unicamp.br*, <sup>†</sup>*agnaldo.farias@ifnmg.edu.br*, <sup>\*</sup>*soniag@unicamp.br*, <sup>§</sup>*wesleyp@lncc.br*,  
<sup>¶</sup>*boness@ci.ufpb.br*, <sup>||</sup>*valentin@lncc.br*

This work proposes a family of multiscale hybrid-mixed methods for the two-dimensional linear elasticity problem on general polygonal meshes. The new methods approximate displacement, stress, and rotation variables using two-scale discretizations. The first scale level setting consists of approximating the traction variable (Lagrange multiplier) in discontinuous polynomial spaces, and of computing rigid-body modes element wisely. In the second scale level, the methods are made effective by solving completely independent local Neumann elasticity problems written in a mixed form with weak symmetry enforced via a rotation multiplier. Since the finite-dimensional space for the traction variable constrains the discrete space for the local stress tensor, the discrete stress field lies in the  $H(\text{div})$  space globally and stays in local equilibrium with external forces. We propose different choices to approximate local problems based on locally stable pairs of finite elements defined on affine second-level meshes. Those choices generate the family of multiscale finite element methods for which stability and convergence are proved in a unified framework. Notably, we prove that the methods are optimal and high-order convergent in the natural norms. Also, it emerges that the approximate displacement and stress divergence are super-convergent in the  $L^2$ -norm. Numerical verification assess theoretical results and highlight the high precision of the new methods on coarse meshes for multilayered heterogeneous material problems.

*Keywords:* Multiscale; mixed finite elements; linear elasticity; hybridization.

\*Corresponding author

## 1. Introduction

Mixed finite element (FE) methods for elasticity problems, based on the Hellinger-Reissner principle, have been used since the very beginning of finite element history. They are formulated simultaneously for stress and displacement variables, which are of primary interest. When correctly designed, mixed methods usually give optimal stress accuracy, and local momentum conservation, without locking-behavior for incompressible or nearly incompressible materials.

We focus our study on conforming mixed formulations, meaning that approximations for the stress tensor  $\underline{\sigma}$  have continuous normal traces along the inter-element boundaries (i.e. the stress approximation space  $\tilde{\mathcal{S}}$  should be  $H(\text{div})$ -conforming), but without requiring stress symmetry. The displacement variable  $\underline{u}$  is searched in a discontinuous space  $\tilde{\mathcal{U}}$ . The idea is to impose a weak symmetry condition through the use of a Lagrange multiplier (rotation) living in an appropriate approximation space  $\tilde{\mathcal{Q}}$ . We denote this class of methods by the acronym MFEM-WS, and refer to Ref. 3, 16 for overviews on this matter.

Our purpose is to create a multiscale hybrid approach for the MFEM-WS. It shall be denoted by the acronym MHM-WS, for its design is in the spirit of the Multiscale Hybrid Mixed (MHM) methods (e.g, as in the contexts of Ref. 19, 15). In summary, this means that the MHM-WS scheme can be interpreted as a discrete version of a characterization of the exact solution in terms of Neumann boundary value problems locally defined on each (general polygonal) subregion  $\Omega_i$  of a (non-conformal) macro-partition  $\mathcal{T} = \{\Omega_i\}$ , which are assembled by using an inter-element connection. The stress tensor is supposed to have normal components strongly constrained to a given coarse finite dimensional trace space  $\tilde{\Lambda}_{sk}$  defined over the subregion boundaries (mesh skeleton), making the referred inter-element connection. This property implies that, in fact, the stress tensor is globally  $H(\text{div})$ -conforming.

The global system to be solved is expressed only in terms of the newly introduced normal trace variable in  $\tilde{\Lambda}_{sk}$ , and of a coarse displacement approximation, piecewise-defined by rigid-body modes in each subregion. Small details are resolved by the local problems in the subregions, using stable MFEM-WS for composite finite element spaces  $\{\tilde{\mathcal{S}}(\Omega_i), \tilde{\mathcal{U}}(\Omega_i), \tilde{\mathcal{Q}}(\Omega_i)\}$ , based on internal conformal shape-regular partitions  $\mathcal{T}^{\Omega_i}$ . Approximation spaces inside the subdomains can be enriched, with respect to the boundary trace resolution, using different strategies: refining the internal mesh, increasing the polynomial degree, or both. Element geometry and mesh resolutions in the subdomains may vary between them. For neighboring subdomains  $\Omega_i$  and  $\Omega_j$ ,  $\mathcal{T}^{\Omega_i}$  and  $\mathcal{T}^{\Omega_j}$  are allowed to be non-conformal over  $\Gamma_{i,j} = \partial\Omega_i \cap \partial\Omega_j$ . However, some mesh and space consistencies should be satisfied (see Sec. 3.1).

As shall be proved in Sec. 5.2, an important analysis aspect of the MHM-WS method is that it may be interpreted as an equivalent stable MFEM-WS formulation of the model problem in the whole domain, based on  $H(\text{div})$ -conforming tensor spaces with normal traces constrained to  $\tilde{\Lambda}_{sk}$ . The required stability conditions,

namely, divergence-constraint and Stokes-constraint with respect to the potential and rotation local spaces, are verified. In fact, we extend the methodology proposed in Ref. 14 to construct new stable Stokes-compatible pairs: the pair used for stability analysis at the coarser one-scale space setting (with mesh-width and polynomial degree determined by  $\tilde{\Lambda}_{sk}$ ) is incremented with extra refined composite bubble terms for the velocity in order to restore stability when using enlarged pressure spaces  $\tilde{\mathcal{Q}}(\Omega_i)$ , in the spirit of the methodology suggested in Ref. 6. Classical tools applied to this equivalent MFEM-WS framework also guides the error analysis of the MHM-WS solutions. We prove optimal and high-order convergence in the natural norms. Stress and rotation variables are approximated with the same accuracy order as for the trace variable. Notably, superconvergence in the  $L^2$ -norm for the divergence of the stress and enhanced displacement may be reached.

The original MHM method for elasticity problems, denoted here by MHM- $H^1$ , was proposed in Ref. 19. It is based on a primal hybrid formulation, using  $H^1$ -conforming instead of mixed local solvers. Another difference between these two MHM methods occurs in the way the Neumann boundary conditions are imposed by their local solvers. For the MHM-WS scheme the tensor normal traces are strongly imposed at the subdomain boundaries, whilst in the primal formulation they are weakly imposed. Furthermore, the attractive properties of momentum conservation at the micro-mesh scale, and locking-free behavior for nearly incompressible materials, typical for conforming mixed methods, are valid for MHM-WS. To be self contained, some aspects of the MHM- $H^1$  method are described in Appendix A.

Recently, in Ref. 22, it was pointed out that the resolution of multiscale elasticity problems by mixed stress-displacement formulations, based on domain decomposition, had not been considered before. They proposed and analyzed a multiscale mixed formulation using the mortar domain decomposition with non-matching grids, and weakly imposed stress symmetry. The mortar spaces use displacement Lagrange multipliers to (weakly) enforce interface continuity of the normal stress. Following a similar “divide-and-conquer” principle, but designed in the different MHM context, the MHM-WS method also helps filling this gap.

Some other multiscale finite element methods have been applied to elasticity problems. The Multiscale Finite Element Method (MsFEM) was applied in Ref. 7, 8. Each level in the MsFEM has its mesh and interpolation spaces that, in general, fit inside the interpolations of lower levels. The MsFEMs have no local problems associated with the source function neither a rigorous mathematical structure to guide the choice of local boundaries. The Localized Orthogonal Decomposition (LOD) method of Ref. 24 is a multiscale method that requires low regularity on the variational problem. To avoid the use of additional regularity, their multiscale basis functions must be computed on a set (*patch*) of macro elements. A generalized finite element method (GFEMs) using LOD is presented in Ref. 21.

### 1.1. Model problem and preliminary notation

Let  $\Omega \subset \mathbb{R}^2$  be a polygonal domain occupied by a linearly elastic body. The equations of static elasticity in Hellinger-Reissner form determine the stress  $\underline{\underline{\sigma}}$  and the displacement  $\underline{u}$  fields satisfying the following equilibrium and constitutive equations

$$-\nabla \cdot \underline{\underline{\sigma}} = \underline{f} \text{ in } \Omega, \quad (1.1)$$

$$\underline{\underline{\sigma}} = \underline{\underline{A}} \underline{\underline{\varepsilon}}(\underline{u}) \text{ in } \Omega, \quad (1.2)$$

$$\underline{u} = \underline{g} \text{ on } \partial\Omega, \quad (1.3)$$

where  $\underline{\underline{\varepsilon}}(\underline{u}) = \frac{\nabla \underline{u} + \nabla \underline{u}^T}{2}$  is the infinitesimal strain tensor,  $\underline{f}$  is the body force, and  $\underline{g}$  is a given Dirichlet boundary data. The material properties are described by the stiffness tensor  $\underline{\underline{A}} = \underline{\underline{A}}(x, y)$ , which is a self-adjoint, bounded, and uniformly positive definite linear operator acting on symmetric tensors  $\mathbb{S}$ . We assume that  $\underline{\underline{A}}$  can be extended to general second-order tensors  $\mathbb{M} = \mathbb{R}^{2 \times 2}$  with the same properties. In particular, in the case of homogeneous and isotropic body,  $\underline{\underline{A}} \underline{\underline{\varepsilon}} = 2\mu \underline{\underline{\varepsilon}} + \lambda \text{tr}(\underline{\underline{\varepsilon}}) \underline{\underline{I}}$ ,  $\lambda$  and  $\mu$  being the Lamé parameters, and  $\underline{\underline{I}}$  the  $2 \times 2$  identity matrix. The variables shall be assumed to be normalized, such that all considered formulations are dimensionless.

Throughout this paper, for a region  $D \subseteq \Omega$ ,  $\underline{n}^D$  denotes the external unitary normal to  $\partial D$ . The scalar Hilbert spaces  $L^2(D, \mathbb{R})$  and  $H^s(D, \mathbb{R})$  have the usual meaning and norms. Spaces  $L^2(D, \mathbb{E})$  and  $H^s(D, \mathbb{E})$ , taking values in finite dimensional spaces  $\mathbb{E}$ , shall be considered for  $\mathbb{E} = \mathbb{R}^2$ ,  $\mathbb{E} = \mathbb{M}$ , or for symmetric tensors  $\mathbb{E} = \mathbb{S} \subset \mathbb{M}$ . These spaces inherit the corresponding norms associated to  $L^2(D, \mathbb{R})$  and  $H^s(D, \mathbb{R})$ . The space  $H(\text{div}, D, \mathbb{R}^2)$  is composed by square-integrable vector functions, for which the divergence is also square integrable. Similarly, we shall consider tensor functions in  $H(\text{div}, D, \mathbb{E})$ , taking values in  $\mathbb{E} = \mathbb{M}$  or  $\mathbb{E} = \mathbb{S}$ . We recall that for tensor fields, the divergence is the vector field obtained by taking the divergence of each row. The notation  $(\cdot, \cdot)_D$  is used for the  $L^2$ -inner products, and  $\langle \cdot, \cdot \rangle_{\partial D}$  refers to the duality pairing between  $H^{1/2}(\partial D, \mathbb{R}^2) = \left\{ \underline{\mu} = \underline{u}|_{\partial D}, \underline{u} \in H^1(D, \mathbb{R}^2) \right\}$  and  $H^{-1/2}(\partial D, \mathbb{R}^2) = \left\{ \underline{\mu} = \underline{\tau} \underline{n}^D|_{\partial D}, \underline{\tau} \in H(\text{div}, D, \mathbb{M}) \right\}$ . The subscript  $D$  is dropped if  $D = \Omega$ .

### 1.2. Mixed formulation with weakly imposed stress symmetry

Problem (1.1) - (1.3) can be equivalently expressed, without a priori assuming stress symmetry, in the following form

$$\begin{aligned} -\nabla \cdot \underline{\underline{\sigma}} &= \underline{f} \text{ in } \Omega, \\ \underline{\underline{A}}^{-1} \underline{\underline{\sigma}} &= \nabla \underline{u} - \underline{\underline{\gamma}}(\underline{u}) \text{ in } \Omega, \\ \underline{\underline{\sigma}} - \underline{\underline{\sigma}}^T &= 0 \text{ in } \Omega, \\ \underline{u} &= \underline{g}, \text{ on } \partial\Omega. \end{aligned}$$

Note that the original constitutive equation  $\underline{\underline{\sigma}} = \underline{\underline{A}} \underline{\underline{\varepsilon}}(\underline{u})$  has been modified by using the relation  $\underline{\underline{\varepsilon}}(\underline{u}) = \nabla \underline{u} - \underline{\underline{\gamma}}(\underline{u})$ , where  $\underline{\underline{\gamma}}(\underline{u}) = \frac{1}{2} \begin{bmatrix} 0 & \partial_2 u_1 - \partial_1 u_2 \\ \partial_1 u_2 - \partial_2 u_1 & 0 \end{bmatrix}$ . The new added equation  $\underline{\underline{\sigma}} - \underline{\underline{\sigma}}^T = 0$  enforces the desired stress symmetry. In addition to the displacement  $\underline{u}$ , and the stress tensor  $\underline{\underline{\sigma}}$ , without symmetry requirement, a new variable  $q = \frac{1}{2} \text{asym } \nabla \underline{u}$  is introduced, where  $\text{asym } \underline{\underline{\tau}} = \tau_{12} - \tau_{21}$  is the asymmetry measure defined for tensors  $\underline{\underline{\tau}} = \begin{bmatrix} \tau_{11} & \tau_{12} \\ \tau_{21} & \tau_{22} \end{bmatrix}$ .

Under this point of view, given  $\underline{g} \in H^{\frac{1}{2}}(\partial\Omega, \mathbb{R}^2)$ , and  $\underline{f} \in L^2(\Omega, \mathbb{R}^2)$ , the mixed formulation with weakly imposed stress symmetry searches for  $(\underline{\underline{\sigma}}, \underline{u}, q) \in H(\text{div}, \Omega, \mathbb{M}) \times L^2(\Omega, \mathbb{R}^2) \times L^2(\Omega, \mathbb{R})$ , satisfying

$$(\underline{\underline{A}}^{-1} \underline{\underline{\sigma}}, \underline{\underline{\tau}}) + (\underline{u}, \nabla \cdot \underline{\underline{\tau}}) + (q, \text{asym } \underline{\underline{\tau}}) = (\underline{\underline{\tau}} \underline{n}^\Omega, \underline{g}), \quad \forall \underline{\underline{\tau}} \in H(\text{div}, \Omega, \mathbb{M}), \quad (1.4)$$

$$-(\nabla \cdot \underline{\underline{\sigma}}, \underline{v}) = (\underline{f}, \underline{v}), \quad \forall \underline{v} \in L^2(\Omega, \mathbb{R}^2), \quad (1.5)$$

$$(\text{asym } \underline{\underline{\sigma}}, w) = 0, \quad \forall w \in L^2(\Omega, \mathbb{R}). \quad (1.6)$$

### 1.3. MFEM-WS

There exist in the literature a variety of finite dimensional approximation spaces to be used in discrete versions of the stress formulation (1.4) - (1.6), here denoted by Mixed Finite Element Method with Weak Symmetry (MFEM-WS). Classical stable MFEM-WS stress formulations use FE space configurations  $\tilde{\mathcal{E}} = \tilde{\mathcal{S}} \times \tilde{\mathcal{U}} \times \tilde{\mathcal{Q}} \subset H(\text{div}, \Omega, \mathbb{M}) \times L^2(\Omega, \mathbb{R}^2) \times L^2(\Omega, \mathbb{R})$ . They are defined in terms of finite dimensional local FE spaces  $S(K, \mathbb{M})$ ,  $U(K, \mathbb{R}^2)$  and  $Q(K, \mathbb{R})$  for the elements  $K \in \mathcal{T}$  of usual triangular or quadrilateral geometry, where  $\mathcal{T}$  is a regular partition of  $\Omega$ . The functions  $\underline{\underline{\tau}} \in \tilde{\mathcal{S}}$  must have continuous normal traces over element interfaces, but for  $\underline{v} \in \tilde{\mathcal{U}}$  and  $\varphi \in \tilde{\mathcal{Q}}$  no interface continuity is required.

The applications of higher order schemes can lead to complications for the enforcement of the  $H(\text{div})$ -conformity, and of the stability divergence-constraint

$$\nabla \cdot \tilde{\mathcal{S}} \subset \tilde{\mathcal{U}}. \quad (1.7)$$

One natural way to cope with that is to form  $\tilde{\mathcal{S}}$  and  $\tilde{\mathcal{U}}$  using Poisson-compatible pair of spaces  $\tilde{\mathcal{V}} \subset H(\text{div}, \Omega, \mathbb{R}^2)$  and  $\tilde{\mathcal{P}} \subset L^2(\Omega, \mathbb{R})$ . Having stress and displacement approximation spaces verifying the above requirements, the finite dimensional rotation approximation space  $\tilde{\mathcal{Q}}$  may be taken from a Stokes-compatible pair of spaces  $\{\tilde{\mathcal{W}}, \tilde{\mathcal{Q}}\}$  such that the following stability Stokes-constraint is satisfied:

$$\underline{\underline{\nabla}} \times \tilde{\mathcal{W}} \subset \tilde{\mathcal{S}} \quad (1.8)$$

Based on the FE space configuration  $\tilde{\mathcal{E}}$ , the MFEM-WS scheme searches for  $(\tilde{\underline{\underline{\sigma}}}, \tilde{\underline{u}}, \tilde{q}) \in \tilde{\mathcal{S}} \times \tilde{\mathcal{U}} \times \tilde{\mathcal{Q}}$  such that

$$(\underline{A}^{-1} \underline{\tilde{\sigma}}, \underline{\tau}) + (\underline{\tilde{u}}, \nabla \cdot \underline{\tau}) + (\tilde{q}, \text{asym } \underline{\tau}) = \langle \underline{\tau} \underline{n}^\Omega, \underline{g} \rangle, \quad \forall \underline{\tau} \in \tilde{\mathcal{J}}, \quad (1.9)$$

$$-(\nabla \cdot \underline{\tilde{\sigma}}, \underline{v}) = (\underline{f}, \underline{v}), \quad \forall \underline{v} \in \tilde{\mathcal{U}}, \quad (1.10)$$

$$(\text{asym } \underline{\tilde{\sigma}}, w) = 0, \quad \forall w \in \tilde{\mathcal{Q}}. \quad (1.11)$$

Under the aforementioned stability conditions (divergence-constraint (1.7) and Stokes-constraint (1.8)), the resulting MFEM-WS stress formulation is well-posed, as originally proposed in Ref. 17 (see also Ref. 4, and 1). Some aspects of the required Poisson-consistent and Stokes-consistent FE pairs are included in Appendix B. Based on them, suitable mixed elasticity elements with reduced stress symmetry are easier to analyze and implement.

#### 1.4. Outline of the paper

The new characterization of the exact solution by a local-global hybrid variational formulation is presented in Sec. 2. Next, Sec. 3 is dedicated to finite element discretizations for this formulation, namely, the new MHM-WS method. In Section 4 the MHM-WS method is proved to be equivalent to a MFEM-WS formulation using FE spaces with constrained tensor traces. Examples of three families of two-scale FE space configurations for the MHM-WS are included in Sec. 5. Stability for them is proved in Sec. 6 using the equivalence with two-scale MFEM-WS schemes. Error analysis of the resulting MHM-WS solutions is developed in Sec. 7, also via the two-scale MFEM-WS with constrained tensor traces. The paper concludes with some computational simulations in Sec. 8, which confirm the predicted theoretical convergence results of Sec. 7, and includes comparative results with the ones given by the MHM- $H^1$  version. We also show the application of the MHM-WS method for a heterogeneous media with high-contrast layers. Concluding remarks, emphasizing the main aspects of the obtained results, are listed in Sec. 9, followed by two appendix sections containing some auxiliary results.

## 2. Hybridization and characterization of the exact solution

The main focus and results of the current research are on a new equivalent hybrid version at the continuous level of the formulation (1.4) - (1.6), and of its discretization. It is a modification of the MHM- $H^1$  formulation by replacing the local downscaling problems (A.4) - (A.5) by stress mixed versions, with weakly imposed stress symmetry, and using the corresponding solutions to adapt the upscaling system. Namely, the hybridization requires a partition  $\mathcal{T} = \{\Omega_i\}$  of the computational domain, and associated to  $\mathcal{T}$  a mesh skeleton  $\Gamma$  is formed by the union of the boundaries  $\partial\Omega_i$ . The following trace space plays an important role

$$\Lambda := \Lambda(\Gamma, \mathbb{R}^2) = \{\underline{\mu}; \underline{\mu} = \underline{\tau} \underline{n}|_{\partial\Omega_i}, \underline{\tau} \in H(\text{div}, \Omega, \mathbb{M}), \Omega_i \in \mathcal{T}\},$$

where  $\underline{n}$  is a given vector field defined over  $\Gamma$  and normal to  $\partial\Omega_i$ , such that  $\underline{n}|_{\Omega_i} = \delta_i \underline{n}^{\Omega_i}$ , where  $\delta_i(e) = \underline{n} \cdot \underline{n}^{\Omega_i}|_e$  for all edges  $e \subset \partial\Omega_i$ . Notice that  $\delta_i(e) = -\delta_j(e)$  for interface edges  $e \subset \Omega_i \cap \Omega_j$ .

Similarly to the local-global hybrid primal formulation initially proposed in Ref. 19, the displacement variable  $\underline{u}$  is decomposed in the form  $\underline{u} = \underline{u}_{rm} + \underline{u}^\perp$ , where  $\underline{u}_{rm}$  is searched in the finite dimensional space  $\mathcal{U}_{rm}$ , defined over  $\mathcal{T}$  by piecewise rigid-body modes

$$\mathcal{U}_{rm} = \{\underline{u} \in L^2(\Omega, \mathbb{R}^2); \underline{u}_i = \underline{u}|_{\Omega_i} \in \mathcal{U}_{rm}(\Omega_i), \Omega_i \in \mathcal{T}\},$$

where each  $\underline{u}_i$  verifies  $\underline{\varepsilon}(\underline{u}_i) = 0$ , i. e.,  $\underline{u}_i = (\alpha_i, \beta_i) + \rho_i(-y, x)$  with  $\alpha_i, \beta_i, \rho_i \in \mathbb{R}$ . The term  $\underline{u}^\perp = \underline{u} - \underline{u}_{rm}$  is a function in  $\mathcal{U}_{rm}^\perp \subset L^2(\Omega, \mathbb{R}^2)$ , the  $L^2$ -orthogonal complement of  $\mathcal{U}_{rm}$  in  $L^2(\Omega, \mathbb{R}^2)$ . Consider also

$$\mathcal{S} = \{\underline{\tau} \in H(\text{div}, \Omega, \mathbb{M}); \underline{\tau} \underline{n}|_{\partial\Omega_i} = 0, \Omega_i \in \mathcal{T}\}.$$

Based on the above functional framework, consider the local (downscaling) and global (upscaling) stages:

- *Downscaling stage:* For  $\underline{\lambda} \in \Lambda$ ,  $\underline{\lambda} \neq 0$ , and  $\underline{f} \in L^2(\Omega, \mathbb{R}^2)$ , let operators  $\{T^\sigma(\underline{\lambda}), \hat{T}^\sigma(\underline{f})\} \in H(\text{div}, \Omega, \mathbb{M}) \times H(\text{div}, \Omega, \mathbb{M})$ ,  $\{T^u(\underline{\lambda}), \hat{T}^u(\underline{f})\} \in \mathcal{U}_{rm}^\perp \times \mathcal{U}_{rm}^\perp$ , and  $\{T^q(\underline{\lambda}), \hat{T}^q(\underline{f})\} \in L^2(\Omega, \mathbb{R}) \times L^2(\Omega, \mathbb{R})$  be defined by the local mixed formulations with weakly imposed stress symmetry and Neumann boundary conditions:

$$(\nabla \cdot T^\sigma(\underline{\lambda}), \underline{v})_{\Omega_i} = 0, \quad \forall \underline{v} \in \mathcal{U}_{rm}^\perp, \quad (2.1)$$

$$(\underline{A}^{-1} T^\sigma(\underline{\lambda}), \underline{\tau})_{\Omega_i} + (T^u(\underline{\lambda}), \nabla \cdot \underline{\tau})_{\Omega_i} + (T^q(\underline{\lambda}), \text{asym } \underline{\tau})_{\Omega_i} = 0, \quad \forall \underline{\tau} \in \mathcal{S}, \quad (2.2)$$

$$(\text{asym } T^\sigma(\underline{\lambda}), \varphi)_{\Omega_i} = 0, \quad \forall \varphi \in L^2(\Omega, \mathbb{R}), \quad (2.3)$$

$$T^\sigma(\underline{\lambda}) \underline{n}|_{\partial\Omega_i} = \underline{\lambda}|_{\partial\Omega_i}. \quad (2.4)$$

$$-(\nabla \cdot \hat{T}^\sigma(\underline{f}), \underline{v})_{\Omega_i} = (\underline{f}, \underline{v})_{\Omega_i}, \quad \forall \underline{v} \in \mathcal{U}_{rm}^\perp, \quad (2.5)$$

$$(\underline{A}^{-1} \hat{T}^\sigma(\underline{f}), \underline{\tau})_{\Omega_i} + (\hat{T}^u(\underline{f}), \nabla \cdot \underline{\tau})_{\Omega_i} + (\hat{T}^q(\underline{f}), \text{asym } \underline{\tau})_{\Omega_i} = 0, \quad \forall \underline{\tau} \in \mathcal{S}, \quad (2.6)$$

$$(\text{asym } \hat{T}^\sigma(\underline{f}), \varphi)_{\Omega_i} = 0, \quad \forall \varphi \in L^2(\Omega, \mathbb{R}), \quad (2.7)$$

$$\hat{T}^\sigma(\underline{f}) \underline{n}|_{\partial\Omega_i} = 0. \quad (2.8)$$

- *Upscaling stage:* Given  $\underline{f} \in L^2(\Omega, \mathbb{R}^2)$ , and  $\underline{g} \in H^{\frac{1}{2}}(\partial\Omega, \mathbb{R}^2)$ , find  $\underline{u}_{rm} \in \mathcal{U}_{rm}$  and  $\underline{\lambda} \in \Lambda$  that solve

$$(\underline{A}^{-1} T^\sigma(\underline{\lambda}), T^\sigma(\underline{\mu})) + (\underline{u}_{rm}, \nabla \cdot T^\sigma(\underline{\mu})) = -(\underline{f}, T^u(\underline{\mu})) + \langle \underline{\mu}, \underline{g} \rangle, \quad \forall \underline{\mu} \in \Lambda, \quad (2.9)$$

$$-(\nabla \cdot T^\sigma(\underline{\lambda}), \underline{v}) = (\underline{f}, \underline{v}), \quad \forall \underline{v} \in \mathcal{U}_{rm}. \quad (2.10)$$

Neumann boundary value problems of linear elasticity are singular, with kernel formed by the rigid motions of the body. This ambiguity can be removed by enforcing that the solution is free of rigid-body modes, and by requiring balanced

force and Newmann boundary terms (see Ref. 23 for a discussion of this topic in the context of algebraic multigrid).

Define  $R_{rm} : \Lambda \rightarrow \mathcal{U}_{rm}$  by  $(R_{rm}(\underline{\lambda}), \underline{v})_{\Omega_i} = \langle \delta_i \underline{\lambda}, \underline{v} \rangle_{\partial\Omega_i}, \forall \underline{v} \in \mathcal{U}_{rm}$ . The variables  $T^{\underline{\sigma}}(\underline{\lambda}) \in H(\text{div}, \Omega, \mathbb{M}), T^{\underline{u}}(\underline{\lambda}) \in \mathcal{U}_{rm}^{\perp}$ , and  $T^q(\underline{\lambda}) \in L^2(\Omega, \mathbb{R})$ , provided by the local mixed solvers (2.1) - (2.4), can be interpreted as solution, in the distributional sense, of the boundary value problems

$$\begin{aligned} -\underline{\nabla} \cdot \underline{\sigma} &= R_{rm}(\underline{\lambda}) \text{ in } \Omega_i, \\ \underline{A}^{-1} \underline{\sigma} &= \underline{\nabla} \underline{u} - \underline{\gamma}(\underline{u}) \text{ in } \Omega_i, \\ \underline{\sigma} - \underline{\sigma}^T &= 0 \text{ in } \Omega_i, \\ \underline{\sigma} \underline{n}|_{\partial\Omega_i} &= \underline{\lambda}, \end{aligned}$$

for  $\underline{u}$  free of rigid-body modes, with balanced force  $R_{rm}(\underline{\lambda})$  and Newmann boundary condition  $\underline{\lambda}$ . Consequently, the solution is unique. Analogously,  $\hat{T}^{\underline{\sigma}}(\underline{f}) \in H(\text{div}, \Omega, \mathbb{M}), \hat{T}^{\underline{u}}(\underline{f}) \in \mathcal{U}_{rm}^{\perp}$ , and  $\hat{T}^q(\underline{f}) \in L^2(\Omega, \mathbb{R})$ , correspond to the unique weak solution of the problem

$$\begin{aligned} -\underline{\nabla} \cdot \underline{\sigma} &= \underline{f} - \Pi^{rm}(\underline{f}), \text{ in } \Omega_i, \\ \underline{A}^{-1} \underline{\sigma} &= \underline{\nabla} \underline{u} - \underline{\gamma}(\underline{u}) \text{ in } \Omega_i, \\ \underline{\sigma} - \underline{\sigma}^T &= 0 \text{ in } \Omega_i, \\ \underline{\sigma} \underline{n}|_{\partial\Omega_i} &= 0, \end{aligned}$$

where  $\Pi^{rm}(\underline{f})$  is the  $L^2$ -orthogonal projection of  $\underline{f} \in L^2(\Omega, \mathbb{R}^2)$  onto  $\mathcal{U}_{rm}$ .

#### Remarks

- (1) If  $(\underline{u}_{rm}, \underline{\lambda})$  solve the upscaling equations (2.9)-(2.10), then  $-\underline{\nabla} \cdot T^{\underline{\sigma}}(\underline{\lambda}) = R_{rm}(\underline{\lambda}) = \Pi^{rm}(\underline{f})$ , for (2.1) and (2.10).
- (2)  $R_{rm}$  is a surjective operator. In fact, given  $\underline{v}^* \in \mathcal{U}_{rm}$ , let  $\underline{\lambda}^*|_{\partial\Omega_i} = \underline{\sigma}^* \underline{n}|_{\partial\Omega_i} \in \Lambda$ , where  $\underline{\sigma}^* \in H^1(\Omega, \mathbb{S})$  satisfy  $\underline{\nabla} \cdot \underline{\sigma}^* = \underline{v}^*$ . Thereby,  $\|\underline{v}^*\|_{L^2(\Omega, \mathbb{R}^2)}^2 = \sum_{\Omega_i} (\underline{v}^*, \underline{v}^*)_{\Omega_i} = \sum_{\Omega_i} \langle \underline{\sigma}^* \underline{n}^{\Omega_i}, \underline{v}^* \rangle_{\partial\Omega_i} = \sum_{\Omega_i} \langle \delta_i \underline{\lambda}^*, \underline{v}^* \rangle_{\partial\Omega_i} = \sum_{\Omega_i} \langle R_{rm}(\underline{\lambda}^*), \underline{v}^* \rangle_{\partial\Omega_i}$ . Then, the adjoint application of  $R_{rm}$  is injective with closed range, which implies the result. The surjectivity of  $R_{rm}$  is key to prove the well-posedness of (2.9)-(2.10), as shall be addressed next.

**Theorem 2.1.** *The global upscaling system (2.9) - (2.10) has a unique solution  $(\underline{u}_{rm}, \underline{\lambda}) \in \mathcal{U}_{rm} \times \Lambda$ . Moreover,  $(\underline{\sigma}, \underline{u}, q)$  is the recovered solution from  $(\underline{u}_{rm}, \underline{\lambda})$  by*

$$\underline{\sigma} = T^{\underline{\sigma}}(\underline{\lambda}) + \hat{T}^{\underline{\sigma}}(\underline{f}), \quad \underline{u} = \underline{u}_{rm} + T^{\underline{u}}(\underline{\lambda}) + \hat{T}^{\underline{u}}(\underline{f}), \quad q = \frac{1}{2} \text{asym } \underline{\nabla} \underline{u}_{rm} + T^q(\underline{\lambda}) + \hat{T}^q(\underline{f}),$$

*if and only  $(\underline{\sigma}, \underline{u}, q)$  solves the weak formulation (1.4) - (1.6).*

**Proof.** To verify the uniqueness of the upscaling system, take zero data  $\underline{f} = 0$  and  $\underline{g} = 0$ . Then system (2.9) - (2.10) becomes

$$\begin{aligned} (\underline{A}^{-1}T^\sigma(\underline{\lambda}), T^\sigma(\underline{\mu})) + (\underline{u}_{rm}, \underline{\nabla} \cdot T^\sigma(\underline{\mu})) &= 0, \quad \forall \underline{\mu} \in \Lambda, \\ (\underline{\nabla} \cdot T^\sigma(\underline{\lambda}), \underline{v}) &= 0, \quad \forall \underline{v} \in \mathcal{U}_{rm}. \end{aligned}$$

Taking test functions  $\underline{\mu} = \underline{\lambda}$  and  $\underline{v} = \underline{\nabla} \cdot T^\sigma(\underline{\lambda}) \in \mathcal{U}_{rm}$ , these equations turn into

$$\begin{aligned} (\underline{A}^{-1}T^\sigma(\underline{\lambda}), T^\sigma(\underline{\lambda})) + (\underline{u}_{rm}, \underline{\nabla} \cdot T^\sigma(\underline{\lambda})) &= 0, \\ (\underline{\nabla} \cdot T^\sigma(\underline{\lambda}), \underline{\nabla} \cdot T^\sigma(\underline{\lambda})) &= 0, \end{aligned}$$

implying that  $\underline{\nabla} \cdot T^\sigma(\underline{\lambda}) = 0$ , from which  $(\underline{A}^{-1}T^\sigma(\underline{\lambda}), T^\sigma(\underline{\lambda})) = 0$  holds. The positive definiteness of the tensor  $\underline{A}$  implies that  $T^\sigma(\underline{\lambda}) = 0$  (meaning that  $\underline{\lambda} = 0$ ,  $T^u(\underline{\lambda}) = 0$ , and  $T^q(\underline{\lambda}) = 0$  as well). Finally,  $\underline{u}_{rm} = 0$  follows from the remaining relation  $(\underline{u}_{rm}, \underline{\nabla} \cdot T^\sigma(\underline{\mu})) = 0$ ,  $\forall \underline{\mu} \in \Lambda$ , recalling that  $\underline{\nabla} \cdot T^\sigma(\underline{\mu}) = -R_{rm}(\underline{\mu})$ , and that  $R_{rm}(\underline{\mu})$  is a surjective operator over  $\mathcal{U}_{rm}$ .

Suppose  $(\underline{u}_{rm}, \underline{\lambda}) \in \mathcal{U}_{rm} \times \Lambda$  solves (2.9) - (2.10), and let  $(\underline{\sigma}, \underline{u}, q)$  be recovered by  $\underline{\sigma} = T^\sigma(\underline{\lambda}) + \hat{T}^\sigma(f)$ ,  $\underline{u} = \underline{u}_{rm} + T^u(\underline{\lambda}) + \hat{T}^u(f)$ ,  $q = \frac{1}{2} \text{asym } \underline{\nabla} \underline{u}_{rm} + T^q(\underline{\lambda}) + \hat{T}^q(f)$ . On the other side, let  $(\underline{s}, \underline{w}, r)$  be the solution of (1.4) - (1.6), define  $\underline{\nu} = \underline{s} \underline{n}|_\Gamma$  and decompose  $\underline{w} = \underline{w}_{rm} + \underline{w}^\perp$ .

By testing (1.5) with  $\underline{v} \in \mathcal{U}_{rm}^\perp$ , and (1.4) with  $\underline{\tau} \in \mathcal{S}$ , both with support in  $\Omega_i$ , and using the fact that  $(\underline{w}_{rm}, \underline{\nabla} \cdot \underline{\tau})_{\Omega_i} = -\frac{1}{2}(\text{asym } \underline{\nabla} \underline{w}_{rm}, \text{asym } \underline{\tau})_{\Omega_i}$ , we obtain

$$(\underline{A}^{-1} \underline{s}, \underline{\tau})_{\Omega_i} + (\underline{w}^\perp, \underline{\nabla} \cdot \underline{\tau})_{\Omega_i} + (r - \frac{1}{2} \text{asym } \underline{\nabla} \underline{w}_{rm}, \text{asym } \underline{\tau})_{\Omega_i} = 0, \quad (2.11)$$

$$-(\underline{\nabla} \cdot \underline{s}, \underline{v})_{\Omega_i} = (\underline{f}, \underline{v}). \quad (2.12)$$

For arbitrary  $\underline{\mu} \in \Lambda$ , take  $\underline{\tau} = T^\sigma(\underline{\mu})$  to test (1.4). Noticing that  $(r, \text{asym } T^\sigma(\underline{\mu})) = 0$  (for (2.3)), and  $(\underline{w}^\perp, \underline{\nabla} \cdot T^\sigma(\underline{\mu})) = 0$  (for (2.1)), then Eq. (1.4) becomes

$$(\underline{A}^{-1} \underline{s}, T^\sigma(\underline{\mu})) + (\underline{w}_{rm}, \underline{\nabla} \cdot T^\sigma(\underline{\mu})) = \langle \underline{\mu}, \underline{g} \rangle, \quad (2.13)$$

and, from Eq. (1.5), we obtain

$$-(\underline{\nabla} \cdot \underline{s}, \underline{v}) = (\underline{f}, \underline{v}), \quad \forall \underline{v} \in \mathcal{U}_{rm}. \quad (2.14)$$

By confronting (2.11)-(2.14) and (1.4) with the set of equations (2.1)-(2.8), the following identities hold for the differences  $\underline{s} - \underline{\sigma}$ ,  $\underline{w}^\perp - \underline{u}^\perp$ , and  $r - q$ :

$$\begin{aligned} (\underline{\nabla} \cdot [\underline{s} - \underline{\sigma}], \underline{v})_{\Omega_i} &= 0, \quad \forall \underline{v} \in \mathcal{U}_{rm}^\perp, \\ (\underline{A}^{-1} [\underline{s} - \underline{\sigma}], \underline{\tau})_{\Omega_i} + (\underline{w}^\perp - \underline{u}^\perp, \underline{\nabla} \cdot \underline{\tau})_{\Omega_i} + (r - q, \text{asym } \underline{\tau})_{\Omega_i} &= 0, \quad \forall \underline{\tau} \in \mathcal{S}, \\ (\text{asym}[\underline{s} - \underline{\sigma}], \varphi)_{\Omega_i} &= 0, \quad \forall \varphi \in L^2(\Omega, \mathbb{R}), \\ (\underline{s} - \underline{\sigma}) \underline{n}|_{\partial\Omega_i} &= \underline{\nu} - \underline{\lambda}. \end{aligned}$$

These equations and (2.16) imply that  $\underline{s} - \underline{\sigma} = T^\sigma(\underline{\nu} - \underline{\lambda})$  having vanishing divergence,  $\underline{w}^\perp - \underline{u}^\perp = T^u(\underline{\nu} - \underline{\lambda})$ , and  $r - q = T^q(\underline{\nu} - \underline{\lambda})$ . Furthermore, since Eq. (2.5),

(2.2), and (2.7) imply that

$$\begin{aligned} (\underline{f}, T^{\underline{u}}(\underline{\mu}))_{\Omega_i} &= -(\nabla \cdot \hat{T}^{\underline{\sigma}}(\underline{f}), T^{\underline{u}}(\underline{\mu}))_{\Omega_i} \\ &= (\underline{A}^{-1} T^{\underline{\sigma}}(\underline{\mu}), \hat{T}^{\underline{\sigma}}(\underline{f}))_{\Omega_i} + (T^q(\underline{\mu}), \text{asym } \hat{T}^{\underline{\sigma}}(\underline{f}))_{\Omega_i} \\ &= (\underline{A}^{-1} T^{\underline{\sigma}}(\underline{\mu}), \hat{T}^{\underline{\sigma}}(\underline{f}))_{\Omega_i} = (T^{\underline{\sigma}}(\underline{\mu}), \underline{A}^{-1} \hat{T}^{\underline{\sigma}}(\underline{f}))_{\Omega_i}, \end{aligned}$$

and by recalling that  $(T^{\underline{\sigma}}(\underline{f}), \underline{v}) = 0, \forall \underline{v} \in \mathcal{U}_{rm}$ , we conclude from (2.9) - (2.10) and (2.13) - (2.13) that

$$(\underline{A}^{-1} [\underline{s} - \underline{\sigma}], T^{\underline{\sigma}}(\underline{\mu})) + (\underline{w}_{rm} - \underline{u}_{rm}, \nabla \cdot T^{\underline{\sigma}}(\underline{\mu})) = 0, \quad \forall \underline{\mu} \in \Lambda, \quad (2.15)$$

$$-(\nabla \cdot [\underline{s} - \underline{\sigma}], \underline{v}) = 0, \quad \forall \underline{v} \in \mathcal{U}_{rm}. \quad (2.16)$$

By setting  $\underline{\mu} = \underline{\nu} - \underline{\lambda}$  and  $\underline{v} = \underline{w}_{rm} - \underline{u}_{rm}$  in (2.15) - (2.16), and using the positive definiteness property of  $\underline{A}^{-1}$ , we conclude that  $\underline{s} = \underline{\sigma}$  (i.e.,  $(\underline{\nu} = \underline{\lambda})$ ). Thus  $\underline{w}^\perp = \underline{u}^\perp$  and  $r = q$  as well. Finally, Eq. (2.15) becomes  $(\underline{w}_{rm} - \underline{u}_{rm}, \nabla \cdot T^{\underline{\sigma}}(\underline{\mu})) = 0, \forall \underline{\mu} \in \Lambda$ , implying that  $\underline{w}_{rm} = \underline{u}_{rm}$ , from Remark (2). By uniqueness of the solutions in both contexts, the equivalence property holds, and then the existence of a solution for (2.9) - (2.10) follows from the existence of a solution for (1.4) - (1.6).  $\square$

### 3. The MHM-WS Method

This section is dedicated to discrete MHM-WS versions for the local-global stress formulation (2.1) - (2.10) proposed and analyzed in Sec. 2. Firstly, let us present the assumptions of the partitions and on the FE approximations. Notably, the first-level mesh  $\mathcal{T}$  is general in the sense that non-convex polygonal elements are accepted under mild condition, and can form a non-conformal decomposition of  $\Omega$ .

#### 3.1. Setting the main assumptions

We assume that a family of shape-regular conformal local partitions  $\mathcal{T}^{\Omega_i} = \{K\}$  can be defined in each subdomain  $\Omega_i \in \mathcal{T}$ . The meshes  $\mathcal{T}^{\Omega_i}$  and  $\mathcal{T}^{\Omega_j}$ , for neighboring subdomains  $\Omega_i$  and  $\Omega_j$ , may be non-conformal over  $\partial\Omega_i \cap \partial\Omega_j$ . The examples discussed here are for affine triangles or quadrilateral elements  $K \in \mathcal{T}^{\Omega_i}$  (but general frameworks with non-affine elements could be admitted as well, as in Ref. 1, 14, 27). For each edge  $e \subset \Gamma$  there is a partition  $\mathcal{T}^e$ , forming a partition  $\mathcal{T}^\Gamma$  of the mesh skeleton. The geometry and mesh resolutions inside the subdomains may vary between them.

*Hypotheses for the internal FE space configurations:* Concerning the FE spaces based on the local partitions  $\mathcal{T}^{\Omega_i}$ , the basic requirements are:

- (i) Finite dimensional composite local spaces  $\tilde{\mathcal{F}}(\Omega_i) \subset H(\text{div}, \Omega_i, \mathbb{M})$ ,  $\tilde{\mathcal{W}}(\Omega_i) \subset L^2(\Omega_i, \mathbb{R}^2)$ , and  $\tilde{\mathcal{Q}}(\Omega_i) \subset L^2(\Omega_i, \mathbb{R})$  should be constructed by piecewise polynomials based on  $\mathcal{T}^{\Omega_i}$ . The representations  $\tilde{\mathcal{F}}(\Omega_i) = \tilde{\mathcal{F}}^\partial(\Omega_i) \oplus \tilde{\mathcal{F}}^\circ(\Omega_i)$  hold in

terms of functions of interior type  $\mathring{\mathcal{S}}(\Omega_i)$ , with vanishing normal traces over  $\partial\Omega_i$ , and functions associated to the subdomain edges  $\mathring{\mathcal{S}}^\partial(\Omega_i)$ .

- (ii) The local FE space configurations  $\mathcal{E}(\Omega_i) = \mathring{\mathcal{S}}(\Omega_i) \times \mathring{\mathcal{W}}(\Omega_i) \times \mathring{\mathcal{Q}}(\Omega_i)$  should be stable for the MFEM-WS formulation for elasticity problems defined in  $\Omega_i$ . For instance, the stability constraints (1.7) and (1.8) are supposed to be valid locally.
- (iii) Uniformly bounded interpolants  $\boldsymbol{\pi}^{\Omega_i} : H^1(\Omega_i, \mathbb{M}) \rightarrow \mathring{\mathcal{S}}(\Omega_i)$  can be defined verifying the divergence-commuting property, i. e.,

$$\left( \nabla \cdot (\underline{\tau} - \boldsymbol{\pi}^{\Omega_i} \underline{\tau}), \underline{v} \right)_{\Omega_i} = 0, \quad \forall \underline{v} \in \mathring{\mathcal{W}}(\Omega_i). \quad (3.1)$$

- (iv) Moreover, it is assumed that  $\mathcal{U}_{rm}(\Omega_i) \subset \nabla \cdot \mathring{\mathcal{S}}(\Omega_i) \subset \mathring{\mathcal{W}}(\Omega_i)$ , and that  $\mathbb{P}_0(\Omega_i, \mathbb{R}) \subset \mathring{\mathcal{Q}}(\Omega_i)$ .

*Hypotheses for the the normal traces:* Assume there is a finite dimensional subspace  $\tilde{\Lambda}_{sk} \subset \Lambda$  verifying the following properties:

- $\tilde{\Lambda}_{sk} \subset \Lambda$  is piecewise defined by polynomials based on  $\mathcal{T}^\Gamma$ , with degree  $k_{sk} \geq 1$ .
- $\tilde{\Lambda}_{sk}$  should verify

$$\tilde{\Lambda}_{sk} \subset \tilde{\Lambda} = \left\{ \underline{\mu}; \underline{\mu} = \underline{\tau} \underline{n}|_{\partial\Omega_i}, \quad \forall \underline{\tau} \in \mathring{\mathcal{S}}(\Omega_i), \quad \Omega_i \in \mathcal{T} \right\}. \quad (3.2)$$

This trace space embedding property is valid under the following circumstances.

- (1) There is a coarse conformal shape-regular partition  $\mathcal{T}_{sk} = \{\bar{K}\}$  of  $\Omega$ , formed by the union of coarse sub-meshes  $\mathcal{T}_{sk}^{\Omega_i}$  satisfying:
  - (a)  $\mathcal{T}^\Gamma$  is the partition induced over  $\Gamma$  by  $\mathcal{T}_{sk}$ .
  - (b)  $\mathcal{T}^{\Omega_i}$  is obtained by refinement of the subdomain partition  $\mathcal{T}_{sk}^{\Omega_i}$ .
- (2) The polynomial degree  $k_{sk}$  used in  $\tilde{\Lambda}_{sk}$  should not exceed the one of  $\tilde{\Lambda}$ .

Notice that the interpolants  $\boldsymbol{\pi}^{\Omega_i}$  verifying the divergence-commuting property (3.1) can be obtained component-wise directly from the interpolants of the associated Poisson-compatible pair of spaces (see B.1): for  $\underline{\tau} = [\underline{\psi}_1 \ \underline{\psi}_2] \in \mathring{\mathcal{S}}(\Omega_i)$ , let  $\boldsymbol{\pi}^{\Omega_i} \underline{\tau} = [\boldsymbol{\pi}^{D, \Omega_i} \underline{\psi}_1 \ \boldsymbol{\pi}^{D, \Omega_i} \underline{\psi}_2]$ . Accordingly, the representation  $\boldsymbol{\pi}_{sk}^{\Omega_i} \underline{\tau} = \boldsymbol{\pi}^{\Omega_i, \partial} \underline{\tau} + \mathring{\boldsymbol{\pi}}^{\Omega_i} [\underline{\tau} - \boldsymbol{\pi}^{\Omega_i, \partial} \underline{\tau}]$  holds, where  $\boldsymbol{\pi}^{\Omega_i, \partial} \underline{\tau} \in \mathring{\mathcal{S}}^\partial(\Omega_i)$ , and  $\mathring{\boldsymbol{\pi}}^{\Omega_i} [\underline{\tau} - \boldsymbol{\pi}_{sk}^{\Omega_i, \partial} \underline{\tau}] \in \mathring{\mathcal{S}}(\Omega_i)$ .

Some aspects of the partitions and FE space configurations for the MHM-WS method are illustrated in Fig. 1. A macro-partition  $\mathcal{T}$  and a skeleton mesh  $\mathcal{T}^\Gamma$  are shown in the top-left and top-center sides. The local meshes of the top-right side do not verify the mesh hierarchy. In fact, there is one element induced by the local mesh  $\mathcal{T}^{\Omega_1}$  over the edge  $e = \Gamma_{1,2}$  which is not totally included in one of the elements of  $\mathcal{T}^e$ . To form a proper mesh hierarchy, firstly consider a conformal partition  $\mathcal{T}_{sk}$  inducing  $\mathcal{T}^\Gamma$  over  $\Gamma$ , as shown in Fig. 1 (bottom-left side). Then, local refined partitions  $\mathcal{T}^{\Omega_i}$  are constructed by subdivisions of the partitions  $\mathcal{T}_{sk}^{\Omega_i} = \mathcal{T}_{sk}|_{\Omega_i}$ , as shown in the

bottom-right side of Fig. 1. The kind of polynomial spaces verifying trace space hierarchy that can be used for the MHM-WS method is also illustrated.

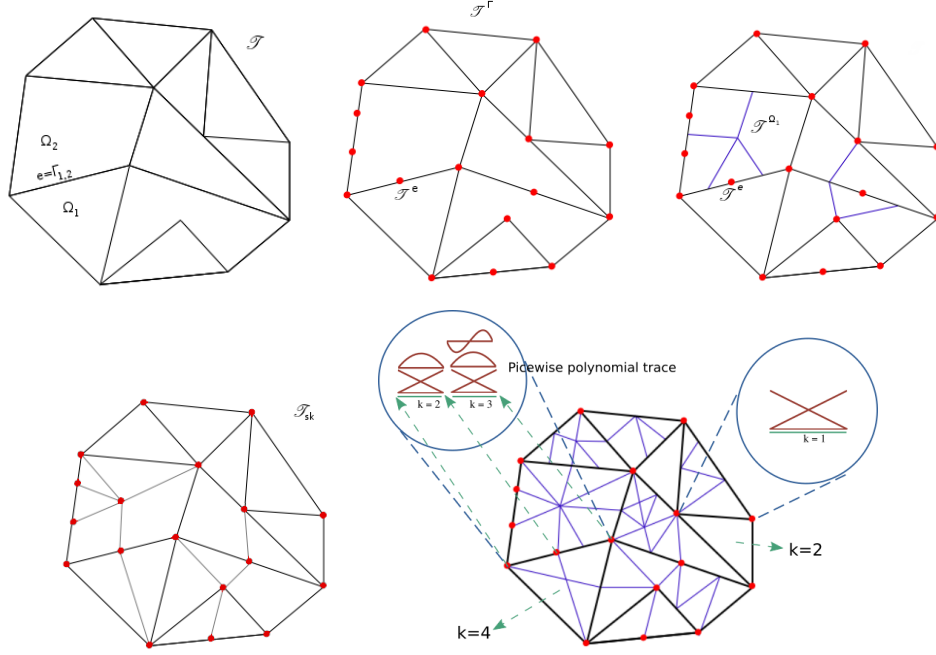


Fig. 1: Diagram illustration of some aspects of MHM-WS partitions and FE space configurations: a macro-partition  $\mathcal{T}$  (top-left side), a skeleton mesh  $\mathcal{T}^\Gamma$  (top-center side), and example of not allowed refined partitions  $\mathcal{T}^{\Omega_i}$  (top-right side); conformal partition  $\mathcal{T}_{sk}$  inducing  $\mathcal{T}^\Gamma$  over  $\Gamma$  (bottom-left side); allowed refined partitions  $\mathcal{T}^{\Omega_i}$ , and FE space configurations verifying the trace space hierarchy (bottom-right side).

### 3.2. The method

Let FE spaces  $\tilde{\mathcal{S}} \subset H(\text{div}, \Omega, \mathbb{M})$ ,  $\tilde{\mathcal{U}} \subset L^2(\Omega, \mathbb{R}^2)$ , and  $\tilde{\mathcal{Q}} \subset L^2(\Omega, \mathbb{R})$  be constructed by the assembly of the local FE spaces  $\tilde{\mathcal{S}}(\Omega_i)$ ,  $\tilde{\mathcal{U}}(\Omega_i)$ , and  $\tilde{\mathcal{Q}}(\Omega_i)$ . Consider also  $\tilde{\mathcal{U}}_{rm}^\perp$ , the  $L^2$ -orthogonal complement of  $\mathcal{U}_{rm}$  in  $\tilde{\mathcal{U}}$ , and define

$$\mathring{\tilde{\mathcal{S}}} = \left\{ \underline{\tau} \in \tilde{\mathcal{S}}; \underline{\tau} \cdot \underline{n}|_{\partial\Omega_i} = 0, \Omega_i \in \mathcal{T} \right\}. \quad (3.3)$$

Following the principles of the local-global setting for the stress mixed method for elasticity with weakly imposed symmetry, and based on the aforementioned finite dimensional FE spaces, consider the corresponding discrete downscaling-upscaling stages, which correspond to the MHM-WS method.

- *Downscaling stage:* For  $\tilde{\lambda} \in \tilde{\Lambda}_{sk}$ ,  $\tilde{\lambda} \neq 0$ , and  $\underline{f} \in L^2(\Omega, \mathbb{R}^2)$ , approximations  $\tilde{T}^\sigma(\tilde{\lambda}), \tilde{T}^\sigma(\underline{f}) \in \tilde{\mathcal{S}}$ ,  $\tilde{T}^u(\tilde{\lambda}), \tilde{T}^u(\underline{f}) \in \tilde{\mathcal{U}}_{rm}^\perp$ , and  $\tilde{T}^q(\tilde{\lambda}), \tilde{T}^q(\underline{f}) \in \tilde{\mathcal{Q}}$  are determined in each subregion  $\Omega_i$  such that

$$(\nabla \cdot \tilde{T}^\sigma(\tilde{\lambda}), \underline{v})_{\Omega_i} = 0, \quad \forall \underline{v} \in \tilde{\mathcal{U}}_{rm}^\perp, \quad (3.4)$$

$$(\underline{A}^{-1} \tilde{T}^\sigma(\tilde{\lambda}), \underline{\tau})_{\Omega_i} + (\tilde{T}^u(\tilde{\lambda}), \nabla \cdot \underline{\tau})_{\Omega_i} + (\tilde{T}^q(\tilde{\lambda}), \text{asym } \underline{\tau})_{\Omega_i} = 0, \quad \forall \underline{\tau} \in \tilde{\mathcal{S}}, \quad (3.5)$$

$$(\text{asym } \tilde{T}^\sigma(\tilde{\lambda}), \varphi)_{\Omega_i} = 0, \quad \forall \varphi \in \tilde{\mathcal{Q}}, \quad (3.6)$$

$$\tilde{T}^\sigma(\tilde{\lambda}) \underline{n}|_{\partial\Omega_i} = \tilde{\lambda}|_{\partial\Omega_i}. \quad (3.7)$$

$$-(\nabla \cdot \tilde{T}^\sigma(\underline{f}), \underline{v})_{\Omega_i} = (\underline{f}, \underline{v})_{\Omega_i}, \quad \forall \underline{v} \in \tilde{\mathcal{U}}_{rm}^\perp, \quad (3.8)$$

$$(\underline{A}^{-1} \tilde{T}^\sigma(\underline{f}), \underline{\tau})_{\Omega_i} + (\tilde{T}^u(\underline{f}), \nabla \cdot \underline{\tau})_{\Omega_i} + (\tilde{T}^q(\underline{f}), \text{asym } \underline{\tau})_{\Omega_i} = 0, \quad \forall \underline{\tau} \in \tilde{\mathcal{S}}, \quad (3.9)$$

$$(\text{asym } \tilde{T}^\sigma(\underline{f}), \varphi)_{\Omega_i} = 0, \quad \forall \varphi \in \tilde{\mathcal{Q}}, \quad (3.10)$$

$$\tilde{T}^\sigma(\underline{f}) \underline{n}|_{\partial\Omega_i} = 0. \quad (3.11)$$

- *Upscaling stage:*  $\tilde{\underline{u}}_{rm} \in \mathcal{U}_{rm}$  and  $\tilde{\lambda} \in \tilde{\Lambda}_{sk}$  are determined by the global system

$$(\underline{A}^{-1} \tilde{T}^\sigma(\tilde{\lambda}), \tilde{T}^\sigma(\underline{\mu})) + (\tilde{\underline{u}}_{rm}, \nabla \cdot \tilde{T}^\sigma(\underline{\mu})) = -(\underline{f}, \tilde{T}^u(\underline{\mu})) + \langle \underline{\mu}, \underline{g} \rangle, \quad \forall \underline{\mu} \in \tilde{\Lambda}_{sk}, \quad (3.12)$$

$$-(\nabla \cdot \tilde{T}^\sigma(\tilde{\lambda}), \underline{v}) = (\underline{f}, \underline{v}), \quad \forall \underline{v} \in \mathcal{U}_{rm}. \quad (3.13)$$

### Remarks

- (i) By construction,  $\tilde{\underline{\sigma}} = \tilde{T}^\sigma(\tilde{\lambda}) + \tilde{T}^\sigma(\underline{f}) \in \tilde{\mathcal{S}}$  has normal trace over  $\Gamma$  included in  $\tilde{\Lambda}_{sk}$ . In other words,  $\tilde{\underline{\sigma}} \in \tilde{\mathcal{S}}_{sk}$ , where

$$\tilde{\mathcal{S}}_{sk} = \{\underline{\tau} \in \tilde{\mathcal{S}}; \underline{\tau} \cdot \underline{n}|_\Gamma \in \tilde{\Lambda}_{sk}\}.$$

- (ii) The strong interface normal trace constraint imposed in the MHM-WS method is a process that can be accomplished in a similar manner of conforming constrained functions commonly used in  $hp$ -adaptive strategies. Neumann boundary conditions in the MHM- $H^1$  method are imposed in a weak multiplier sense.
- (iii) The approximate displacement  $\tilde{\underline{u}}$  given by the MHM-WS method decomposes into the form  $\tilde{\underline{u}} = \tilde{\underline{u}}_{rm} + \tilde{\underline{u}}^\perp$ , as in the MHM- $H^1$  version. However, unlike the approximation given by the MHM- $H^1$  formulation, for  $\tilde{\underline{u}}^\perp$  no continuity constraint is required inside  $\Omega_i$ , over element interfaces of  $\mathcal{T}^{\Omega_i}$ . This aspect, combined with the global  $H(\text{div})$ -conformity of the tensor  $\tilde{\underline{\sigma}}$ , is crucial in the proof of the local conservation property verified by the MHM-WS method at the micro scale level, over the partitions  $\mathcal{T}^{\Omega_i}$ , which is essential for ensuring a locally equilibrated approximation. Furthermore, for  $\underline{f} = 0$ , the resulting tensor  $\tilde{\underline{\sigma}}$  is strongly divergence-free, due to the divergence-compatibility condition (1.7) valid for tensor and displacement local spaces  $\tilde{\mathcal{S}}(\Omega_i)$ , and  $\tilde{\mathcal{U}}(\Omega_i)$ .

The next result is paramount for the well-posedness of (3.12) - (3.13).

**Lemma 3.1.** *The mapping  $\tilde{R}_{rm} : \tilde{\Lambda}_{sk} \rightarrow \mathcal{U}_{rm}$ , defined by  $\tilde{R}_{rm} = R_{rm}|_{\tilde{\Lambda}_{sk}}$ , is surjective.*

**Proof.** Recall that, for  $\underline{\mu} \in \tilde{\Lambda}_{sk}$ ,  $(\tilde{R}_{rm}\underline{\mu}, \underline{v})_{\Omega_i} = \langle \delta_i \underline{\mu}, \underline{v} \rangle_{\partial\Omega_i}$ ,  $\forall \underline{v} \in \mathcal{U}_{rm}$ . As in the continuous setting analysed in Sec. 2, given  $\underline{v}^* \in \mathcal{U}_{rm}$ , let  $\underline{\sigma}^* \in H^1(\Omega, \mathbb{S})$  satisfying  $\nabla \cdot \underline{\sigma}^* = \underline{v}^*$ . Then, define  $\tilde{\lambda}^* = \underline{\sigma}^* \underline{n}|_{\partial\Omega_i}$ ,  $\Omega_i \in \mathcal{T}$ , where  $\underline{\sigma}^* = \Pi_{1,sk}^{\underline{\sigma}} \underline{\sigma}^* \in \tilde{\mathcal{S}}_{sk}$ , and the interpolant  $\Pi_{1,sk}^{\underline{\sigma}}$ , defined for  $\underline{\tau} \in H^1(\Omega, \mathbb{M})$ , is such that  $(\nabla \cdot (\underline{\tau} - \Pi_{1,sk}^{\underline{\sigma}} \underline{\tau}), \underline{v}) = 0$ ,  $\forall \underline{v} \in \tilde{\mathcal{W}}$ . The existence of such mapping is postponed to Theorem 4.2. Thus,  $\tilde{\lambda}^* \in \tilde{\Lambda}_{sk}$ , and the assumption  $\mathcal{U}_{rm} \subset \tilde{\mathcal{W}}$  implies that  $\nabla \cdot \underline{\sigma}^* = \underline{v}^*$ . Consequently,  $(\tilde{v}^*, \underline{v})_{\Omega_i} = \langle \underline{\sigma}^* \underline{n}^{\Omega_i}, \underline{v} \rangle_{\partial\Omega_i} = \langle \delta_i \tilde{\lambda}^*, \underline{v} \rangle_{\partial\Omega_i}$ , meaning that  $\tilde{R}_{rm}(\tilde{\lambda}^*) = \underline{v}^*$ , and the result follows.  $\square$

**Theorem 3.1.** *Solution uniqueness holds for the MHM-WS defined by the local solvers (3.4) - (3.7) and (3.8) - (3.11), and by the global system (3.12) - (3.13).*

**Proof.** Due to the stability assumptions on the FE spaces  $\tilde{\mathcal{S}}(\Omega_i) \times \tilde{\mathcal{W}}(\Omega_i) \times \tilde{\mathcal{Q}}(\Omega_i)$ , the local upscaling solvers (3.4) - (3.7) are well-posed MFEM-WS versions in  $\Omega_i$  of the local mixed formulations (2.1) - (2.4). Thus, uniqueness holds for  $(\tilde{T}^{\underline{\sigma}}(\tilde{\lambda}), \tilde{T}^u(\lambda), \tilde{T}^q(\lambda)) \in \tilde{\mathcal{S}}_{sk} \times \tilde{\mathcal{W}} \times \tilde{\mathcal{Q}}$ . Analogously,  $(\tilde{T}^{\underline{\sigma}}(\underline{f}), \tilde{T}^u(\underline{f}), \tilde{T}^q(\underline{f})) \in \tilde{\mathcal{S}}_{sk} \times \tilde{\mathcal{W}} \times \tilde{\mathcal{Q}}$  are locally defined by unique solutions of well-posed MFEM-WS formulations (3.8) - (3.11) in the subdomains  $\Omega_i$ .

Uniqueness for the solution of the upscaling stage (3.12) - (3.13) follows by similar proof steps, as observed for the formulations in the continuous level. Take zero data  $\underline{f} = 0$  and  $\underline{g} = 0$ . Thus, the well-posedness of the local problem (3.8) - (3.11) implies that  $\tilde{T}^u(\underline{f}) = 0$ ,  $\tilde{T}^{\underline{\sigma}}(\underline{f}) = 0$  (and  $\tilde{T}^q(\underline{f}) = 0$ ). The upscaling system (3.12) - (3.13) becomes

$$\begin{aligned} (\underline{A}^{-1} \tilde{T}^{\underline{\sigma}}(\tilde{\lambda}), \tilde{T}^{\underline{\sigma}}(\underline{\mu})) + (\tilde{u}_{rm}, \nabla \cdot \tilde{T}^{\underline{\sigma}}(\underline{\mu})) &= 0, \quad \forall \underline{\mu} \in \tilde{\Lambda}_{sk}, \\ (\nabla \cdot \tilde{T}^{\underline{\sigma}}(\tilde{\lambda}), \underline{v}) &= 0, \quad \forall \underline{v} \in \mathcal{U}_{rm}. \end{aligned}$$

Testing with  $\underline{\mu} = \tilde{\lambda}$  and  $\underline{v} = \nabla \cdot \tilde{T}^{\underline{\sigma}}(\tilde{\lambda}) \in \mathcal{U}_{rm}$  (for (3.4)), these equations turn into

$$\begin{aligned} (\underline{A}^{-1} \tilde{T}^{\underline{\sigma}}(\tilde{\lambda}), \tilde{T}^{\underline{\sigma}}(\tilde{\lambda})) + (\tilde{u}_{rm}, \nabla \cdot \tilde{T}^{\underline{\sigma}}(\tilde{\lambda})) &= 0, \\ (\nabla \cdot \tilde{T}^{\underline{\sigma}}(\tilde{\lambda}), \nabla \cdot \tilde{T}^{\underline{\sigma}}(\tilde{\lambda})) &= 0, \end{aligned}$$

implying that  $\nabla \cdot \tilde{T}^{\underline{\sigma}}(\tilde{\lambda}) = 0$ , from which  $(\underline{A}^{-1} \tilde{T}^{\underline{\sigma}}(\tilde{\lambda}), \tilde{T}^{\underline{\sigma}}(\tilde{\lambda})) = 0$  holds. The positive definiteness of the tensor  $\underline{A}$  implies that  $\tilde{T}^{\underline{\sigma}}(\tilde{\lambda}) = 0$ , meaning that  $\tilde{\lambda} = 0$  (and thus  $\tilde{T}^u(\tilde{\lambda}) = 0$  and  $\tilde{T}^q(\tilde{\lambda}) = 0$  as well). Consequently, the remaining relation is  $(\tilde{u}_{rm}, \nabla \cdot \tilde{T}^{\underline{\sigma}}(\underline{\mu})) = 0$ ,  $\forall \underline{\mu} \in \tilde{\Lambda}_{sk}$ . Noting that  $-\nabla \cdot \tilde{T}^{\underline{\sigma}}(\underline{\mu}) = \tilde{R}_{rm}(\underline{\mu})$  in  $\Omega_i$ , for  $\underline{\mu} \in \tilde{\Lambda}_{sk}$ , and since from Lemma 3.1 there exists  $\underline{\mu}^* \in \tilde{\Lambda}_{sk}$  such that  $\tilde{R}_{rm}(\underline{\mu}^*) = \tilde{u}_{rm}$ , we conclude that  $\tilde{u}_{rm} = 0$ , and the result follows.  $\square$

#### 4. The MHM-WS method as a MFEM-WS

The purpose of this section is to establish the relation between this MFEM-WS solution with the approximate variables given by the MFEM-WS scheme based on the same FE space setting  $\tilde{\mathcal{E}}_{sk}$ .

**Theorem 4.1.** *Assume the FE space configuration  $\tilde{\mathcal{E}}_{sk} = \tilde{\mathcal{I}}_{sk} \times \tilde{\mathcal{U}} \times \tilde{\mathcal{Q}}$  verify the divergence and Stokes compatibility constraints. Then the well-posed MFEM-WS based on  $\tilde{\mathcal{E}}_{sk}$  is equivalent to the MHM-WS method using the same FE space configuration.*

**Proof.** Let us follow similar steps as in the proof of Theorem 2.1. Firstly, suppose  $(\tilde{\lambda}, \tilde{u}_{rm})$  solves the upscaling system of the MHM-WS method, and consider the recovered solution of the downscaling stage  $\tilde{\underline{\sigma}} = \tilde{T}^\sigma(\tilde{\lambda}) + \tilde{T}^\sigma(f)$ ,  $\tilde{u}^\perp = \tilde{T}^u(\tilde{\lambda}) + \tilde{T}^u(f)$ , and  $\tilde{q} = \frac{1}{2} \text{asym } \tilde{u}_{rm} + \tilde{T}^q(\tilde{\lambda}) + \tilde{T}^q(f)$ . After the combination of the systems (3.4) - (3.7) and (3.8) - (3.11), we obtain the following set of equations in the subdomains:

$$\begin{aligned} -(\nabla \cdot \tilde{\underline{\sigma}}, v)_{\Omega_i} &= (f, v)_{\Omega_i}, \quad \forall v \in \tilde{\mathcal{U}}_{rm}^\perp. \\ (\underline{A}^{-1} \tilde{\underline{\sigma}}, \underline{\tau})_{\Omega_i} + (\tilde{u}^\perp, \nabla \cdot \underline{\tau})_{\Omega_i} + (\tilde{q} - \frac{1}{2} \text{asym } \nabla \tilde{u}_{rm}, \text{asym } \underline{\tau})_{\Omega_i} &= 0, \quad \forall \underline{\tau} \in \tilde{\mathcal{I}}, \\ (\text{asym } \tilde{\underline{\sigma}}, \varphi)_{\Omega_i} &= 0, \quad \forall \varphi \in \tilde{\mathcal{Q}}, \\ \tilde{\underline{\sigma}} \underline{n}|_{\partial\Omega_i} &= \tilde{\lambda}|_{\partial\Omega_i}. \end{aligned}$$

On the other hand side, let  $(\tilde{s}, \tilde{w}, \tilde{r}) \in \tilde{\mathcal{E}}_{sk}$  be the MFEM-WS solution, and set  $\tilde{\nu} = \tilde{s} \underline{n}|_\Gamma$ , and  $\tilde{w} = \tilde{w}_{rm} + \tilde{w}^\perp$ . By confronting the above system of equations with similar one valid for  $(\tilde{s}, \tilde{w}, \tilde{r})$ , we conclude that  $\tilde{\underline{\sigma}} - \tilde{s} = \tilde{T}^\sigma(\tilde{\lambda} - \tilde{\nu})$ ,  $\tilde{u}^\perp - \tilde{w}^\perp = \tilde{T}^u(\tilde{\lambda} - \tilde{\nu})$ , and  $\tilde{q} - \tilde{r} = \tilde{T}^q(\tilde{\lambda} - \tilde{\nu})$ .

For arbitrary  $\mu \in \tilde{\Lambda}_{sk}$ , (3.8), (3.5), and (3.10) imply that  $(f, \tilde{T}^u(\mu))_{\Omega_i} = (\tilde{T}^\sigma(\mu), \underline{A}^{-1} \tilde{T}^\sigma(f))_{\Omega_i}$ . Using this relation and the properties  $\mu|_{\partial\Omega} = \tilde{T}^\sigma(\mu) \underline{n}^\Omega$  (by (3.11)), and  $(\nabla \cdot \tilde{T}^\sigma(f), v) = 0$ ,  $\forall v \in \mathcal{U}_{rm}$ , Eq. (3.12) and (3.13) become

$$\begin{aligned} (\underline{A}^{-1} \tilde{\underline{\sigma}}, \tilde{T}^\sigma(\mu)) + (\tilde{u}_{rm}, \nabla \cdot \tilde{T}^\sigma(\mu)) &= \langle \mu, g \rangle, \quad \forall \mu \in \tilde{\Lambda}_{sk} \\ -(\nabla \cdot \tilde{\underline{\sigma}}, v) &= (f, v), \quad \forall v \in \mathcal{U}_{rm}. \end{aligned}$$

Analogously, using in Eq. (1.9) the facts that  $(\tilde{r}, \text{asym } T^\sigma(\mu)) = 0$ , and  $(\tilde{w}^\perp, \nabla \cdot T^\sigma(\mu)) = 0$ , and recalling Eq. (1.10), we obtain

$$\begin{aligned} (\underline{A}^{-1} \tilde{s}, T^\sigma(\mu)) + (\tilde{w}_{rm}, \nabla \cdot T^\sigma(\mu)) &= \langle \mu, g \rangle, \quad \forall \mu \in \tilde{\Lambda}_{sk}, \\ -(\nabla \cdot \tilde{s}, v) &= (f, v), \quad \forall v \in \mathcal{U}_{rm}. \end{aligned}$$

Consequently,

$$\begin{aligned} (\underline{A}^{-1} [\tilde{\underline{\sigma}} - \tilde{s}], \tilde{T}^\sigma(\mu)) + (\tilde{u}_{rm} - \tilde{w}_{rm}, \nabla \cdot \tilde{T}^\sigma(\mu)) &= 0, \quad \forall \mu \in \tilde{\Lambda}_{sk}. \\ -(\nabla \cdot [\tilde{\underline{\sigma}} - \tilde{s}], v) &= 0, \quad \forall v \in \mathcal{U}_{rm}. \end{aligned}$$

By setting  $\underline{\mu} = \tilde{\lambda} - \tilde{\nu}$  and  $\underline{v} = \tilde{u}_{rm} - \tilde{w}_{rm}$  in the above relations, and since we already know that  $\underline{\tilde{\sigma}} - \underline{\tilde{s}} = \tilde{T}^\sigma(\tilde{\lambda} - \tilde{\nu})$ , the positive definiteness property of  $\underline{A}^{-1}$  implies that  $\underline{\tilde{\sigma}} = \underline{\tilde{s}}$  (i.e.,  $\tilde{\lambda} = \tilde{\nu}$ ). Thus  $\underline{\tilde{u}}^\perp = \underline{w}^\perp$  and  $\tilde{q} = \tilde{r}$  as well. Finally, the remaining equation  $(\tilde{u}_{rm} - \tilde{w}_{rm}, \nabla \cdot T^\sigma(\underline{\mu})) = 0$ ,  $\forall \underline{\mu} \in \tilde{\Lambda}_{sk}$ , and Lemma 3.1, concerning the surjectivity over  $\mathcal{U}_{rm}$  of  $\nabla \cdot \tilde{T}^\sigma(\underline{\mu}) = -R_{rm}(\underline{\mu})$ ,  $\underline{\mu} \in \Lambda_{sk}$ , imply that  $\tilde{u}_{rm} = \tilde{w}_{rm}$ . By uniqueness of MHM-WS and MFEM-WS solutions in  $\tilde{\mathcal{E}}_{sk}$ , these methods are equivalent.  $\square$

As shall be used in further sections, the equivalence result of Theorem 4.1 is an important tool for stability and error analyses of the MHM-WS method via some known methodologies for the MFEM-WS, which require the construction appropriate interpolants, as defined in Ref. 4. Then error estimates are bounded in terms of the interpolation errors. The next theorem shows how these operators can be defined for the particular cases of interest in the context of the MHM-WS method.

**Theorem 4.2.** *Assume the composite FE space configuration  $\tilde{\mathcal{E}}_{sk} = \tilde{\mathcal{S}}_{sk} \times \tilde{\mathcal{U}} \times \tilde{\mathcal{Q}}$  verify the divergence and Stokes compatibility stability constraints. Then, a bounded interpolation operator  $\Pi_{sk}^\sigma : H^1(\Omega, \mathbb{M}) \rightarrow \tilde{\mathcal{S}}_{sk}$  can be defined satisfying*

$$\begin{aligned} \left( \nabla \cdot (\underline{\tau} - \Pi_{sk}^\sigma \underline{\tau}), \underline{v} \right) + \left( \text{asym}(\underline{\tau} - \Pi_{sk}^\sigma \underline{\tau}), \varphi \right) &= 0, \quad \forall \underline{v} \in \tilde{\mathcal{U}}, \quad \forall \varphi \in \tilde{\mathcal{Q}}, \\ \|\Pi_{sk}^\sigma \underline{\tau}\|_{H(\text{div}, \Omega, \mathbb{M})} &\leq C \|\underline{\tau}\|_{H(\text{div}, \Omega, \mathbb{M})}. \end{aligned} \quad (4.1)$$

**Proof.** The construction of  $\Pi_{sk}^\sigma \underline{\tau} = \Pi_{1,sk}^\sigma \underline{\tau} + \Pi_{2,sk}^\sigma \underline{\tau}$  is done in two steps, as suggested in Ref. 4. Firstly, for divergence consistent pairs  $\tilde{\mathcal{S}}_{sk} \times \tilde{\mathcal{U}}$ , the mapping  $\Pi_{1,sk}^\sigma : H^1(\Omega, \mathbb{M}) \rightarrow \tilde{\mathcal{S}}_{sk}$  is constructed such that

$$\left( \nabla \cdot (\underline{\tau} - \Pi_{1,sk}^\sigma \underline{\tau}), \underline{v} \right) = 0, \quad \forall \underline{v} \in \tilde{\mathcal{U}}. \quad (4.2)$$

It can be formed by the combination of local versions  $\pi_{sk}^{\Omega_i} : H^1(\Omega_i, \mathbb{M}) \rightarrow \tilde{\mathcal{S}}_{sk}(\Omega_i)$  verifying (4.2) in  $\Omega_i$ . As for the one-scale FE settings, a direct sum decomposition for the constrained tensor space  $\tilde{\mathcal{S}}_{sk}(\Omega_i) = \tilde{\mathcal{S}}_{sk}^\partial(\Omega_i) \oplus \mathring{\mathcal{S}}(\Omega_i)$  also holds, playing a crucial role in the definition of  $\pi_{sk}^{\Omega_i}$ . Precisely, in the spirit of the projection-based interpolants  $\pi^{\Omega_i}$  hold by the one-level frameworks  $\mathcal{S}(\Omega_i)$ ,  $\pi_{sk}^{\Omega_i} \underline{\tau}$  can be factorized in terms of edge and internal terms as  $\pi_{sk}^{\Omega_i} \underline{\tau} = \pi_{sk}^{\Omega_i, \partial} \underline{\tau} + \mathring{\pi}^{\Omega_i} [\underline{\tau} - \pi_{sk}^{\Omega_i, \partial} \underline{\tau}]$ ,  $\pi_{sk}^{\Omega_i, \partial} \underline{\tau} \in \tilde{\mathcal{S}}_{sk}^\partial(\Omega_i)$ , and  $\mathring{\pi}^{\Omega_i} [\underline{\tau} - \pi_{sk}^{\Omega_i, \partial} \underline{\tau}] \in \mathring{\mathcal{S}}(\Omega_i)$ , where the edge component is modified to be constrained by  $\tilde{\Lambda}_{sk}$  (instead of  $\tilde{\Lambda}$  for the unconstrained cases),

$$\langle \underline{\pi}^{\Omega_i, \partial} \underline{\tau} \cdot \underline{n}, \mu \rangle_{\partial\Omega_i} = \langle \underline{\tau} \cdot \underline{n}, \mu \rangle_{\partial\Omega_i}, \quad \forall \mu \in \tilde{\Lambda}_{sk}.$$

The uniform boundness of  $\pi_{sk}^{\Omega_i} \underline{\tau}$  and the required divergence-commuting property hold as for unconstrained one-scale spaces.

For the divergence-free correction  $\Pi_{2,sk}^\sigma : H^1(\Omega, \mathbb{M}) \rightarrow \tilde{\mathcal{S}}_{sk}$  such that

$$\left( \text{asym} \Pi_{2,sk}^\sigma \underline{\tau}, \varphi \right) = \left( \text{asym} (\Pi_{1,sk}^\sigma \underline{\tau} - \underline{\tau}), \varphi \right), \quad \forall \varphi \in \tilde{\mathcal{Q}}, \quad (4.3)$$

consider the Stokes-compatible pair  $\{\tilde{\mathcal{W}}_{sk}, \tilde{\mathcal{Q}}\}$ , which is assumed to exist so that the stability constraint  $\underline{\nabla} \times \tilde{\mathcal{W}}_{sk} \subset \tilde{\mathcal{S}}_{sk}$  is satisfied. To construct  $\Pi_{2,sk}^{\underline{\sigma}, \underline{\tau}}$ , let  $\underline{\phi} = [\phi_1 \ \phi_2] \in \tilde{\mathcal{W}}_{sk}$  solving the Stokes problem such that  $-(\nabla \cdot \underline{\phi}, \varphi) = (\text{asym}(\Pi_{1,sk}^{\underline{\sigma}, \underline{\tau}} - \underline{\tau}), \varphi)$ ,  $\forall \varphi \in \tilde{\mathcal{Q}}$ , and define  $\Pi_{2,sk}^{\underline{\sigma}, \underline{\tau}} = \underline{\nabla} \times \underline{\phi} = \begin{bmatrix} \partial_2 \phi_1 & -\partial_1 \phi_1 \\ \partial_2 \phi_2 & -\partial_1 \phi_2 \end{bmatrix} \in \tilde{\mathcal{S}}_{sk}$ . It can be verified that  $\Pi_{2,sk}^{\underline{\sigma}, \underline{\tau}}$  is divergence free and

$$\|\Pi_{2,sk}^{\underline{\sigma}, \underline{\tau}}\|_{H(\text{div}, \Omega, \mathbb{M})} = \|\Pi_{2,\gamma}^{\underline{\sigma}, \underline{\tau}}\|_{L^2(\Omega, \mathbb{M})} \leq C \|\Pi_{1,\gamma}^{\underline{\sigma}, \underline{\tau}} - \underline{\tau}\|_{L^2(\Omega, \mathbb{M})}. \quad (4.4)$$

Since  $\text{asym} \Pi_{2,sk}^{\underline{\sigma}, \underline{\tau}} = -\partial_1 \phi_1 - \partial_2 \phi_2 = -\nabla \cdot \underline{\phi}$ , the required property (4.3) holds.  $\square$

## 5. Examples of FE Spaces for the MHM-WS

We know from Theorem 4.1 that, under divergence and Stokes compatibility constraints of a FE space setting  $\tilde{\mathcal{E}}_{sk} = \tilde{\mathcal{S}}_{sk} \times \tilde{\mathcal{U}} \times \tilde{\mathcal{Q}}$ , the MHM-WS method and the MFEM-WS formulation based on it are equivalent. Some stable two-scale examples shall be derived and analyzed in this section. Their constructions start from basic stable one-scale composite frameworks.

### 5.1. The one-scale FE space cases

Suppose partitions  $\mathcal{T}_h^e$  of  $e \subset \Gamma$  are given, with characteristic size  $h > 0$ . Internal partitions  $\mathcal{T}_h^{\Omega_i}$  of the subdomains  $\Omega_i$  are defined with the same characteristic mesh-size  $h$ , and verifying the geometric properties stated in Sec. 3.1, excepting that they are supposed to be compatible with the edge partitions  $\mathcal{T}_h^e$  for each  $e$  in  $\partial\Omega_i$ , so that  $\mathcal{T}_h = \cup \mathcal{T}_h^{\Omega_i}$  is a conformal shape-regular partition of  $\Omega$ . Let us also assume that aspect ratios of  $\mathcal{T}_h$  are independent of  $h$ .

Consider one-scale FE spaces  $\tilde{\mathcal{E}}_{h,k} = \tilde{\mathcal{S}}_{h,k} \times \tilde{\mathcal{U}}_{h,k} \times \tilde{\mathcal{Q}}_{h,k}$  composed by stable discrete local settings  $\tilde{\mathcal{S}}_{h,k}(\Omega_i) \times \tilde{\mathcal{U}}_{h,k}(\Omega_i) \times \tilde{\mathcal{Q}}_{h,k}(\Omega_i)$  for the MFEM-WS in  $\Omega_i$ , based on  $\mathcal{T}_h^{\Omega_i}$ , for which the assumptions made in Sec. 3.1 hold. For them, define the trace space  $\tilde{\Lambda}_{h,k}, k \geq 1$ , of piecewise scalar polynomials of degree  $k$  based on  $\mathcal{T}_h^e, e \subset \partial\Omega_i$ , so that  $\underline{\tau}|_e \in \tilde{\Lambda}_{h,k}|_e$ , for  $\underline{\tau} \in \tilde{\mathcal{S}}_{h,k}(\Omega_i)$ .

For  $k \geq 1$ , let parameters  $t, r \in \{-1, 0, 1\}$  be such that the local approximation spaces  $S(K, \mathbb{M}), U(K, \mathbb{R}^2)$ , and  $Q(K, \mathbb{R}), K \in \mathcal{T}_h^{\Omega_i}$ , used in the construction of the one-sale space settings  $\tilde{\mathcal{S}}_{h,k}(\Omega_i) \times \tilde{\mathcal{U}}_{h,k}(\Omega_i) \times \tilde{\mathcal{Q}}_{h,k}(\Omega_i)$ , satisfy the following properties:

$$\mathbb{P}_k(K, \mathbb{M}) \subset S(K, \mathbb{M}), \quad (5.1)$$

$$\mathbb{P}_{k+t}(K, \mathbb{M}) \subset U(K, \mathbb{R}^2), \quad (5.2)$$

$$\mathbb{P}_{k+r}(K, \mathbb{M}) \subset Q(K, \mathbb{R}). \quad (5.3)$$

Table 1 summarizes some examples of stable one-scale FE space settings verifying these properties. Notice that  $\tilde{\mathcal{E}}_{\mathcal{BDM}_k^+}$  and  $\tilde{\mathcal{E}}_{\mathcal{BDM}_k^{++}}$ , and  $\tilde{\mathcal{E}}_{\mathcal{RT}_{[k]}^+}$  are recently constructed stable enhanced versions of  $\tilde{\mathcal{E}}_{\mathcal{BDM}_k}$  and  $\tilde{\mathcal{E}}_{\mathcal{RT}_{[k]}}$  methods, respectively.

They are obtained by an enrichment procedure enforced by incrementing the tensor space with extra bubble terms to restore divergence-constraint and/or Stokes-constraint for stability condition when higher order displacement and/or rotation spaces are applied. The parameters  $(t, r)$  characterize their optimal conditions (5.2) and (5.3). Condition (5.1), with  $k \geq 1$ , is valid in all the cases. Eventually, their stability analyses require two new auxiliary types of Stokes-compatible space configurations, namely, the enriched versions of Crouzier-Raviat  $\mathcal{CR}_{k+1}^+$  for triangles or Girault-Raviart  $\mathcal{GR}_{[k+1]}^+$  for quadrilaterals. More details shall be given in Sec. 6 for these and for general two-scale FE space configurations.

Table 1: One-scale stable FE methods  $\tilde{\mathcal{E}}_{h,k}$ ,  $k \geq 1$  for the MFEM-WS for triangular (T) and affine quadrilateral (Q) elements  $K$ : Stokes pairs, FE spaces  $S(K, \mathbb{M})$ ,  $U(K, \mathbb{R}^2)$ , and  $Q(K, \mathbb{R})$ , for  $K \in \mathcal{T}_h^{\Omega_i}$ ; the accuracy parameters  $(t, r)$  verify (5.2) and (5.3).

$K$	$\tilde{\mathcal{E}}_{h,k}$	Stokes	$S(K, \mathbb{M})$	$U(K, \mathbb{R}^2)$	$Q(K, \mathbb{R})$	$(t, r)$	Ref.
T	$\mathcal{BDM}_k$	-	$\mathbb{P}_k^0(K, \mathbb{M}) \oplus \hat{\mathbb{P}}_k(K, \mathbb{M})$	$\mathbb{P}_{k-1}(K, \mathbb{R}^2)$	$\mathbb{P}_{k-1}(K)$	$(-1, -1)$	[3]
	$\mathcal{BDM}_k^+$	$\mathcal{CR}_{k+1}$	$\mathbb{P}_k^0(K, \mathbb{M}) \oplus \hat{\mathbb{P}}_{k+1}(K, \mathbb{M})$	$\mathbb{P}_k(K, \mathbb{R}^2)$	$\mathbb{P}_k(K, \mathbb{R})$	$(0, 0)$	[14]
	$\mathcal{BDM}_k^{++}$	$\mathcal{CR}_{k+1}^+$	$\mathbb{P}_k^0(K, \mathbb{M}) \oplus \hat{\mathbb{P}}_{k+2}(K, \mathbb{M})$	$\mathbb{P}_{k+1}(K, \mathbb{R}^2)$	$\mathbb{P}_{k+1}(K, \mathbb{R})$	$(1, 1)$	[14]
Q	$\mathcal{RT}_{[k]}$	$\mathcal{GR}_{[k+1]}$	$S_{\mathcal{RT}_{[k]}}(K, \mathbb{M})$	$\mathbb{Q}_{k,k}(K, \mathbb{R}^2)$	$\mathbb{P}_k(K, \mathbb{R})$	$(0, 0)$	[1]
	$\mathcal{RT}_{[k]}^+$	$\mathcal{GR}_{[k+1]}^+$	$S_{\mathcal{RT}_{[k]}}^0(K, \mathbb{M}) \oplus \hat{S}_{\mathcal{RT}_{[k+1]}}(K, \mathbb{M})$	$U_{\mathcal{RT}_{[k+1]}}(K, \mathbb{R}^2)$	$\mathbb{P}_{k+1}(K, \mathbb{R})$	$(1, 1)$	[14]

## 5.2. The two-scale space cases

The family of two-scale MHM-WS methods are parametrized by  $\gamma = (\gamma_{sk}, \gamma_{in})$ , where  $\gamma_{sk}$  and  $\gamma_{in}$  represent the pair of mesh widths and polynomial degrees associated to the trace and local FE spaces. Specifically,

- $\gamma_{sk} = (h_{sk}, k_{sk})$ ,  $k_{sk} \geq 1$ , are parametrers for a fixed coarse one-scale stable setting  $\tilde{\mathcal{E}}_{\gamma_{sk}}$  for the MFEM-WS. Namely, the trace space  $\tilde{\Lambda}_{\gamma_{sk}}$  is piecewise defined by polynomials of degree  $k_{sk}$  based on a skeleton partition  $\mathcal{T}_{h_{sk}}^\Gamma$  of characteristic mesh-size  $h_{sk}$ , and the FE spaces  $\tilde{\mathcal{E}}_{\gamma_{sk}}$  are based on a conformal shape regular partition  $\mathcal{T}_{h_{sk}}$  of  $\Omega$  formed by the union of local meshes  $\mathcal{T}_{h_{sk}}^{\Omega_i}$ .
- $\gamma_{in} = (h_{in}, k_{in})$  are the parameters for refined local FE spaces inside the subregions,  $\tilde{\mathcal{E}}_{\gamma_{in}}(\Omega_i) = \tilde{\mathcal{S}}_{\gamma_{in}}(\Omega_i) \times \tilde{\mathcal{U}}_{\gamma_{in}}(\Omega_i) \times \tilde{\mathcal{Q}}_{\gamma_{in}}(\Omega_i)$ , based on the partitions  $\mathcal{T}_{h_{in}}^{\Omega_i}$ .
- It is assumed that  $h_{in} = h_{sk}/2^\ell$ ,  $\ell \geq 0$ , and  $k_{in} = k_{sk} + n$ ,  $n \geq 0$ . Thus,  $\tilde{\mathcal{E}}_{\gamma_{sk}}(\Omega_i) \subset \tilde{\mathcal{E}}_{\gamma_{in}}(\Omega_i)$ . For the particular case  $\tilde{\mathcal{E}}_{\mathcal{BDM}\mathcal{M}\gamma_{in}}(\Omega_i)$ , with  $k_{sk} = 1$ , we assume  $n \geq 1$  (such that  $\mathcal{U}_{rm}(\Omega_i) \subset \tilde{\mathcal{U}}_{\gamma_{in}}(\Omega_i)$  holds).

Owing to the previous assumptions, observe that the requirements stated in Sec. 3.1 concerning the well-definition of the MHM-WS method hold. Precisely, we get

- (1) The local FE spaces  $\tilde{\mathcal{E}}_{\gamma_{in}}(\Omega_i) = \tilde{\mathcal{S}}_{\gamma_{in}}(\Omega_i) \times \tilde{\mathcal{U}}_{\gamma_{in}}(\Omega_i) \times \tilde{\mathcal{Q}}_{\gamma_{in}}(\Omega_i)$  verify the stability constraints for the MFEM-WS scheme for elasticity problems in  $\Omega_i$ .
- (2)  $\mathcal{U}_{rm}(\Omega_i) \subset \tilde{\mathcal{U}}_{\gamma_{in}}(\Omega_i)$  and  $\mathbb{P}_0(\Omega_i, \mathbb{R}) \subset \tilde{\mathcal{Q}}_{\gamma_{in}}(\Omega_i)$ .
- (3) Trace hierarchy naturally holds:  $\tilde{\Lambda}_{\gamma_{sk}} \subset \tilde{\Lambda}_{\gamma_{in}}$ .

Let us define the following two-scale local FE spaces:

$$\tilde{\mathcal{S}}_{\gamma}(\Omega_i) := \tilde{\mathcal{S}}_{h_{sk}, k_{sk}}^{\partial}(\Omega_i) \oplus \mathring{\mathcal{S}}_{h_{in}, k_{in}}(\Omega_i), \quad (5.4)$$

$$\tilde{\mathcal{U}}_{\gamma_{in}}(\Omega_i) := \tilde{\mathcal{U}}_{h_{in}, k_{in}}(\Omega_i). \quad (5.5)$$

$$\tilde{\mathcal{Q}}_{\gamma_{in}}(\Omega_i) := \tilde{\mathcal{Q}}_{h_{in}, k_{in}}(\Omega_i). \quad (5.6)$$

Recall that the internal tensors  $\mathring{\mathcal{S}}_{h_{in}, k_{in}}(\Omega_i)$ , with vanishing normal traces over  $\partial\Omega_i$ , are enriched versions of  $\mathring{\mathcal{S}}_{h_{sk}, k_{sk}}(\Omega_i) \subset \mathring{\mathcal{S}}_{h_{in}, k_{in}}(\Omega_i)$  by uniformly refining the local meshes  $\mathcal{T}_{h_{sk}}^{\Omega_i}$  to get  $\mathcal{T}_{h_{in}}^{\Omega_i}$ , and/or by adding internal tensors of higher degree  $k_{sk} + n$ . However, the edge tensors  $\tilde{\mathcal{S}}_{h_{sk}, k_{sk}}^{\partial}(\Omega_i)$  are maintained at the coarser level, their normal traces over  $\partial\Omega_i$  being constrained to the coarse space  $\tilde{\Lambda}_{\gamma_{sk}} \subset \tilde{\Lambda}_{\gamma_{in}}$ . This means that if

$$\tilde{\mathcal{S}}_{\gamma} = \{\underline{\tau} \in H(\text{div}, \Omega, \mathbb{M}); \underline{\tau}|_{\Omega_i} \in \tilde{\mathcal{S}}_{\gamma}(\Omega_i)\},$$

then the interface normal trace constraint  $\underline{\tau} \cdot \underline{n}|_{\Gamma} \in \tilde{\Lambda}_{\gamma_{sk}}$  holds for all  $\underline{\tau} \in \tilde{\mathcal{S}}_{\gamma}$ .

Following the general construction described in Sec 3.2, here the focus is on the analysis of MHM-WS methods relying on the two-scale FE space configurations  $\tilde{\mathcal{E}}_{\gamma} = \tilde{\mathcal{S}}_{\gamma} \times \tilde{\mathcal{U}}_{\gamma_{in}} \times \tilde{\mathcal{Q}}_{\gamma_{in}}$ .

#### Remarks

- The two-scale pairs  $\tilde{\mathcal{S}}_{\gamma}(\Omega_i) \times \tilde{\mathcal{U}}_{\gamma_{in}}(\Omega_i)$  can be interpreted as being constructed from two-scale Poisson-compatible pairs  $\tilde{\mathcal{V}}_{\gamma}(\Omega_i) \times \tilde{\mathcal{P}}_{\gamma_{in}}(\Omega_i)$  defined in Ref. 15, where  $\tilde{\mathcal{V}}_{\gamma}(\Omega_i) = \tilde{\mathcal{V}}_{h_{sk}, k_{sk}}^{\partial}(\Omega_i) \oplus \mathring{\mathcal{V}}_{h_{in}, k_{in}}(\Omega_i)$  and  $\tilde{\mathcal{P}}_{\gamma_{in}}(\Omega_i) = \mathring{\mathcal{P}}_{h_{in}, k_{in}}(\Omega_i)$ .
- It should be mentioned that more generic stable one-scale FE space configurations can be used to form two-scale FE spaces  $\tilde{\mathcal{E}}_{\gamma}$  for the MHM-WS method. For instance, the cases proposed in Ref. 30 and 9 could be considered. They are constructed by the inclusion of some extra divergence-free bubble tensor functions to an approximation space formed with rows taken from standard Poisson-compatible FE spaces. Their stability are not based on a Stokes-constraint, as for the cases considered in Table 1 and analysed in the following section.

## 6. Unified Stability Analysis for the Two-Scale MHM-WS Methods

This section is dedicated to the stability analysis for the MHM-WS methods based on the two-scale FE space configurations  $\tilde{\mathcal{E}}_{\mathcal{BDM}_{\gamma}}$ ,  $\tilde{\mathcal{E}}_{\mathcal{BDM}_{\gamma}^+}$ , and  $\tilde{\mathcal{E}}_{\mathcal{RT}_{[\gamma]}}$ , derived from the one-scale settings  $\tilde{\mathcal{E}}_{h, \mathcal{BDM}_k}$ ,  $\tilde{\mathcal{E}}_{h, \mathcal{BDM}_k^+}$ , and  $\tilde{\mathcal{E}}_{h, \mathcal{RT}_{[k]}}$ , for  $k \geq 1$ , displayed in Table 1.

Recalling the statement of Theorem 4.1, the principle is to prove stability of these MHM-WS methods via the equivalent MFEM-WS methods (generally denoted by MFEM-WS( $\gamma$ )) that search for two-scale approximations  $(\underline{\tilde{\sigma}}, \underline{\tilde{u}}, \underline{\tilde{q}}) \in \tilde{\mathcal{E}}_\gamma = \tilde{\mathcal{S}}_\gamma \times \tilde{\mathcal{U}}_{\gamma_{in}} \times \tilde{\mathcal{Q}}_{\gamma_{in}}$  satisfying

$$(\underline{A}^{-1} \underline{\tilde{\sigma}}, \underline{\tau}) + (\underline{\tilde{u}}, \underline{\nabla} \cdot \underline{\tau}) + (\underline{\tilde{q}}, \text{asym } \underline{\tau}) = \langle \underline{\tau}, \underline{n}^\Omega, g \rangle, \quad \forall \underline{\tau} \in \tilde{\mathcal{S}}_\gamma, \quad (6.1)$$

$$-(\underline{\nabla} \cdot \underline{\tilde{\sigma}}, \underline{v}) = (\underline{f}, \underline{v}), \quad \forall \underline{v} \in \tilde{\mathcal{U}}_{\gamma_{in}}, \quad (6.2)$$

$$(\text{asym } \underline{\tilde{\sigma}}, \underline{\varphi}) = 0, \quad \forall \underline{\varphi} \in \tilde{\mathcal{Q}}_{\gamma_{in}}. \quad (6.3)$$

By construction, the divergence-constraint  $\underline{\nabla} \cdot \tilde{\mathcal{S}}_\gamma \subset \tilde{\mathcal{U}}_{\gamma_{in}}$  is verified by the FE pairs  $\tilde{\mathcal{S}}_\gamma(\Omega_i) \times \tilde{\mathcal{U}}_{\gamma_{in}}(\Omega_i)$ . To complete stability of the MFEM-WS( $\gamma$ ) scheme, enriched pairs  $\{\tilde{\mathcal{W}}_\gamma, \tilde{\mathcal{Q}}_{\gamma_{in}}\}$  of Stokes-compatible spaces verifying the constraint  $\underline{\nabla} \times \tilde{\mathcal{W}}_\gamma \subset \tilde{\mathcal{S}}_\gamma$  are required, which shall be constructed in this section.

As already mentioned, the stability of some particular scenarios were analyzed in Ref. 14 for one-scale triangular or quadrilateral meshes (i.e.  $h_{in} = h_{sk}$ ), when only internal polynomial degree enrichments  $k_{in} = k_{sk} + 1$  or  $k_{in} = k_{sk} + 2$  were adopted (see Table 1). A similar methodology can be successfully applied to the more general two-scale composite FE space settings  $\tilde{\mathcal{E}}_\gamma$ , as shall be detailed in Sec. 6.1 and Sec. 6.2, and summarized in Table 2. The construction of these two-scale Stokes-compatible FE pairs is guided by incrementing the velocity spaces  $W_{\mathcal{CR}_{k_{sk}+1}}(\bar{K}, \mathbb{R}^2)$  or  $W_{\mathcal{GR}_{[k_{sk}]+1}}(\bar{K}, \mathbb{R}^2)$  for  $\bar{K} \in \mathcal{T}_{h_{sk}}^{\Omega_i}$  with some bubble vector functions to recover stability when pressure spaces are enlarged (see Ref. 6). These extra terms are defined by the multiplication of appropriate vector spaces, containing the gradient of the enlarged rotation elements, by a fixed scalar bubble function defined for each  $\bar{K} \in \mathcal{T}_{h_{sk}}^{\Omega_i}$ . As far as we understand, these two-scale Stokes-compatible FE pairs, for the Girault-Raviart family for affine quadrilaterals, and for the Crouzeix-Raviart spaces for triangles, are new in the literature.

Table 2: Two-scale Stokes-compatible FE pairs  $\{\tilde{\mathcal{W}}_\gamma(\Omega_i), \tilde{\mathcal{Q}}_{\gamma_{in}}(\Omega_i)\}$ : local spaces in  $\bar{K} \in \mathcal{T}_{h_{sk}}^{\Omega_i}$  for triangular (T) and affine quadrilateral (Q) elements.

$\bar{K}$	Spaces	$\tilde{\mathcal{Q}}_{k_{in}}(\mathcal{T}_{h_{in}}^{\bar{K}}, \mathbb{R})$	$W_\gamma(\bar{K}, \mathbb{R}^2)$
T	$\mathcal{CR}_\gamma$	$\mathbb{P}_{k_{sk}+n-1}(\mathcal{T}_{h_{in}}^{\bar{K}}, \mathbb{R})$	$W_{\mathcal{CR}_{k_{sk}+1}}(\bar{K}, \mathbb{R}^2) + \mathring{B}_{\mathcal{CR}_{k_{in}}}(\mathcal{T}_{h_{in}}^{\bar{K}}, \mathbb{R}^2)$
Q	$\mathcal{GR}_{[\gamma]}$	$\mathbb{P}_{k_{sk}+n}(\mathcal{T}_{h_{in}}^{\bar{K}}, \mathbb{R})$	$W_{\mathcal{GR}_{[k_{sk}+1]}}(\bar{K}, \mathbb{R}^2) + \mathring{B}_{\mathcal{GR}_{[k_{in}]}}(\mathcal{T}_{h_{in}}^{\bar{K}}, \mathbb{R}^2)$

The next two sections describe the construction of two-scale Stokes-compatible FE pairs to be applied in the stability analysis of the MFEM-WS( $\gamma$ ) schemes.

### 6.1. Stokes-constraint for local triangular meshes

Let us consider two families of FE space settings  $\tilde{\mathcal{E}}_\gamma$  for triangular local meshes  $\mathcal{T}_{h_{in}}^{\Omega_i}$ .

*Family  $\tilde{\mathcal{E}}_{\mathcal{BDM}_\gamma}$ :* Consider first the FE space settings based on the conformal coarse partitions  $\mathcal{T}_{h_{sk}}^{\Omega_i}$  (without internal mesh refinement) and polynomial increment  $k_{in} = k_{sk} + 1$ , for which the local spaces are defined by

$$\{\tilde{\mathcal{S}}_{h_{sk}, \mathcal{BDM}_{k_{sk}}}^\partial(\Omega_i) \oplus \tilde{\mathcal{S}}_{h_{sk}, \mathcal{BDM}_{k_{sk}+1}}^\partial(\Omega_i), \tilde{\mathcal{U}}_{h_{sk}, \mathcal{BDM}_{k_{sk}+1}}(\Omega_i), \tilde{\mathcal{Q}}_{h_{sk}, \mathcal{BDM}_{k_{sk}+1}}(\Omega_i)\}.$$

They correspond to the  $\mathcal{BDM}_{h_{sk}, k_{sk}}^+(\Omega_i)$  cases considered in Ref. 14. For them, a stable choice  $\tilde{\mathcal{Q}}_{h_{sk}, \mathcal{BDM}_{k_{sk}+1}}(\Omega_i) := \mathbb{P}_{k_{sk}}(\mathcal{T}_{h_{sk}}^{\Omega_i}, \mathbb{R})$  for the rotation space is guided by considering the Stokes-compatible Crouzeix-Raviart spaces  $\mathcal{CR}_{k_{sk}+1}(\Omega_i)$ , with local FE spaces  $W_{\mathcal{CR}_{k_{sk}+1}}(\bar{K}, \mathbb{R}^2) = \mathbb{P}_{k_{sk}+1}(K, \mathbb{R}^2) + b_K \mathbb{P}_{k_{sk}-1}(\bar{K}, \mathbb{R}^2)$  for velocity, and  $\mathbb{P}_{k_{sk}}(\bar{K}, \mathbb{R})$  for pressure, in  $\bar{K} \in \mathcal{T}_{h_{sk}}^{\Omega_i}$ .

For a general two-scale scenario, using internal polynomial degree increment  $k_{in} = k_{sk} + n$ , and internal refined partitions  $\mathcal{T}_{h_{in}}^{\Omega_i}$ , with  $h_{in} = h_{sk}/2^\ell$ , stability of the new proposed two-scale FE space settings

$$\{\tilde{\mathcal{S}}_{h_{sk}, \mathcal{BDM}_{k_{sk}}}^\partial(\Omega_i) \oplus \tilde{\mathcal{S}}_{h_{in}, \mathcal{BDM}_{k_{sk}+n}}^\partial(\Omega_i), \tilde{\mathcal{U}}_{h_{in}, \mathcal{BDM}_{k_{sk}+n}}(\Omega_i), \tilde{\mathcal{Q}}_{h_{in}, \mathcal{BDM}_{k_{sk}+n}}(\Omega_i)\}$$

requires two-scale Stokes-compatible Crouzeix-Raviart spaces  $\tilde{\mathcal{W}}_{\mathcal{CR}_\gamma}(\Omega_i) \subset H^1(\Omega_i, \mathbb{R}^2)$ ,  $\tilde{\mathcal{Q}}_{\mathcal{CR}_{\gamma_{in}}}(\Omega_i) \subset L^2(\Omega_i, \mathbb{R})$ . They are defined for  $\bar{K} \in \mathcal{T}_{h_{sk}}^{\Omega_i}$  by the composite pressure space  $\tilde{\mathcal{Q}}_{\mathcal{CR}_{\gamma_{in}}}(\bar{K}) = \mathbb{P}_{k_{sk}+n-1}(\mathcal{T}_{h_{in}}^{\bar{K}}, \mathbb{R}) = \tilde{\mathcal{Q}}_{h_{in}, \mathcal{BDM}_{k_{sk}+n}}(\bar{K})$ , piecewise-defined over the refined partition  $\mathcal{T}_{h_{in}}^{\bar{K}}$  induced on  $\bar{K}$ , and the velocity space  $W_{\mathcal{CR}_{k_{sk}+1}}(\bar{K}, \mathbb{R}^2) + \mathring{B}_{\mathcal{CR}_{k_{in}}}(\mathcal{T}_{h_{in}}^{\bar{K}}, \mathbb{R}^2)$ , where the stabilizing bubble spaces are

$$\mathring{B}_{\mathcal{CR}_{k_{in}}}(\mathcal{T}_{h_{in}}^{\bar{K}}, \mathbb{R}^2) = \{\underline{w} \in H^1(\bar{K}, \mathbb{R}^2); \underline{w}|_K = b_K \nabla \mathbb{P}_{k_{sk}+n-1}(K, \mathbb{R}), K \in \mathcal{T}_{h_{in}}^{\bar{K}}\}.$$

Using these local FE pairs, the requirements of Corollary of Theorem 2 in Ref. 6 are fulfilled, and the Stokes-compatibility of the resulting two-scale space configuration holds. Furthermore,  $\underline{\nabla} \times \mathring{B}_{\mathcal{CR}_{k_{in}}}(\mathcal{T}_{h_{in}}^{\bar{K}}, \mathbb{R}^2)$  are divergence-free bubble functions in  $\bar{K} \in \mathcal{T}_{h_{sk}}^{\Omega_j}$ , with degree  $k_{sk} + n$ . Therefore, the required property  $\underline{\nabla} \times \tilde{\mathcal{W}}_{\mathcal{CR}_\gamma}(\Omega_i) \subset \tilde{\mathcal{S}}_\gamma(\Omega_i) = \tilde{\mathcal{S}}_{h_{sk}, \mathcal{BDM}_{k_{sk}}}^\partial(\Omega_i) \oplus \tilde{\mathcal{S}}_{h_{in}, \mathcal{BDM}_{k_{sk}+n}}^\partial(\Omega_i)$  holds. Consequently,  $\tilde{\mathcal{Q}}_{\gamma_{in}}(\Omega_i) = \mathbb{P}_{k_{sk}+n-1}(\mathcal{T}_{h_{in}}^{\Omega_i}, \mathbb{R})$  is a stable rotation choice for  $\tilde{\mathcal{E}}_{\mathcal{BDM}_\gamma}(\Omega_i)$ .

*Family  $\tilde{\mathcal{E}}_{\mathcal{BDM}_\gamma^+}$ :* As for its original one-scale setting, it is clear that the local FE spaces  $\{\tilde{\mathcal{S}}_{\mathcal{BDM}_\gamma^+}(\Omega_i), \tilde{\mathcal{U}}_{\mathcal{BDM}_{\gamma_{in}}^+}(\Omega_i), \tilde{\mathcal{Q}}_{\mathcal{BDM}_{\gamma_{in}}^+}(\Omega_i)\}$  of this two-scale family verify

$$\begin{aligned} \tilde{\mathcal{S}}_{\mathcal{BDM}_\gamma^+}^\partial(\Omega_i) &= \tilde{\mathcal{S}}_{h_{sk}, \mathcal{BDM}_{k_{sk}}}^\partial(\Omega_i), & \mathring{\tilde{\mathcal{S}}}_{\mathcal{BDM}_\gamma^+}(\Omega_i) &= \mathring{\tilde{\mathcal{S}}}_{h_{in}, \mathcal{BDM}_{k_{in}+1}}(\Omega_i), \\ \tilde{\mathcal{U}}_{\mathcal{BDM}_{\gamma_{in}}^+}(\Omega_i) &= \tilde{\mathcal{U}}_{h_{in}, \mathcal{BDM}_{k_{in}+1}}(\Omega_i), & \tilde{\mathcal{Q}}_{\mathcal{BDM}_{\gamma_{in}}^+}(\Omega_i) &= \tilde{\mathcal{Q}}_{h_{in}, \mathcal{BDM}_{k_{in}+1}}(\Omega_i). \end{aligned}$$

In other words,  $\tilde{\mathcal{E}}_{\mathcal{BDM}_\gamma^+} = \tilde{\mathcal{E}}_{\mathcal{BDM}_{\gamma^+}}$ , where  $\gamma^+ = (\gamma_{sk}, \gamma_{in}^+)$ , and  $\gamma_{in}^+ = (h_{in}, k_{in} + 1)$ . Thus, the stability analysis valid for  $\tilde{\mathcal{E}}_{\mathcal{BDM}_{\gamma^+}}$  ensures that  $\tilde{\mathcal{E}}_{\mathcal{BDM}_\gamma^+}$  is also stable.

## 6.2. Stokes-constraint for local affine quadrilateral meshes

Firstly, let us recall the FE space settings based on the conformal quadrilateral partitions  $\mathcal{T}_{h_{sk}}^{\Omega_i}$  (without internal mesh refinement) and polynomial increment  $k_{in} = k_{sk} + 1$ , for which the local spaces are defined by

$$\{\tilde{\mathcal{S}}_{h_{sk}, \mathcal{RT}_{[k_{sk}]}}^{\partial}(\Omega_i) \oplus \mathring{\mathcal{S}}_{h_{sk}, \mathcal{RT}_{[k_{sk}+1]}}(\Omega_i), \tilde{\mathcal{U}}_{h_{sk}, \mathcal{BDM}_{k_{sk}+1}}(\Omega_i), \tilde{\mathcal{Q}}_{h_{sk}, \mathcal{RT}_{[k_{sk}+1]}}(\Omega_i)\}.$$

They correspond to the  $\mathcal{RT}_{[h_{sk}, k_{sk}]}^+$ ( $\Omega_i$ ) cases considered in Ref. 14. For them, a stable choice  $\tilde{\mathcal{Q}}_{h_{sk}, \mathcal{RT}_{[k_{sk}+1]}}(\Omega_i) = \mathbb{P}_{k_{sk}+1}(\mathcal{T}_{h_{sk}}^{\Omega_i}, \mathbb{R})$  for the rotation space is guided by considering enriched Stokes-compatible Girault-Raviart spaces  $\mathcal{GR}_{[k_{sk}+1]}^+(\Omega_i)$ , with local FE spaces  $W_{\mathcal{GR}_{[k_{sk}+1]}^+}(\bar{K}, \mathbb{R}^2) = \mathbb{Q}_{k_{sk}+1, k_{sk}+1}(\bar{K}, \mathbb{R}^2) + \mathring{B}_{\mathcal{GR}_{[k_{sk}+1]}}(\bar{K}, \mathbb{R}^2)$  for velocity, and  $\mathbb{P}_{k_{sk}+1}(\bar{K}, \mathbb{R})$  for pressure, in  $\bar{K} \in \mathcal{T}_{h_{sk}}^{\Omega_i}$ . Functions  $\underline{w}$  in the bubble spaces  $\mathring{B}_{\mathcal{GR}_{[k_{sk}+1]}}(\bar{K}, \mathbb{R}^2)$  are of the form  $\underline{w} = b_{\bar{K}} \mathbb{Q}_{k_{sk}, k_{sk}}(\bar{K}, \mathbb{R})$ ,  $b_{\bar{K}}$  being the basic bubble function on  $\bar{K}$ .

This enrichment methodology can also be extended to prove stability for general local FE space scenarios  $\mathcal{ER}_{\mathcal{T}_{[\gamma]}}$ , with local spaces

$$\{\tilde{\mathcal{S}}_{h_{sk}, \mathcal{RT}_{[k_{sk}]}^{\partial}}(\Omega_i) \oplus \mathring{\mathcal{S}}_{h_{in}, k_{sk}+n}(\Omega_i), \tilde{\mathcal{U}}_{h_{in}, \mathcal{RT}_{[k_{sk}+n]}}(\Omega_i), \tilde{\mathcal{Q}}_{h_{in}, \mathcal{RT}_{[k_{sk}+n]}}(\Omega_i)\},$$

where both internal polynomial degree increment and partition refinement are applied. The stability of the rotation space  $\tilde{\mathcal{Q}}_{h_{in}, \mathcal{RT}_{[k_{sk}+n]}}(\Omega_i) = \mathbb{P}_{k_{sk}+n}(\mathcal{T}_{h_{in}}^{\Omega_i}, \mathbb{R})$  is guided by the FE Stokes pair  $\{\tilde{\mathcal{W}}_{\mathcal{GR}_{[\gamma]}}(\Omega_i), \tilde{\mathcal{Q}}_{\mathcal{GR}_{[\gamma_{in}]}}(\Omega_i)\} \subset H^1(\Omega_i, \mathbb{R}^2) \times L^2(\Omega_i, \mathbb{R})$ , with local pressure space  $\tilde{\mathcal{Q}}_{\mathcal{GR}_{[\gamma_{in}]}}(\bar{K}) = \mathbb{P}_{k_{sk}+n}(\mathcal{T}_{h_{in}}^{\bar{K}}, \mathbb{R})$ ,  $\bar{K} \in \mathcal{T}_{h_{sk}}^{\Omega_i}$ , piecewise defined over the partition  $\mathcal{T}_{h_{in}}^{\bar{K}}$  induced in  $\bar{K}$ , and the local velocity space  $W_{\mathcal{GR}_{[k_{sk}+1]}}(\bar{K}, \mathbb{R}^2) + \mathring{B}_{\mathcal{GR}_{[k_{in}]}}(\mathcal{T}_{h_{in}}^{\bar{K}}, \mathbb{R}^2)$ , where the bubble spaces  $\mathring{B}_{\mathcal{GR}_{[k_{in}]}}(\mathcal{T}_{h_{in}}^{\bar{K}}, \mathbb{R}^2) \subset H^1(\bar{K}, \mathbb{R}^2)$  is composed by the functions  $\underline{w}$  such that  $\underline{w}|_K = b_K \mathbb{Q}_{k_{sk}+n-1, k_{sk}+n-1}(K, \mathbb{R})$ ,  $K \in \mathcal{T}_{h_{in}}^{\bar{K}}$ . Since  $\mathbb{Q}_{k_{sk}+n-1, k_{sk}+n-1}(K, \mathbb{R})$  contains  $\mathbb{P}_{k_{sk}+n-1}(K, \mathbb{R}^2) = \nabla \mathbb{P}_{k_{sk}+n}(K, \mathbb{R})$ , and according to Corollary of Theorem 2 in Ref. 6, the stability of the resulting enriched Stokes-compatible space configuration holds. Furthermore, the tensors in  $\underline{\nabla} \times \mathring{B}_{\mathcal{GR}_{[k_{in}]}}(\mathcal{T}_{h_{in}}^{\bar{K}}, \mathbb{R}^2)$  are divergence-free bubble functions with degree  $k_{sk} + n$  defined in  $\bar{K} \in \mathcal{T}_{h_{sk}}^{\Omega_i}$ . Therefore, as in the previous cases, the required property  $\underline{\nabla} \times \tilde{\mathcal{W}}_{\mathcal{RT}_{[\gamma]}} \subset \tilde{\mathcal{S}}_{\mathcal{RT}_{[\gamma]}}$  holds, concluding that  $\tilde{\mathcal{Q}}_{\mathcal{RT}_{[\gamma_{in}]}}$  is a stable choice for the rotation space in  $\tilde{\mathcal{ER}}_{\mathcal{T}_{[\gamma]}}$ .

The conclusions of this section are summarized in the following theorem.

**Theorem 6.1.** *The MFEM-WS( $\gamma$ ) formulation (6.1) - (6.3) is well-posed for any of the two-scale FE spaces  $\tilde{\mathcal{E}}_{\mathcal{BDM}_{\gamma}}$ ,  $\tilde{\mathcal{E}}_{\mathcal{BDM}_{\gamma}^+}$ , or  $\tilde{\mathcal{E}}_{\mathcal{RT}_{[\gamma]}}$ . Moreover, it is equivalent to the respective MHM-WS method defined by (3.4) - (3.13) by means of Theorem 4.1.*

## 7. Unified Error Analysis

An unified error analysis is presented for stable MHM-WS schemes derived via an equivalent MFEM-WS( $\gamma$ ) formulation (6.1) - (6.3). Namely, we shall consider stable two-scale FE spaces  $\tilde{\mathcal{E}}_\gamma$  defined in Sec 5.2, which are composed by local approximations  $\tilde{\mathcal{S}}_\gamma(\Omega_i) \times \tilde{\mathcal{U}}_{\gamma_{in}}(\Omega_i) \times \tilde{\mathcal{Q}}_{\gamma_{in}}(\Omega_i)$  proposed in (5.4) - (5.6), the tensors being constrained to the trace vector space  $\tilde{\Lambda}_{\gamma_{sk}}$ . The analysis is general enough to be applied to the three stable families  $\tilde{\mathcal{E}}_{\mathcal{BDM}_\gamma}$ ,  $\tilde{\mathcal{E}}_{\mathcal{BDM}_\gamma^+}$ , or  $\tilde{\mathcal{E}}_{\mathcal{RT}_{[\gamma]}}$  considered in the previous section, but also to other stable two-scale FE settings eventually constructed from other examples of Poisson-compatible FE pairs under similar circumstances.

### 7.1. Interpolation error estimates

For stable two-scale FE space configurations  $\tilde{\mathcal{E}}_\gamma = \tilde{\mathcal{S}}_\gamma \times \tilde{\mathcal{U}}_{\gamma_{in}} \times \tilde{\mathcal{Q}}_{\gamma_{in}}$ , verifying the divergence and Stokes compatibility constraints, consider interpolants  $\Pi_{\tilde{\gamma}}^\sigma : H^s(\Omega, \mathbb{M}) \rightarrow \tilde{\mathcal{S}}_\gamma$ , as presented in Theorem 4.2, satisfying (4.1). In order to derive interpolation error estimates, recall the three mesh parameters involved in the discretizations:  $H$  (size of subregions),  $h_{sk} \leq H$  (mesh size of the elements in the skeleton partition), and  $h_{in} \leq h_{sk}$  referring to the mesh spacing of the shape-regular refined partitions  $\mathcal{T}_{h_{in}}^{\Omega_i}$ , which are obtained from  $\mathcal{T}_{h_{sk}}^{\Omega_i}$  by uniform subdivisions. There are also two polynomial degrees used in the construction of the FE spaces:  $k_{sk}$  referring to the trace approximations over the mesh skeleton, and  $k_{in}$  of the internal local FE approximations.

**Theorem 7.1.** *For a stable two-scale FE space configuration  $\tilde{\mathcal{E}}_\gamma = \tilde{\mathcal{S}}_\gamma \times \tilde{\mathcal{U}}_{\gamma_{in}} \times \tilde{\mathcal{Q}}_{\gamma_{in}}$ , consider the interpolant  $\Pi_{\tilde{\gamma}}^\sigma : H^s(\Omega, \mathbb{M}) \rightarrow \tilde{\mathcal{S}}_\gamma$  being defined for sufficiently smooth tensors, and let  $\Pi_{\gamma_{in}}^u : L^2(\Omega, \mathbb{R}^2) \rightarrow \tilde{\mathcal{U}}_{\gamma_{in}}$ , and  $\Pi_{\gamma_{in}}^q : L^2(\Omega, \mathbb{R}^2) \rightarrow \tilde{\mathcal{Q}}_{\gamma_{in}}$  be  $L^2$ -orthogonal-projections. If the properties (5.1) - (5.3) are verified, then:*

$$\|\underline{\mathcal{T}} - \Pi_{\tilde{\gamma}}^\sigma \underline{\mathcal{T}}\|_{\mathbf{L}^2(\Omega, \mathbb{M})} \lesssim h_{sk}^{k_{sk}+1} \|\underline{\mathcal{T}}\|_{H^{k_{sk}+1}(\Omega, \mathbb{M})}, \quad (7.1)$$

$$\|\nabla \cdot (\underline{\mathcal{T}} - \Pi_{\tilde{\gamma}}^\sigma \underline{\mathcal{T}})\|_{L^2(\Omega, \mathbb{R}^2)} \lesssim h_{in}^{k_{in}+t+1} \|\nabla \cdot \underline{\mathcal{T}}\|_{H^{k_{in}+t+1}(\Omega, \mathbb{R}^2)}, \quad (7.2)$$

$$\|\underline{v} - \Pi_{\gamma_{in}}^u \underline{v}\|_{L^2(\Omega, \mathbb{R}^2)} \lesssim h_{in}^{k_{in}+t+1} \|\underline{v}\|_{H^{k_{in}+t+1}(\Omega, \mathbb{R}^2)}, \quad (7.3)$$

$$\|\varphi - \Pi_{\gamma_{in}}^q \varphi\|_{L^2(\Omega, \mathbb{R})} \lesssim h_{in}^{k_{in}+r+1} \|\varphi\|_{H^{k_{in}+r+1}(\Omega, \mathbb{R})}, \quad (7.4)$$

where  $t$  and  $r$  are the optimal parameters defined in (5.2) and (5.3). The leading constants appearing on the right hand sides are independent of  $\gamma$ .

**Proof.** Being a  $L^2$ -projection over  $\tilde{\mathcal{U}}_{\gamma_{in}}(\Omega)$ ,  $\Pi_{\gamma_{in}}^u$  is bounded in  $L^2(\Omega, \mathbb{R}^2)$ , with unitary norm. Then, the estimation (7.3) follows from usual  $L^2$ -projection convergence errors valid in the one-level FE space configuration with mesh size  $h_{in}$  and containing polynomial spaces with degree  $k_{in} + t$ .

For the same reason, (7.2) holds due to the divergence-compatibility property derived in (4.2), meaning that  $\nabla \cdot \Pi_{\tilde{\gamma}}^\sigma \underline{\mathcal{T}}$  is the  $L^2$ -projection over  $\tilde{\mathcal{U}}_{\gamma_{in}}$  of  $\nabla \cdot \underline{\mathcal{T}}$ .

Similarly, the estimation (7.4) follows from usual  $L^2$ -projection convergence errors by recalling that  $\tilde{\mathcal{Q}}_{\gamma_{in}}(\Omega_i)$  are composite spaces over the local meshes  $\mathcal{T}_{h_{in}}^{\Omega_i}$  piecewise defined by scalar local spaces containing polynomials of degree  $k_{in} + t$ .

Concerning the error estimation (7.1), firstly observe that it holds for  $\Pi_{1,\gamma}^{\underline{\sigma}}$ . In fact, this is a consequence of the corresponding interpolation error for  $\pi_{\gamma}^D : H^s(\Omega, \mathbb{R}^2) \rightarrow \tilde{\mathcal{V}}_{\gamma}$  associated to two-scale Poisson-compatible space configurations, proved in Ref. 15. It is valid as a consequence of classic arguments, where the leading constant appearing on the right hand side only depends on the shape-regularity factors of the meshes  $\mathcal{T}_h^{\Omega_j}$ , which are supposed to be independent of the mesh-widths, and on the bound for the projection  $\hat{\pi}^D$  on the corresponding master element  $\hat{K}$ ,  $K \in \mathcal{T}_h^{\Omega_j}$  (see Theorem 4.1 in Ref.2). Recalling (4.4), we obtain  $\|\Pi_{2,\gamma}^{\underline{\sigma}}\|_{L^2(\Omega, \mathbb{M})} \leq C \|\Pi_{1,\gamma}^{\underline{\sigma}} - \underline{\tau}\|_{L^2(\Omega, \mathbb{M})}$ , completing the proof of (7.1), as a consequence of the error estimation hold for  $\Pi_{1,\gamma}^{\underline{\sigma}}$ .  $\square$

We should observe that:

- (i) Interpolation errors for tensors are limited to order  $O(h_{sk}^{k_{sk}+1})$ , independently of internal enrichment, because the edge terms live in the coarser discretization level of the normal traces over the skeleton interfaces.
- (ii) Divergence of the tensor, displacement and rotation projection errors can reach arbitrary high accuracy orders, profiting from finer meshes and higher polynomial degrees used for the approximations in  $\tilde{\mathcal{U}}_{\gamma_{in}}$  and in  $\tilde{\mathcal{Q}}_{\gamma_{in}}$ .

## 7.2. Convergence error estimates

As a consequence of the interpolation errors given in Theorem 7.1, the following convergence error estimates hold for the two-scale MFEM-WS( $\gamma$ ) formulation.

**Theorem 7.2.** *For a convex region  $\Omega$ , let  $\tilde{\mathcal{E}}_{\gamma} = \tilde{\mathcal{S}}_{\gamma} \times \tilde{\mathcal{U}}_{\gamma_{in}} \times \tilde{\mathcal{Q}}_{\gamma_{in}}$  be a two-scale composite FE space setting for the MFEM-WS( $\gamma$ ) formulation verifying the divergence and Stokes compatibility constraints. If  $\tilde{\underline{\sigma}} \in \mathcal{S}_{\gamma}$ ,  $\tilde{\underline{u}} \in \tilde{\mathcal{U}}_{\gamma_{in}}$ , and  $\tilde{q} \in \tilde{\mathcal{Q}}_{\gamma_{in}}$  are the solutions of (6.1) - (6.3), and the exact fields  $\underline{\sigma}$ ,  $\underline{u}$  and  $q$  verifying (1.4) - (1.6) are regular enough, then the next estimates hold:*

$$\begin{aligned} \|\underline{\sigma} - \tilde{\underline{\sigma}}\|_{\mathbf{L}^2(\Omega, \mathbb{M})} + \|q - \tilde{q}\|_{L^2(\Omega, \mathbb{R})} &\lesssim h_{sk}^{k_{sk}+1} \|\underline{\sigma}\|_{H^{k_{sk}+1}(\Omega, \mathbb{M})} \\ &\quad + h_{in}^{k_{in}+r+1} \|q\|_{H^{k_{in}+r+1}(\Omega, \mathbb{R})}, \end{aligned} \quad (7.5)$$

$$\|\nabla \cdot (\underline{\sigma} - \tilde{\underline{\sigma}})\|_{L^2(\Omega, \mathbb{R}^2)} \lesssim h_{in}^{k_{in}+t+1} \|\nabla \cdot \underline{\sigma}\|_{H^{k_{in}+t+1}(\Omega, \mathbb{R}^2)}, \quad (7.6)$$

$$\begin{aligned} \|\underline{u} - \tilde{\underline{u}}\|_{L^2(\Omega, \mathbb{R}^2)} &\lesssim h_{sk}^{k_{sk}+2} \|\underline{\sigma}\|_{H^{k_{in}+t+1}(\Omega, \mathbb{M})} + h_{in}^{k_{in}+t+1} \|\underline{u}\|_{H^{k_{in}+t+1}(\Omega, \mathbb{R}^2)} \\ &\quad + h_{sk} h_{in}^{k_{in}+r+1} \|q\|_{H^{k_{in}+r+1}(\Omega, \mathbb{R})}, \end{aligned} \quad (7.7)$$

where  $t$  and  $r$  are the optimal parameters defined in (5.2) and (5.3).

**Proof.** The following error estimates hold for the approximate variables in terms

of interpolation errors (see Ref. 14 or the references therein)

$$\|\underline{\sigma} - \tilde{\underline{\sigma}}\|_{L^2(\Omega, \mathbb{M})} + \|q - \tilde{q}\|_{L^2(\Omega, \mathbb{R})} \lesssim \|\underline{\sigma} - \Pi_{\tilde{\gamma}}^{\underline{\sigma}} \underline{\sigma}\|_{L^2(\Omega, \mathbb{M})} + \|q - \Pi_{\tilde{\gamma}_{in}}^q q\|_{L^2(\Omega, \mathbb{R})}, \quad (7.8)$$

$$\|\nabla \cdot (\underline{\sigma} - \tilde{\underline{\sigma}})\|_{L^2(\Omega, \mathbb{R}^2)} \lesssim \|\nabla \cdot (\underline{\sigma} - \Pi_{\tilde{\gamma}}^{\underline{\sigma}} \underline{\sigma})\|_{L^2(\Omega, \mathbb{R}^2)}, \quad (7.9)$$

$$\|\Pi_{\tilde{\gamma}_{in}}^u \underline{u} - \tilde{u}\|_{L^2(\Omega, \mathbb{R}^2)}^2 = (\underline{A}(\underline{\sigma} - \tilde{\underline{\sigma}}), \underline{v} - \Pi_{\tilde{\gamma}}^{\underline{\sigma}} \underline{v}) + (\Pi_{\tilde{\gamma}_{in}}^q q - q, \text{asym}(\underline{v} - \Pi_{\tilde{\gamma}}^{\underline{\sigma}} \underline{v})), \quad (7.10)$$

where  $\underline{v} \in H(\text{div}, \Omega, \mathbb{S})$  is the solution of the elasticity problem  $\nabla \cdot \underline{v} = \Pi_{\tilde{\gamma}_{in}}^u \underline{u} - \tilde{u}$ , and  $\underline{v} = \underline{A}^{-1} \underline{\xi}(w)$  in  $\Omega$ , with  $\underline{w} = \underline{0}$  on  $\partial\Omega$ . Consequently, estimates (7.5) and (7.6) follow directly by inserting the interpolation errors (7.1), (7.2), and (7.4) in (7.8) and (7.9). Using Cauchy-Schwartz inequality in (7.10), we obtain

$$\begin{aligned} \|\Pi_{\tilde{\gamma}_{in}}^u \underline{u} - \tilde{u}\|_{L^2(\Omega, \mathbb{R}^2)}^2 &\leq \|\underline{A}(\underline{\sigma} - \tilde{\underline{\sigma}})\|_{L^2(\Omega, \mathbb{M})} \|\underline{v} - \Pi_{\tilde{\gamma}}^{\underline{\sigma}} \underline{v}\|_{L^2(\Omega, \mathbb{M})} \\ &\quad + \|\Pi_{\tilde{\gamma}_{in}}^q q - q\|_{L^2(\Omega, \mathbb{R})} \|\text{asym}(\underline{v} - \Pi_{\tilde{\gamma}}^{\underline{\sigma}} \underline{v})\|_{L^2(\Omega, \mathbb{R})}. \end{aligned}$$

Since  $\|\underline{v}\|_{H^1(\Omega, \mathbb{M})} \approx \|\underline{w}\|_{H^2(\Omega, \mathbb{M})}$  is bounded by  $\|\Pi_{\tilde{\gamma}_{in}}^u \underline{u} - \tilde{u}\|_{L^2(\Omega, \mathbb{R}^2)}$ , due to the elliptic regularity property, valid for convex  $\Omega$ , and recalling that  $\|\underline{v} - \Pi_{\tilde{\gamma}}^{\underline{\sigma}} \underline{v}\|_{L^2(\Omega, \mathbb{M})} \lesssim h_{sk} \|\underline{v}\|_{H^1(\Omega, \mathbb{M})}$ , and  $\|\text{asym}(\underline{v} - \Pi_{\tilde{\gamma}}^{\underline{\sigma}} \underline{v})\|_{L^2(\Omega, \mathbb{R})} \lesssim h_{sk} \|\underline{v}\|_{H^1(\Omega, \mathbb{M})}$ , we obtain

$$\|\Pi_{\tilde{\gamma}_{in}}^u \underline{u} - \tilde{u}\|_{L^2(\Omega, \mathbb{R}^2)} \lesssim h_{sk} \left( \|\underline{\sigma} - \tilde{\underline{\sigma}}\|_{L^2(\Omega, \mathbb{M})} + \|\Pi_{\tilde{\gamma}_{in}}^q q - q\|_{L^2(\Omega, \mathbb{R})} \right).$$

Finally, (7.7) follows by inserting the above estimate in the triangular inequality

$$\|\underline{u} - \tilde{u}\|_{L^2(\Omega, \mathbb{R}^2)} \leq \|\underline{u} - \Pi_{\tilde{\gamma}_{in}}^u \underline{u}\|_{L^2(\Omega, \mathbb{R}^2)} + \|\Pi_{\tilde{\gamma}_{in}}^u \underline{u} - \tilde{u}\|_{L^2(\Omega, \mathbb{R}^2)},$$

and by recalling the interpolation errors (7.3) and (7.4), and using (7.5).  $\square$

*Remark:* Theorem 7.2 holds for the stable methods  $\tilde{\mathcal{E}}_{\mathcal{RT}_{[\gamma]}}$  and  $\tilde{\mathcal{E}}_{\mathcal{BDM}_{\gamma}^+}$  with  $t = r = 0$ , and  $\tilde{\mathcal{E}}_{\mathcal{BDM}_{\gamma}}$  for  $k_{sk} > 1$ , or  $k_{sk} = 1$  with  $k_{in} > k_{sk}$ , with  $t = r = -1$ .

## 8. Numerical Verification Tests

This section is dedicated to the presentation and discussion of some verification tests for the MHM-WS formulation analyzed in the previous sections, based on two-scale space configurations  $\tilde{\mathcal{E}}_{\gamma}$  corresponding to FE local spaces  $\tilde{\mathcal{S}}_{\gamma}(\Omega_i) \times \tilde{\mathcal{U}}_{\gamma_{in}}(\Omega_i) \times \tilde{\mathcal{Q}}_{\gamma_{in}}(\Omega_i)$ , as defined in (5.4) - (5.5) - (5.6). The results are compared with the ones given by the corresponding one-scale MFEM-WS versions and by the MHM- $H^1$  formulation described in Section A.2. For these implementations,  $H(\text{div})$ -conforming shape functions of edge and internal types, required in the construction of stress approximations, are the ones presented in Ref. 29, 13. The MHM- $H^1$  simulations adopt spaces spanned by the hierarchical shape functions described in Ref. 12. Both types of shape functions are available in the computational framework<sup>a</sup>.

<sup>a</sup>NeoPZ open source platform: <http://github.com/labmec/neoPZ>

### Problem 1: Oscillatory Young's modulus

Consider the elasticity problem defined in the square region  $(0, 1) \times (0, 1)$ , having Poisson ratio  $\nu = 0.3$ , and oscillatory Young's modulus  $E(x, y) = 100(1 + 0.3 \sin(10\pi(x - 0.5)) \cos(10\pi y))$ , with exact displacement solution

$$\underline{u}(x, y) = \begin{pmatrix} \frac{1}{3} \left(\frac{x}{3}\right)^2 y^2 \cos(6\pi x) \sin(7\pi y) \\ \frac{1}{5} e^y \sin(4\pi x) \end{pmatrix}.$$

The plots for  $E(x, y)$ , the components of the displacement and the corresponding stress tension field  $\underline{\underline{\sigma}}$  are shown in Fig. 2.

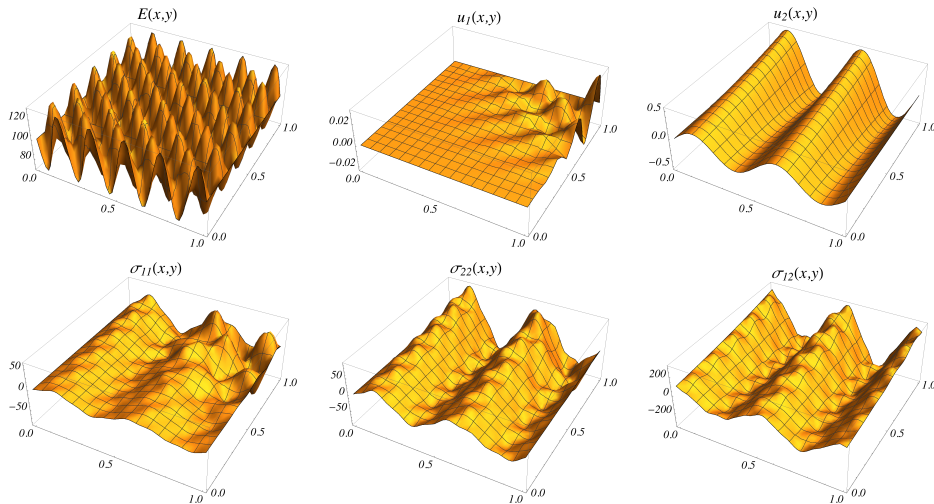


Fig. 2: Problem 1: Young's modulus, analytic displacement and stress tensor components.

The results shown in this section are for enhanced FE approximations  $\tilde{\mathcal{E}}_{\mathcal{RT}[\gamma]}$  based on square meshes, for  $\tilde{\mathcal{E}}_{\mathcal{BDM}_\gamma}$ , and  $\tilde{\mathcal{E}}_{\mathcal{BDM}_\gamma^+}$  based on triangular elements. Two types of convergence curves are considered: mesh-based and space-based convergence rates. In the first scenario, convergence rate is based on the usual  $H$ -refinement of the macro-partition, and taking  $h_{sk} = H$  (no mesh-skeleton refinement). The goal is to verify the error estimates predicted in Theorem 7.2.

Note also that the macro mesh-size  $H$  does not appear explicitly in the error estimates of Theorem 7.2. Thus, convergence is achieved by making  $h_{sk} \rightarrow 0$ , even if  $\mathcal{T}_H$  stays unchanged. Thus, the second case is for a fixed macro-partition, and the skeleton partitions are refined (as well the internal ones). The purpose is to verify if an extra convergence rate of order  $h_{sk}^{1/2}$  occurs, as observed in the numerical tests of Ref. 20, 26 using the MHM- $H^1$  method.

### 8.1. Problem 1: mesh-based convergence with square elements

In this part, all the verification tests for Problem 1 are for FE spaces  $\tilde{\mathcal{E}}_{\mathcal{RT}[\gamma]}$  based on square local partitions.

The results for the tensor component  $\sigma_{11}$  obtained by the application of the MHM-WS method are displayed in Fig. 3, for different FE space configurations. Precisely, the plots are shown for: (a)  $8 \times 8$  subregions,  $H = 2^{-3}$ ,  $h_{sk} = H$ ,  $k_{sk} = 2$ ; (b)  $8 \times 8$  subregions,  $h_{sk} = H/4$ ,  $k_{sk} = 0$ ; and (c)  $32 \times 32$  subregions,  $H = 2^{-5}$ ,  $h_{sk} = H$ ,  $k_{sk} = 2$ . In all the cases,  $h_{in} = 2^{-7}$ , and  $k_{in} = k_{sk} + 1$ . It is clear that the space configuration (a) is not sufficiently refined to capture the essential features of the solution. The other two space configurations, which are equivalent in terms of element sizes on the edges, show similar approximations, but the errors for the configuration in (c) are the smallest ones.

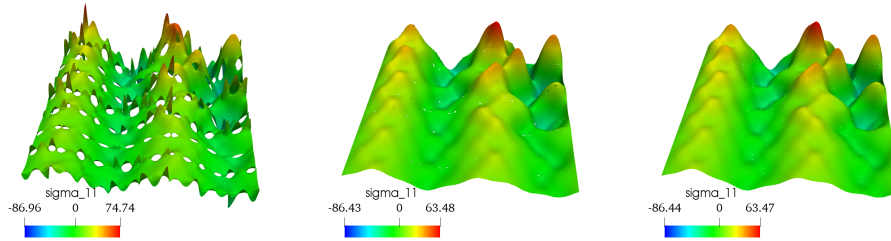


Fig. 3: Problem 1 - tensor component  $\sigma_{11}$  solved with MHM-WS using approximation space configurations  $\tilde{\mathcal{E}}_{\mathcal{RT}[\gamma]}$  for different square partitions:  $8 \times 8$  subregions,  $h_{sk} = H$ ,  $k_{sk} = 2$  (left side);  $8 \times 8$  subregions,  $h_{sk} = H/4$ ,  $k_{sk} = 0$  (middle side); and  $32 \times 32$  subregions,  $h_{sk} = H$ , and  $k_{sk} = 2$ . In all the cases  $k_{in} = k_{sk} + 1$ , and  $h_{in} = 2^{-7}$ .

Concerning the errors for displacement, the three terms in the right hand side of the displacement error estimate (7.10) may have different influence on the results, as shall be illustrated in the simulations of the next section. Fig. 4. For instance, for  $\tilde{\mathcal{E}}_{\mathcal{RT}[\gamma]}$  and  $\tilde{\mathcal{E}}_{\mathcal{BDM}_\gamma^+}$  cases, the last term  $h_{sk} h_{in}^{k_{in}+1}$  is always dominated by  $h_{sk}^{k_{sk}+2}$  (Term 1) and  $h_{in}^{k_{sk}+n+1}$  (Term 2) appearing in the first and second terms. Different regimes may be observed for Term 1 and Term 2, depending on the configuration parameters. For instance, when internal polynomial degree increment is applied with  $n \geq 1$ , the influence of Term 1 dominates Term 2 in the range of  $h_{sk}$  illustrated in Fig. 4 (top side), independently of the internal mesh refinement  $h_{in} = h_{sk}/2^\ell$ ,  $\ell \geq 1$ . These effects shall be verified in the simulations of this section.

Fig. 5 - 8 show  $L^2$ -error curves for  $\underline{u}$ ,  $\underline{\sigma}$ ,  $\nabla \cdot \underline{\sigma}$ ,  $q$ , and energy norm  $\left( \underline{A} \underline{\varepsilon}(\underline{u}), \underline{\varepsilon}(\underline{u}) \right)^{\frac{1}{2}}$ , in terms of the macro mesh size  $H = 2^{-j}$ ,  $j = 1, 2, \dots, 6$ , for the MHM-WS method based on FE spaces  $\tilde{\mathcal{E}}_{\mathcal{RT}[\gamma]}$ , using  $h_{sk} = H$ ,  $k_{sk} = 1, 2$ . For comparison, results are shown for MFEM-WS, using uniform mesh-size  $H$ , and polynomial degrees  $k = 1, 2$ .

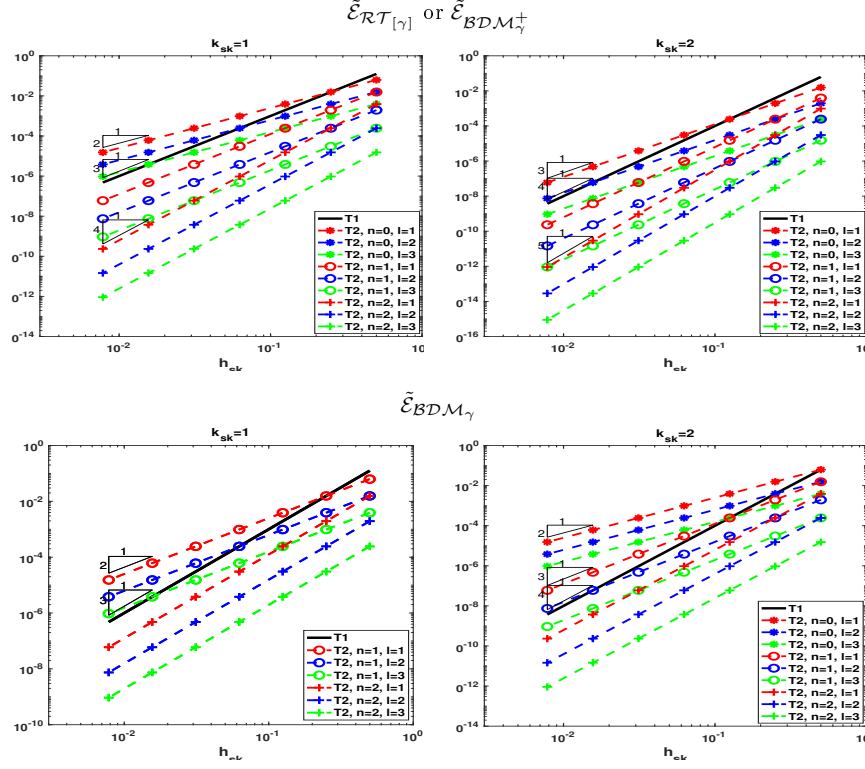


Fig. 4: Effects of  $h_{sk}^{k_{sk}+2}$  in Term 1 (T1), and  $h_{in}^{t+1}$  in Term 2 (T2) in the displacement error estimate:  $k_{sk} = 1, 2$ ,  $k_{in} = k_{sk} + n$ ,  $n = 0, 1, 2$ , and  $h_{in} = h_{sk}/2^\ell$ ,  $\ell = 1, 2, 3$ .

### 8.1.1. Effect of polynomial degree increment

Fig. 5 is for  $k_{sk} = 1$ , and Fig. 6 is for  $k_{sk} = 2$ , both with  $h_{in} = h_{sk}/2$ . The purpose is to analyze the effect of increasing  $k_{in} = k_{sk} + n$ ,  $n = 0, 1, 2$ .

As predicted in (7.5), the errors in  $\underline{\sigma}$  and  $q$  are of order  $k_{sk} + 1$ , independently of  $n$ , and these errors are about the same magnitude, in all the cases. The stress symmetry errors, which are proportional to the stress errors, also have convergence rates of order  $k_{sk} + 1$ , but the increment of the polynomial degrees inside the subregions reduces significantly their magnitudes. As expected, the divergence of the stress systematically improves accuracy to order  $k_{sk} + n + 1$  (recall that  $t = 0$  for  $\tilde{\mathcal{E}}_{\mathcal{RT}[\gamma]}$ ). For these space configurations, the dominant effect of the first term in the displacement error estimate (7.7), of order  $k_{sk} + 2$ , is also verified when  $n = 1, 2$ . For  $n = 0$ , i.e.  $k_{in} = k_{sk}$ , the second term takes place, and convergence rate of order  $k_{sk} + 1$  occurs, in accordance with the illustration of Fig. 4 (top-left-side).

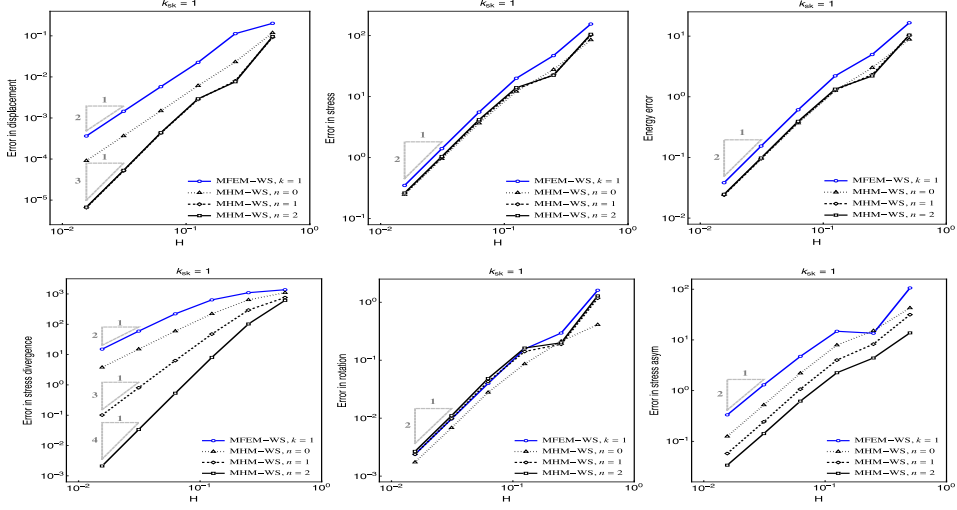


Fig. 5: Problem 1 - Mesh-based convergence for MHM-WS using FE spaces  $\tilde{\mathcal{E}}_{\mathcal{RT}[\gamma]}$ , in terms of the macro-element size  $H = 2^{-j}$ ,  $j = 1, 2, \dots, 6$ :  $h_{sk} = H$ ,  $h_{in} = h_{sk}/2$ ,  $k_{sk} = 1$ , and  $k_{in} = k_{sk} + n$ ,  $n = 0, 1, 2$ ; MFEM-WS for mesh-size  $H$ , and  $k = 1$ .

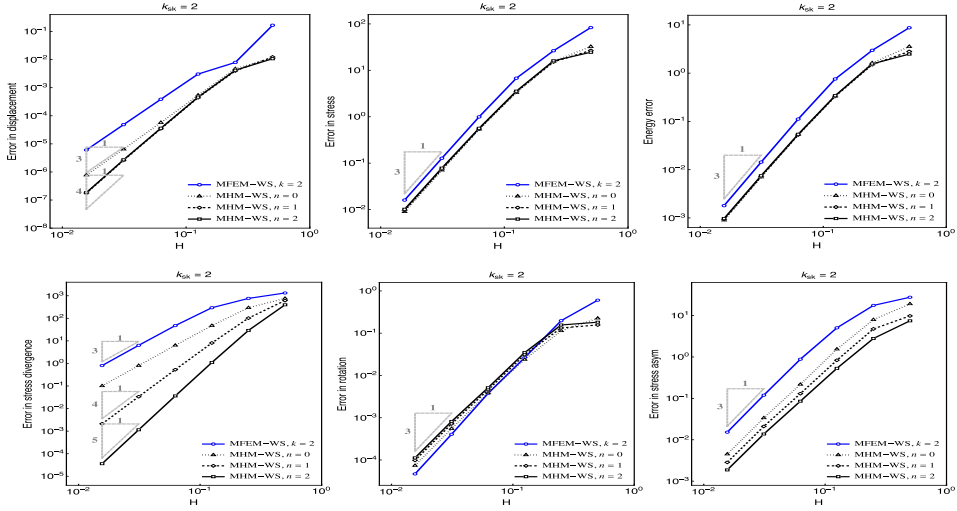


Fig. 6: Problem 1 - Mesh-based convergence for MHM-WS using FE spaces  $\tilde{\mathcal{E}}_{\mathcal{RT}[\gamma]}$ , in terms of the macro-element size  $H = 2^{-j}$ ,  $j = 1, 2, \dots, 6$ :  $h_{sk} = H$ ,  $h_{in} = h_{sk}/2$ ,  $k_{sk} = 1$ , and  $k_{in} = k_{sk} + n$ ,  $n = 0, 1, 2$ ; MFEM-WS for mesh-size  $H$ , and  $k = 2$ .

### 8.1.2. Effect of internal mesh refinement

The purpose in Fig. 7, for  $k_{sk} = 1$ , and Fig. 8, for  $k_{sk} = 2$ , taking  $k_{in} = k_{sk}$ , is to analyze the effect of refining the internal meshes, comparing the cases for

$h_{in} = h_{sk}/2^\ell$ ,  $\ell = 1, 2, 3$ . Again, for coarser levels ( $\ell = 1, 2$ ) the second term in the displacement error is the most significant, of order  $k_{sk} + 1$ , in accordance with the plots of Fig. 4 (top-left-side). However, by further refining the internal grids ( $\ell > 2$ ), the convergence rate tends to order  $k_{sk} + 2$  of the first term in (7.7). It should also be pointed out the different regime for the divergence of the stress, which is now always of fixed order  $k_{sk} + 1$ , but with magnitude reducing as  $\ell$  increases. The behavior of the other variables are not significantly affected by using these space configurations.

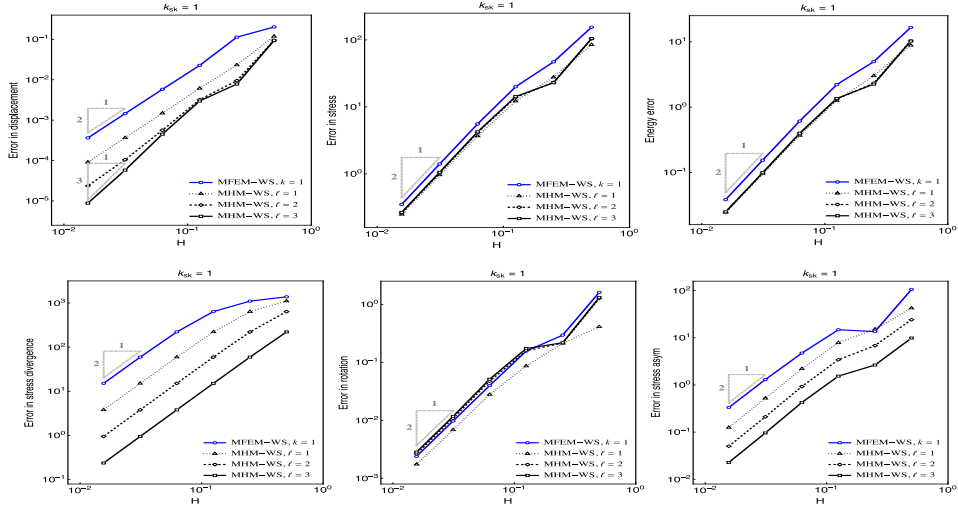


Fig. 7: Problem 1 - Mesh-based convergence for MHM-WS using FE spaces  $\tilde{\mathcal{E}}_{\mathcal{RT}}[\gamma]$ , in terms of the macro-element size  $H = 2^{-j}$ ,  $j = 1, 2, \dots, 6$ :  $h_{sk} = H$ ,  $h_{in} = h_{sk}/2^\ell$ ,  $\ell = 1, 2, 3$ ,  $k_{sk} = 1$ , and  $k_{in} = k_{sk}$ ; MFEM-WS for mesh-size  $H$ , and  $k = 1$ .

### 8.1.3. Comparison of MHM-WS and MHM- $H^1$ methods

Convergence histories for MHM-WS and MHM- $H^1$  methods, are compared in the plots in Fig. 9. The space configurations are for polynomial degree  $k_{sk} = 1, 2$ , without skeleton subdivision ( $h_{sk} = H$ ) and internal polynomial degree enrichment ( $n = 0$ ), but  $\ell$  subdivisions are used to form the micro meshes inside the macro-elements ( $h_{in} = H/2^\ell$ ),  $1 \leq \ell \leq 3$ . For the MHM- $H^1$  method, using scalar polynomials in  $\mathbb{Q}_{k_{sk}, k_{sk}}(K, \mathbb{R})$ ,  $L^2$ -stress and energy errors maintain of order  $k_{sk}$ , but as the internal mesh refinement increases, the error magnitudes decrease. This error decay is faster for  $k_{sk} = 2$ , starting with a convergence rate of order 2 for  $\ell = 1$ , the error curves for the MHM- $H^1$  method approach the ones of the MHM-WS method, having rate of order  $k_{sk} + 1$ , until they almost coincide at  $\ell = 3$ . Concerning the

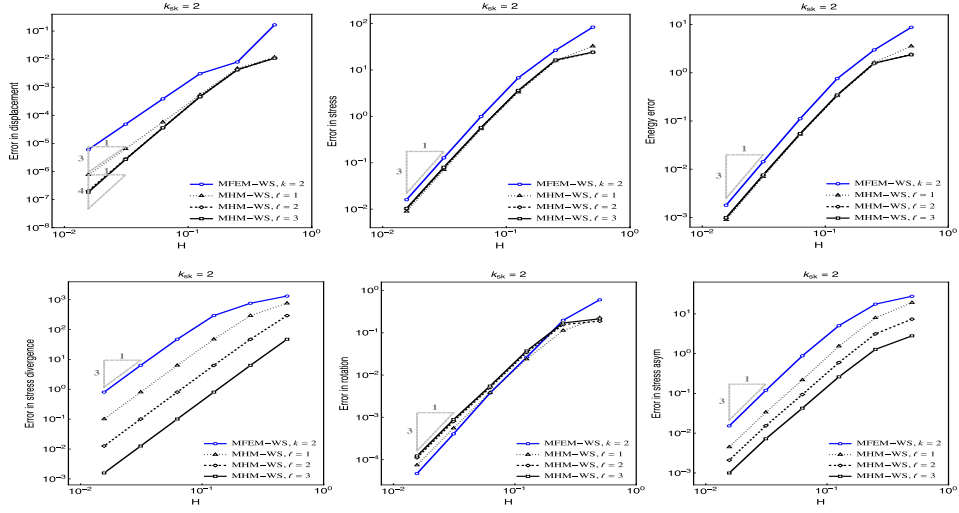


Fig. 8: Problem 1 - Mesh-based convergence for MHM-WS using FE spaces  $\tilde{\mathcal{E}}_{\mathcal{RT}}[\gamma]$ , in terms of the macro-element size  $H = 2^{-j}$ ,  $j = 1, 2, \dots, 5$ :  $h_{sk} = H$ ,  $h_{in} = h_{sk}/2^\ell$ ,  $\ell = 1, 2, 3$ ,  $k_{sk} = 2$ , and  $k_{in} = k_{sk}$ ; MFEM-WS for mesh-size  $H$ , and  $k = 2$ .

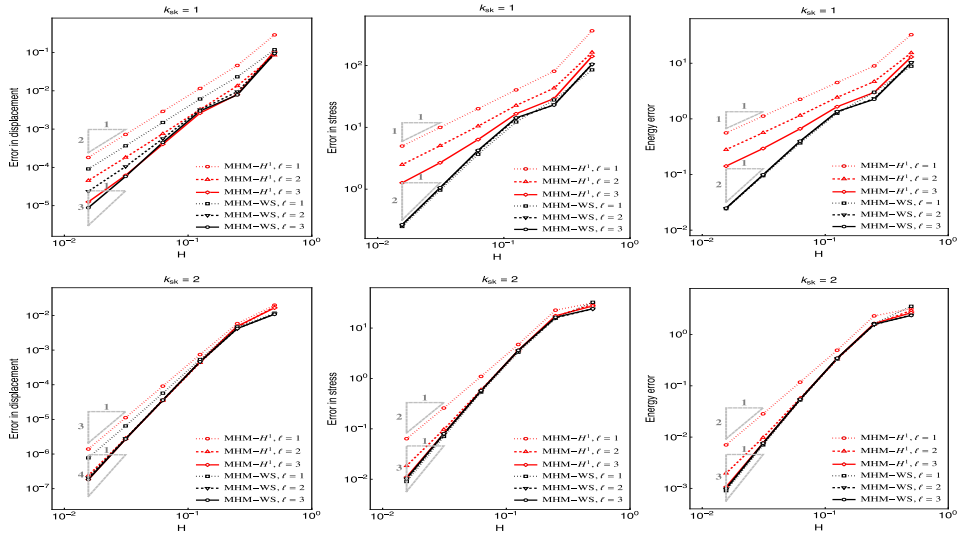


Fig. 9: Problem 1 - Mesh-based convergence for MHM-WS using FE spaces  $\tilde{\mathcal{E}}_{\mathcal{RT}}[\gamma]$ , and MHM- $H^1$  formulations, in terms of the macro-element size  $H = 2^{-j}$ ,  $j = 1, 2, \dots$ ,  $h_{sk} = H$ ,  $k_{sk} = 1, 2$ ,  $h_{in} = h_{sk}/2^\ell$ ,  $\ell = 1, 2, 3$  and  $k_{in} = k_{sk}$ .

displacement variable, both methods show similar behavior, starting with rates of order  $k_{sk} + 1$  at low internal refinement levels, typical of one-level schemes, as predicted by the error estimate in (7.7) for this kind of space configuration ( $n = 0$ ,  $t = 0$ , and  $h_{in} \sim h$ ), whose first term on the right hand side is dominating. However, as  $\ell$  increases, with  $h_{in} \ll h_{sk}$ , the error magnitudes decrease, with fast decay for the higher degree  $k_{sk} = 2$ . The enhanced rate of order  $k_{sk} + 2$  is observed at  $\ell = 3$ , illustrating the domination of the first term on the right hand side of (7.7).

## 8.2. Problem 1: Space-based convergence

Consider now a fixed macro-partition with mesh-size  $H = 2^{-2}$ , and skeleton subdivision, taking  $h_{sk} = 2^{-j}H$ ,  $j = 0, 1, 2, \dots$ . Inside the subregions, uniform partitions  $\mathcal{T}_{h_{in}}^{\Omega_i}$  are taken with  $h_{in} = h_{sk}/2$ . The polynomial degrees used for the trace spaces are  $k_{sk} = 1, 2$ , and  $k_{in} = k_{sk} + 1$  is applied for the local FE spaces inside  $\Omega_i$ .

Space-based error curves in Fig. 10 are for  $\tilde{\mathcal{E}}_{\mathcal{RT}_{[\gamma]}}$  versus the number of equations (DoF) in the condensed systems of the upscaling stage. Mesh-based results are also included, where the macro-partitions and the skeleton discretization use the same grid size  $H = h_{sk}$ , and the other parameters are maintained. These plots show that a desired accuracy can be obtained with about two orders of magnitude less degrees of freedom when the space-based strategy is adopted.

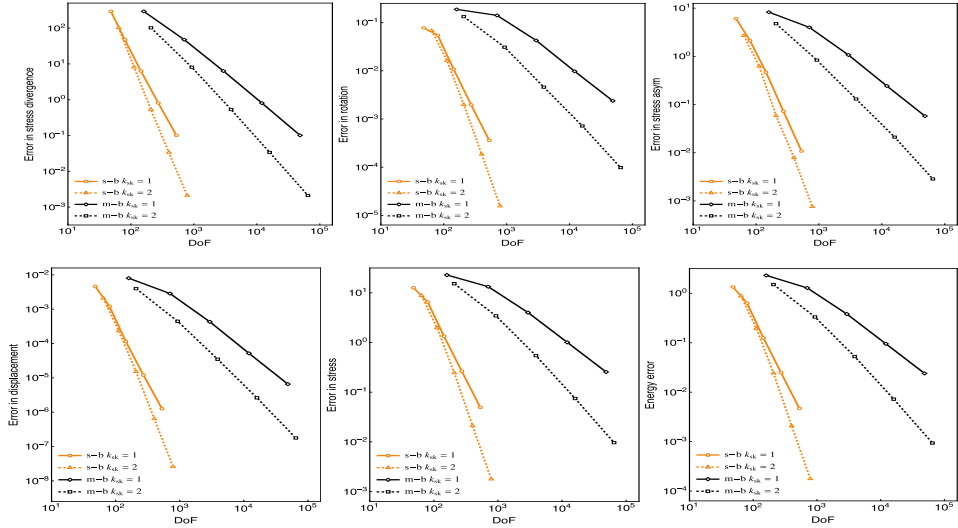


Fig. 10: Problem 1 - Space-based convergence (s-b) for MHM-WS using  $\tilde{\mathcal{E}}_{\mathcal{RT}_{[\gamma]}}$  versus DoF in the condensed upscaling systems: fixed macro-partition with 16 uniform square subregions,  $h_{sk} = 2^{-j}$ ,  $j = 2, \dots, 6$ , for  $k_{sk} = 1, 2$ ,  $h_{in} = h_{sk}/2$ , and  $k_{in} = k_{sk} + 1$ ; mesh-based convergence (m-b) is for macro-partitions with  $H = h_{sk}$ .

Table 3: Problem 1 - Space-based convergence for MHM-WS:  $L^2$ -errors and convergence rates using fixed macro-partition of 16 uniform squares for  $\tilde{\mathcal{E}}_{\mathcal{RT}_{[\gamma]}}$ , or 32 uniform triangles for  $\tilde{\mathcal{E}}_{\mathcal{BDM}_\gamma}$  and  $\tilde{\mathcal{E}}_{\mathcal{BDM}_\gamma^+}$ ;  $h_{sk} = 2^{-j}$ ,  $k_{sk} = 1, 2$ ,  $h_{in} = h_{sk}/2$ , and  $k_{in} = k_{sk} + 1$ .

Square local partitions												
$\tilde{\mathcal{E}}_{\mathcal{RT}_{[\gamma]}}$												
$k_{sk} = 1$												
$j$	stress		displacement		divergence		rotation		asymmetry		energy	
	error	rate	error	rate	error	rate	error	rate	error	rate	error	rate
2	9.4146e+0	--	1.7854e-3	--	4.7550e+1	--	8.8385e-2	--	3.3533e+0	--	9.2503e-1	--
3	1.9264e+0	2.29	1.7689e-4	3.34	6.3514e+0	2.90	1.7487e-2	2.34	6.4913e-1	2.37	1.8732e-1	2.30
4	3.7643e-1	2.36	1.7954e-5	3.30	8.0654e-1	2.98	3.1986e-3	2.45	9.9418e-2	2.71	3.6507e-2	2.36
5	7.0104e-2	2.42	1.7949e-6	3.32	1.0121e-1	2.99	5.8776e-4	2.44	1.5477e-2	2.68	6.7932e-3	2.43
$k_{sk} = 2$												
$j$	stress		displacement		divergence		rotation		asymmetry		energy	
	error	rate	error	rate	error	rate	error	rate	error	rate	error	rate
2	2.5818e+0	--	3.0900e-4	--	8.0800e+0	--	2.1208e-2	--	6.8336e-1	--	2.5349e-1	--
3	2.9517e+1	3.13	1.8120e-5	4.09	5.3177e+1	3.93	2.3865e-3	3.15	7.6440e-2	3.16	2.9117e-2	3.12
4	2.5628e-2	3.53	7.7721e-7	4.54	3.3700e-2	3.98	2.2522e-4	3.41	9.7628e-3	2.97	2.5336e-3	3.52
5	2.1734e-3	3.56	3.1703e-8	4.62	2.1136e-3	3.99	1.9062e-5	3.56	9.2792e-4	3.40	2.1600e-4	3.55
Triangular local partitions												
$\tilde{\mathcal{E}}_{\mathcal{BDM}_\gamma}$												
$k_{sk} = 1$												
$j$	stress		displacement		divergence		rotation		asymmetry		energy	
	error	rate	error	rate	error	rate	error	rate	error	rate	error	rate
2	1.5298e+1	--	6.1570e-3	--	2.3282e+2	--	1.5827e+0	--	5.0094e+0	--	1.5277e+0	--
3	3.8547e+0	1.99	1.2550e-3	2.29	6.6334e+1	1.81	3.8729e-2	2.03	1.3566e+0	1.88	3.7603e-1	2.02
4	7.9571e-1	2.28	2.8845e-4	2.12	1.7167e+1	1.95	7.245e-3	2.42	2.6268e-1	2.37	7.6726e-2	2.29
5	1.6220e-1	2.30	7.1211e-5	2.02	4.3292e+0	1.99	1.4674e-3	2.30	4.8063e-2	2.45	1.5543e-2	2.30
$k_{sk} = 2$												
$j$	stress		displacement		divergence		rotation		asymmetry		energy	
	error	rate	error	rate	error	rate	error	rate	error	rate	error	rate
2	6.5982e+0	--	1.4763e-3	--	1.0815e+1	--	6.8016e-2	--	1.4044e+0	--	6.4350e-1	--
3	1.1056e-1	2.58	1.2802e-4	3.53	1.0815e+1	2.79	1.0762e-2	2.66	1.9111e-1	2.88	1.0699e-1	2.59
4	1.1581e-1	3.25	8.1727e-6	3.97	1.4003e+0	2.95	1.1113e-3	3.28	2.3519e-2	3.02	1.1212e-2	3.20
5	9.4750e-3	3.61	6.4039e-7	3.67	1.7659e-1	2.99	8.5089e-5	3.71	2.6922e-3	3.13	9.2499e-4	3.60
$\tilde{\mathcal{E}}_{\mathcal{BDM}_\gamma^+}$												
$k_{sk} = 1$												
$j$	stress		displacement		divergence		rotation		asymmetry		energy	
	error	rate	error	rate	error	rate	error	rate	error	rate	error	rate
2	1.5909e+1	--	4.7291e-3	--	7.4825e+1	--	1.9752e-1	--	2.6632e+0	--	1.5436e+0	--
3	4.0471e+0	1.97	6.1283e-4	2.95	1.0815e+1	2.79	4.8076e-2	2.04	7.1458e-1	1.90	3.8563e-1	2.00
4	8.2132e-1	2.30	5.8335e-5	3.39	1.4003e+0	2.95	8.4784e-3	2.50	1.2752e-1	2.49	7.7762e-2	2.31
5	1.6348e-1	2.33	6.3446e-6	3.20	1.7659e+1	2.99	1.5663e-3	2.44	1.9175e-2	2.73	1.5442e-2	2.33
$k_{sk} = 2$												
$j$	stress		displacement		divergence		rotation		asymmetry		energy	
	error	rate	error	rate	error	rate	error	rate	error	rate	error	rate
2	6.6848e+0	--	1.4911e-3	--	2.0206e+1	--	7.3370e-2	--	9.1499e+1	--	6.4407e+1	--
3	1.1190e+0	2.58	1.2639e-4	3.56	1.4320e+0	3.82	1.1316e-2	2.70	1.1343e-1	3.01	1.0775e-1	2.58
4	1.1724e-1	3.25	6.8611e-6	4.20	9.2555e-2	3.95	1.1689e-3	3.28	1.5131e-2	2.91	1.1291e-2	3.25
5	9.6566e-3	3.60	2.5853e-7	4.73	5.8340e-3	3.99	9.3046e-5	3.65	1.7545e-3	3.11	9.3336e-4	3.60

Errors and convergence rates are displayed in Table 3 for square and triangular mesh scenarios, with fixed macro-partitions with 16 uniform squares or 32 triangles,

respectively. Excepting the divergence of the stress, all other variables experiment this enhanced accuracy, which is more evident for  $k_{sk} = 2$ . Since  $\underline{\nabla} \cdot \underline{\tilde{\sigma}}$  is the  $L^2$ -orthogonal projection of  $\underline{f}$  over  $\tilde{\mathcal{U}}_{\gamma_{in}}$ , its accuracy is kept in the superconvergence rate of order  $h_{in}^{k_{sk}+t+n+1}$ , as predicted in (7.6). As for MHM- $H^1$  simulations shown in Ref. 20, 26, a tendency in these MHM-WS space-based convergence rates to extrapolate the predicted values by an exponent  $\approx 1/2$  also occurs when using  $\tilde{\mathcal{E}}_{\mathcal{RT}_{[\gamma]}}$  and  $\tilde{\mathcal{E}}_{\mathcal{BDM}_{\gamma}^+}$  families. Once stress convergence rate reaches the order  $h_{sk}^{k_{sk}+3/2}$ , this enhanced accuracy is translated to the displacement error estimate (7.7), improving the Term 1 to order  $h_{sk}^{k_{sk}+5/2}$ . When this term is dominant, the extra  $h_{sk}^{1/2}$  accuracy order reveals, as for the cases of  $\tilde{\mathcal{E}}_{\mathcal{RT}_{[\gamma]}}$  and  $\tilde{\mathcal{E}}_{\mathcal{BDM}_{\gamma}^+}$  families using the mesh sizes and polynomial degree scenario of this test problem. However, this tendency is not confirmed by the displacement errors given by the simulations with  $\tilde{\mathcal{E}}_{\mathcal{BDM}_{\gamma}}$ , a fact that can be justified by a closer look in the bottom-side of Fig. 4: using  $n = 1$  and  $\ell = 1$  the Term 2 dominates the Term 1 as  $h_{sk}$  diminishes.

## Problem 2: Heterogeneous Media

The model set has 16 layers with constant physical properties, covering an area of  $10 \times 10 \times 5$  km, with maximum topography at about 500 m and maximum depth at about 4500 m. From the binary data downloaded from<sup>b</sup>, and as suggested in Ref. 26, the original layers 4 and 12 were replaced by the data of saturated clay:  $\rho = 1760$  kg/m<sup>3</sup>,  $\nu = 0.49$ ,  $E = 15$  MPa.

We consider regridded 3D values sampled at  $h = \Delta x = \Delta y = 19.53125$  m (10000/512), and  $\Delta z = 4500/256 = 17.578125$  m, for the compressional velocity  $V_p$ , shear velocity  $V_s$ , and density  $\rho$ , from which the Poisson coefficient  $\nu$  and Young's modulus  $E$  are obtained by the expressions  $\nu = \frac{V_p^2 - 2V_s^2}{2(V_p^2 - V_s^2)}$  and  $E = 2\rho V_s^2(1 + \nu)$ .

Fig. 11 shows the plots of these parameters defined at the central cross line at  $y = 5000$  m, which is defined as the computational region for Problem 2. The top, left and right sides of the domain are stress free, and the bottom side has zero displacement. The domain is loaded by gravity ( $9.81$  m/s<sup>2</sup>). We chose as a reference value the evolution of  $\underline{\sigma}_{11}$  at the height of 2250.25 m.

MFEM-WS solutions with FE space configuration  $\tilde{\mathcal{E}}_{h, \mathcal{RT}_{[k]}}$ ,  $k = 1, 2$  and compared to conclude that the finest mesh can be used as a reference solution. The plots in Fig. 12 show the reference values of  $\underline{\sigma}_{11}$  along the horizontal center line of the domain for four MHM-WS approximations, and compared with MHM-WS solutions obtained using fixed  $16 \times 8$  subregions (as documented in the right-hand side of Fig. 13). The interior meshes in each subregion are also fixed, and are obtained after five uniform subdivisions of it. The approximations are obtained using  $\tilde{\mathcal{E}}_{\mathcal{RT}_{[\gamma]}}$  spaces for  $k_{sk} = k_{in} = 1$ , and  $\ell = 0, 1, 2$  and 3 divisions of the skeleton mesh. It

<sup>b</sup><http://hpc4e.eu/downloads/datasets-and-software>

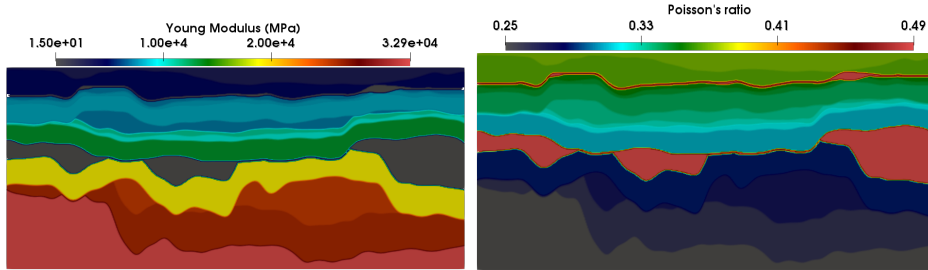


Fig. 11: Problem 2 - Young's modulus (left) and Poisson's ratio (right) at the cross line  $y = 5000$  m.

can be observed that by refining the skeleton mesh, the MHM-WS approximations become closer to the reference solution, with quite well matching for  $\ell = 3$ .

Fig. 13 shows contour plots of  $\underline{\sigma}_{11}$  comparing the reference results (left-hand side) with the finest MHM-WS approximate results (right-hand side), using  $\ell = 3$ .

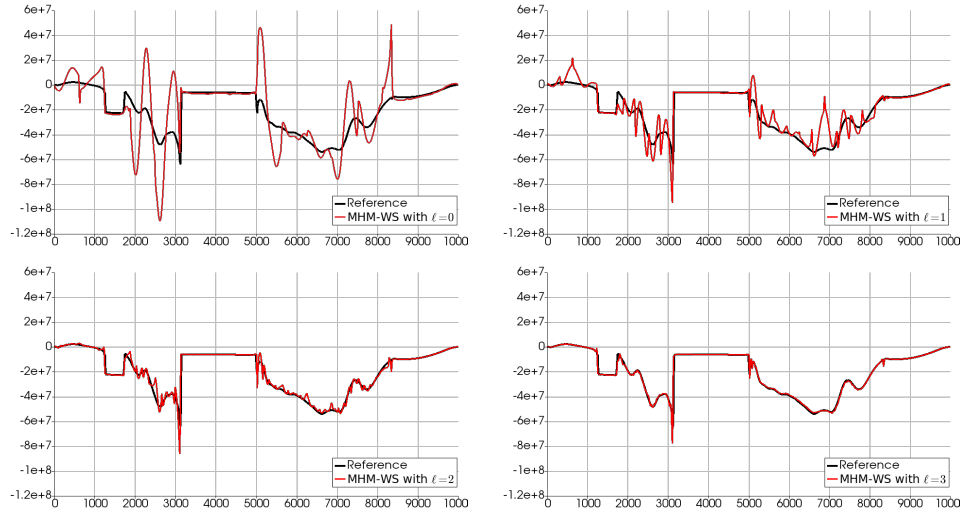


Fig. 12: Problem 2 - Plots of  $\underline{\sigma}_{11}$  at the height of 2250.25 m. The reference solution is in black, and the solutions of MHM-WS, in red,  $\tilde{\mathcal{E}}_\gamma$  based on  $16 \times 8$  macro subregions,  $k_{sk} = k_{in} = 1$ ,  $h_{in} = 10000/512 \approx 19.53$  m,  $h_{sk} = H/2^\ell$  with  $\ell = 0, 1, 2, 3$ .

## 9. Concluding Remarks

The family of stable  $H(\text{div})$ -conforming multiscale mixed-method for elasticity problems proposed in this work impose weakly stress symmetry on general polygonal

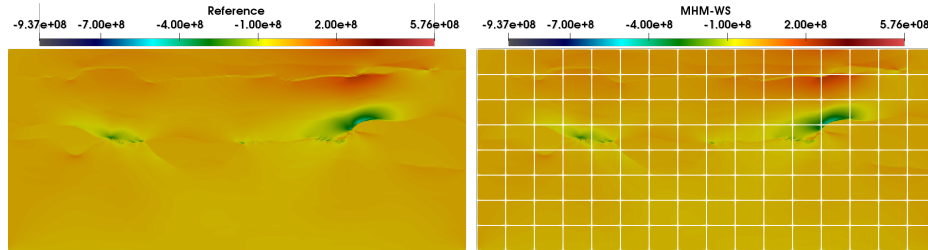


Fig. 13: Problem 2 - Solution  $\underline{\sigma}_{11}$  obtained with reference FE using  $\tilde{\mathcal{E}}_{h, \mathcal{RT}_{[2]}}$  (top), and MHM-WS (right) with  $\tilde{\mathcal{E}}_{\gamma}$  based on a  $16 \times 8$  macro-elements,  $k_{sk} = k_{in} = 1$ ,  $h_{sk} = H/8$ , and  $h_{in} = 10000/512 \approx 19.53$  m.

meshes. Such a feature makes the methodology flexible to represent complex geometries while it yields a systematic way to build multiscale finite element spaces with upscaling-downscaling stages. The multiscale nature of the methods provides a detailed representation of the solution (stress, displacement, and rotation multiplier). Such discrete solutions combine fine scales computations within macro elements, which are entirely independent of one another and prompt to be parallelized, with coarse scales represented by constrained traction (Lagrange multiplier) on mesh skeleton. As a result, the methods achieve optimal and high-order convergence by refining the meshes' frame and local sub-meshes only. Also, local stress fields are in local equilibrium with external forces. Those properties are theoretically demonstrated and validated through numerical tests, which also verified the robustness of the methods on a highly complex multilayer problem using meshes non-aligned with interface layers.

### Acknowledgments

The authors P. R. B. Devloo and S. M. Gomes thankfully acknowledges financial support from CNPq - *Conselho Nacional de Desenvolvimento Científico e Tecnológico* (grants 305823-2017-5, and 306167/2017-4). P. R. B. Devloo also acknowledges financial support from ANP-Brazilian National Agency of Petroleum, Natural Gas and Biofuels (grant 2014/00090-2). F. Valentin has received funding from the European Union's Horizon 2020 Programme (2014-2020) and from the Brazilian Ministry of Science, Technology and Innovation through Rede Nacional de Pesquisa (RNP) under the HPC4E Project ([www.hpc4e.eu](http://www.hpc4e.eu)), grant agreement N° 689772, and from CAPES/Brazil under the PHOTOM project, and CNPq/Brazil. S. M. Gomes is grateful for the support and hospitality received during her visit to *Universidade Federal da Paraíba*, PB, Brazil, whilst this manuscript was prepared.

### Bibliography

1. D. N. Arnold, G. Awanou, B. W. Bestbury and Q. W., Mixed finite elements for elasticity on quadrilateral meshes, *Adv. Comput. Math.* **41** (2015) 553–572.

2. D. N. Arnold, D. Boffi and R. S. Falk, Quadrilateral h(div) finite elements, *SIAM J. Numer. Anal.* **42** (2005) 2429–2451.
3. D. N. Arnold, R. S. Falk and R. Winther, Mixed finite element methods for linear elasticity with weakly imposed symmetry, *Math. Comp.* **76** (2007) 1699–1723.
4. D. Boffi, F. Brezzi and M. Fortin, Reduced symmetry elements in linear elasticity, *Commun. Pure Appl. Anal.* **8** (2009) 95–121.
5. F. Brezzi, D. J. and L. D. Marini, Two families of mixed finite elements for second order elliptic problems, *Numer. Math.* **47** (1985) 217–235.
6. F. Brezzi and J. Pitkäranta, *On the stabilization of finite element approximations of the Stokes equations* (Vieweg+Teubner, 1984).
7. M. Buck, O. Iliev and H. Andrä, Multiscale finite element coarse spaces for the application to linear elasticity, *Cent. Eur. J. Math.* **11** (2013) 608–701.
8. M. Buck, O. Iliev and H. Andrä, Multiscale finite elements for linearelasticity: oscillatory boundary conditions, in *Lect. Not. Comp. Sci.* (Springer International Publishing, 2014), pp. 237–245.
9. B. Cockburn, J. Gopalakrishnan and J. Guzmán, A new elasticity element made for enforcing weak stress symmetry, *Math. Comp.* **79** (2010) 1331–1349.
10. M. Crouzeix and P. A. Raviart, Conforming and nonconforming finite element methods for solving the stationary Stokes equations I, *ESAIM Math. Model. Numer. Anal.* **7** (1973) 33–75.
11. L. Demkowicz, Polynomial Exact Sequences and Projection-Based Interpolation with Application to Maxwell Equations, in *Mixed Finite Elements, Compatibility Conditions, and Applications. Lecture Notes in Mathematics*, eds. D. Boffi and L. Gastaldi (Springer, Berlin, Heidelberg, 2008), volume 1939, pp. 101–158.
12. P. R. B. Devloo, C. M. A. A. Bravo and E. C. Rylo, Systematic and generic construction of shape functions for p-adaptive meshes of multidimensional finite elements, *Comput. Meth. Appl. Mech. Engr.* **198** (2009) 1716–1725.
13. P. R. B. Devloo, A. M. Farias and S. M. Gomes, A remark concerning divergence accuracy order for H(div)-conforming finite element flux approximations, *Comput. Math. Appl.* **77** (2019) 1864–1872.
14. P. R. B. Devloo, S. M. Gomes, T. Quinelato and S. Tian, Enriched two dimensional mixed finite element models for linear elasticity with weak stress symmetry, *Comput. Math. Appl.* 2019. To appear. <hal-01928789>.
15. O. Durán, P. R. B. Devloo, S. M. Gomes and F. Valentin, A multiscale hybrid method for Darcy’s problems using mixed finite element local solvers, *Comput. Meth. Appl. Mech. Engr.* **354** (2019) 213–244.
16. R. S. Falk, Finite Element Methods for Linear Elasticity, in *Mixed Finite Elements, Compatibility Conditions, and Applications. Lecture Notes in Mathematics*, eds. D. Boffi and L. Gastaldi (Springer, Berlin, Heidelberg, 2008), volume 1939, pp. 159–194.
17. M. Farhloul and M. Fortin, Dual hybrid methods for the elasticity and the Stokes problems: a unified approach, *Numer. Math.* **76** (1997) 419–440.
18. V. Girault and P. A. Raviart, *Finite element methods for Navier-Stokes equations: theory and algorithms*, Springer Series in Computational Mathematics (Springer-Verlag, New York, 1991).
19. C. Harder, A. L. Madureira and F. Valentin, A hybrid-mixed method for elasticity, *ESAIM: Math. Model. Numer. Anal.* **50** (2016) 311–336.
20. C. Harder, D. Paredes and F. Valentin, On a multiscale hybrid-mixed method for advective-reactive dominated problems with heterogenous coefficients, *SIAM Multi-scale Model. and Simul.* **3** (2015) 491–518.

21. P. Henning and A. Persson, A multiscale method for linear elasticity reducing poisson locking, *Comput. Meth. Appl. Mech. Engr.* **310** (2016) 156–171.
22. E. Khattatov and I. Yotov, Domain decomposition and multiscale mortar mixed finite elements methods for linear elasticity with weak stress symmetry, *Math. Model. Numer. Anal.*, to appear. ArXiv:1711.09248.
23. M. Kuchta, K.-A. Mardal and M. Mortensen, On the singular Neumann problem in linear elasticity, *Numer. Linear. Algebra. Appl.* **26** (2019) doi:10.1002/nla.2212.
24. A. Målqvist and D. Peterseim, Localization of elliptic multiscale problems, *Math. Comp.* **83** (2014) 2583–2603.
25. L. Mansfield, Finite element subspaces with optimal rates of convergence for the stationary Stokes problem, *RAIRO Anal. Numer.* **16** (1982) 49–66.
26. W. S. Pereira, Multiscale hybrid-mixed methods for heterogeneous elastic models, Ph.D. thesis, LNCC, RJ, BR, Sep. 2019.
27. T. O. Quinelato, A. F. D. Loula, M. R. Correa and T. Arbogast, Full H(div)-approximation of linear elasticity on quadrilateral meshes based on abf finite elements, *Comput. Meth. Appl. Mech. Engr.* **347** (2019) 120–142.
28. P. A. Raviart and J. M. Thomas, Primal hybrid finite element methods for 2nd order elliptic equations, *Math. Comp.* **31** (1997) 391–413.
29. D. Siqueira, P. R. B. Devloo and S. M. Gomes, A new procedure for the construction of hierarchical high order Hdiv and Hcurl finite element spaces, *J. Comput. Appl. Math.* **240** (2013) 204–214.
30. R. Stenberg, A family of mixed finite elements for the elasticity problem, *Numer. Math.* **53** (1988) 513–538.

## Appendix A. The MHM- $H^1$ formulation

In the classic  $H^1$ -conforming approach for linear elasticity problems, the body displacement  $\underline{u} \in H^1(\Omega, \mathbb{R}^2)$  verifying the boundary condition is such that

$$(\underline{A} \underline{\varepsilon}(\underline{u}), \underline{\varepsilon}(\underline{v})) = (\underline{f}, \underline{v}), \quad \forall \underline{v} \in H_0^1(\Omega, \mathbb{R}^2). \quad (\text{A.1})$$

Given a partition  $\mathcal{T} = \{\Omega_i\}$ , the Lagrange multiplier space  $\Lambda$  and the broken space

$$H^1(\mathcal{T}, \mathbb{R}^2) = \left\{ \underline{v} \in L^2(\Omega, \mathbb{R}^2); \underline{v}|_{\Omega_i} \in H^1(\Omega_i, \mathbb{R}^2), \Omega_i \in \mathcal{T} \right\},$$

its hybrid version is formulated as: find  $(\underline{u}, \underline{\lambda}) \in H^1(\mathcal{T}, \mathbb{R}^2) \times \Lambda$  such that

$$\sum_{\Omega_i \in \mathcal{T}} (\underline{A} \underline{\varepsilon}(\underline{u}), \underline{\varepsilon}(\underline{v}))_{\Omega_i} + \langle \underline{\lambda}, \underline{v} \rangle = (\underline{f}, \underline{v}), \quad \forall \underline{v} \in H^1(\mathcal{T}, \mathbb{R}^2), \quad (\text{A.2})$$

$$\sum_{\Omega_i \in \mathcal{T}} \langle \underline{\mu}, \underline{u} \rangle_{\partial\Omega_i} = \langle \underline{\mu}, \underline{g} \rangle, \quad \forall \underline{\mu} \in \Lambda. \quad (\text{A.3})$$

It can be shown that  $(\underline{u}, \underline{\lambda}) \in H^1(\mathcal{T}, \mathbb{R}^2) \times \Lambda$  solves (A.2) - (A.3) if and only if  $\underline{u} \in H^1(\Omega, \mathbb{R}^2)$  is the solution of the  $H^1$ -conforming formulation (A.1). Furthermore, if  $\underline{\sigma} = \underline{A} \underline{\varepsilon}(\underline{u})$  is the stress tensor, then  $\underline{\lambda}|_{\partial\Omega_i} = -\underline{\sigma} \underline{n}^{\partial\Omega_i}$ .

### A.1. An equivalent local-global hybrid primal formulation

Let  $\mathcal{U}_{c,rm}^\perp := \mathcal{U}_c(\mathcal{T}, \mathbb{R}^2)_{rm}^\perp$  denotes  $L^2$ -orthogonal complement of  $\mathcal{U}_{rm}$  in  $H^1(\mathcal{T}, \mathbb{R}^2)$ . The approach for the MHM- $H^1$  method for linear elasticity problems, as proposed

in Ref. 19, is based on the representation  $\underline{u} = \underline{u}_{rm} + \underline{u}^\perp$ , in terms of a coarse approximation  $\underline{u}_{rm} \in \mathcal{U}_{rm}$ , and of  $\underline{u}^\perp = \underline{u} - \underline{u}_{rm} \in \mathcal{U}_{c,rm}^\perp$  containing the smaller scales in  $\underline{u}$ . The local-global hybrid primal formulation is the result of two stages:

- *Downscaling stage:*  $\underline{u}^\perp$  is characterized as  $\underline{u}^\perp = T(\underline{\lambda}) + \hat{T}(\underline{f})$ , where  $\{T(\underline{\lambda}), \hat{T}(\underline{f})\}$  denote the local solvers defined on each  $\Omega_i \in \mathcal{T}$

$$(\underline{A} \underline{\varepsilon}(T(\underline{\lambda})), \underline{\varepsilon}(\underline{v}))_{\Omega_i} = - \langle \underline{\lambda}, \underline{v} \rangle_{\partial\Omega_i}, \quad \forall \underline{v} \in \mathcal{U}_{c,rm}^\perp, \quad (\text{A.4})$$

$$(\underline{A} \underline{\varepsilon}(\hat{T}(\underline{f})), \underline{\varepsilon}(\underline{v}))_{\Omega_i} = (\underline{f}, \underline{v})_{\Omega_i}, \quad \forall \underline{v} \in \mathcal{U}_{c,rm}^\perp. \quad (\text{A.5})$$

- *Upscaling stage:*  $\underline{u}_{rm} \in \mathcal{U}_{rm}$  and  $\underline{\lambda} \in \Lambda$  solve the system

$$\sum_{\Omega_i \in \mathcal{T}} \langle \underline{\mu}, \underline{u}_{rm} + T(\underline{\lambda}) \rangle_{\partial\Omega_i} = - \sum_{\Omega_i \in \mathcal{T}} \langle \underline{\mu}, \hat{T}(\underline{f}) \rangle_{\partial\Omega_i} + \langle \underline{\mu}, \underline{g} \rangle, \quad \forall \underline{\mu} \in \Lambda, \quad (\text{A.6})$$

$$\sum_{\Omega_i \in \mathcal{T}} \langle \underline{\lambda}, \underline{v}_{rm} \rangle_{\partial\Omega_i} = (\underline{f}, \underline{v}_{rm}), \quad \forall \underline{v} \in \mathcal{U}_{rm}. \quad (\text{A.7})$$

It is shown in Ref. 19 that this system can be rewritten in an equivalent form as in (2.9) - (2.10), but using the downscaling solutions of the MHM- $H^1$  context.

## A.2. Discrete MHM formulation with $H^1$ -conforming local solvers

The MHM- $H^1$  formulation is driven into two discretization instances:

- A finite dimensional space  $\tilde{V} = \mathcal{U}_{rm} + \tilde{V}^\perp \subset H^1(\mathcal{T}, \mathbb{R}^2)$ . The construction of this space rely on local  $H^1$ -conforming FE spaces  $\tilde{V}(\Omega_i)$  for each subdomain  $\Omega_i$ , based on refined partitions  $\mathcal{T}^{\Omega_i}$ . The functions  $v \in \tilde{V}(\Omega_i)$  are piecewise defined over the elements  $K \in \mathcal{T}^{\Omega_i}$  by mapping scalar polynomial shape functions in the corresponding master elements. For the presented experiments, they are spanned by a hierarchy of arbitrary high-order shape functions described in Ref. 12.
- A finite dimensional subspace  $\tilde{\Lambda}_{sk} \subset \Lambda$  of piecewise polynomials based on partitions  $\mathcal{T}^e$  of edges  $e \subset \partial\Omega_i$ , embedding the piecewise constant functions.

According to the principles of the local-global hybrid setting (A.4) - (A.7), the MHM- $H^1$  solutions  $(\tilde{\underline{u}}_{rm} + \tilde{\underline{u}}^\perp, \tilde{\underline{\lambda}}) \in \mathcal{U}_{rm} + \tilde{V}^\perp \times \tilde{\Lambda}_{sk}$  are characterized as follows:

- $\tilde{\underline{u}}^\perp = \tilde{T}(\tilde{\underline{\lambda}}) + \tilde{\hat{T}}(\underline{f})$ ,  $\{\tilde{T}(\tilde{\underline{\lambda}}), \tilde{\hat{T}}(\underline{f})\}$  being the discrete local solvers

$$(\underline{A} \underline{\varepsilon}(\tilde{T}(\tilde{\underline{\lambda}})), \underline{\varepsilon}(\underline{v}))_{\Omega_i} = - \langle \tilde{\underline{\lambda}}, \underline{v} \rangle_{\partial\Omega_i}, \quad \forall \underline{v} \in \tilde{V}^\perp, \quad (\text{A.8})$$

$$(\underline{A} \underline{\varepsilon}(\tilde{\hat{T}}(\underline{f})), \underline{\varepsilon}(\underline{v}))_{\Omega_i} = (\underline{f}, \underline{v})_{\Omega_i}, \quad \forall \underline{v} \in \tilde{V}^\perp. \quad (\text{A.9})$$

- $\tilde{\underline{u}}_{rm} \in \mathcal{U}_{rm}$  and  $\tilde{\underline{\lambda}} \in \tilde{\Lambda}_{sk}$  solve the system

$$\sum_{\Omega_i \in \mathcal{T}} \langle \underline{\mu}, \tilde{\underline{u}}_{rm} + \tilde{T}(\tilde{\underline{\lambda}}) \rangle_{\partial\Omega_i} = - \sum_{\Omega_i \in \mathcal{T}} \langle \underline{\mu}, \tilde{\hat{T}}(\underline{f}) \rangle_{\partial\Omega_i} + \langle \underline{\mu}, \underline{g} \rangle, \quad \forall \underline{\mu} \in \tilde{\Lambda}_{sk}, \quad (\text{A.10})$$

$$\sum_{\Omega_i \in \mathcal{T}} \langle \tilde{\underline{\lambda}}, \underline{v} \rangle_{\partial\Omega_i} = (\underline{f}, \underline{v}), \quad \forall \underline{v} \in \mathcal{U}_{rm}. \quad (\text{A.11})$$

This two-scale formulation is analyzed in Ref. 19. For

$$\tilde{V} = \bigoplus_{\Omega_i \in \mathcal{T}} \mathbb{P}_{k_{in}}(\Omega_i, \mathbb{R}^2) \subset H^1(\mathcal{T}, \mathbb{R}^2), \quad \tilde{\Lambda}_{sk} = \bigoplus_{e \in \Gamma} \mathbb{P}_{k_{sk}}(e, \mathbb{R}^2) \subset \Lambda,$$

well-posedness occurs for  $k_{in} \geq k_{sk} + 1$  if  $k_{sk}$  is even, and  $k_{in} \geq k_{sk} + 2$ , otherwise. If  $\tilde{V} = \bigoplus_{\Omega_i \in \mathcal{T}} \mathbb{Q}_{k_{in}}(\Omega_i, \mathbb{R}^2) \subset H^1(\mathcal{T}, \mathbb{R}^2)$ , well-posedness holds provided  $k_{in} \geq k_{sk} + 2$ .

Similar results hold if the local spaces are continuously piecewise constructed on top of refined meshes  $\mathcal{T}^{\Omega_i}$  of each subregion  $\Omega_i$ , under the same polynomial degree constraints. For these kinds of polynomial, or piecewise polynomial approximation spaces, a priori error estimations proved in Ref. 19 states that for a smooth exact solution  $\underline{u}$ , and under mesh shape-egularity and elliptic regularity assumptions,

$$\|\lambda - \tilde{\lambda}\|_{\Lambda} + \|\underline{u}_{rm} - \tilde{\underline{u}}_{rm}\|_{H^1(\mathcal{T}_H)} \lesssim H^{k_{sk}+1} \quad (\text{A.12})$$

$$H\|\underline{u} - \tilde{\underline{u}}\|_{H^1(\mathcal{T})} + \|\underline{u} - \tilde{\underline{u}}\|_{L^2} \lesssim H^{k_{sk}+2}, \quad (\text{A.13})$$

where  $H$  is the characteristic macro-partition size of the subdomains  $\Omega_i \in \mathcal{T}$ ,  $\|\cdot\|_{\Lambda}$ ,  $\|\cdot\|_{H^1(\mathcal{T})}$  and  $|\cdot|_{H^1(\mathcal{T})}$  denoting standard norm for  $H^{-\frac{1}{2}}(\Gamma, \mathbb{R}^2)$ , norm and semi-norm for  $H^1(\mathcal{T}, \mathbb{R}^2)$ , respectively.

In the recent work of Ref. 26, the MHM- $H^1$  formulation was extended to more general families of approximation spaces and meshes, allowing the use of polygons in 2D and polyhedra in 3D. It is proved and verified numerically that there is a superconvergence in the displacement when refining either the global partition or the skeleton mesh. The accuracy of the MHM- $H^1$  method on non-aligned coarse partitions was highlighted there using an elasticity problem in a high-contrast heterogeneous domain. An especial treatment proposed in Ref. 26, using Galerkin Least Squares local solvers, also shows that this new MHM- $H^1$  method is locking-free, a property that fails for classical  $H^1$ -conforming low-order numerical methods.

## Appendix B. Classical FE Pairs for Poisson and Stokes Problems

For an element  $K$ , there is a master element  $\hat{K}$  and a geometric invertible map  $F_K : \hat{K} \rightarrow K$  transforming  $\hat{K}$  onto  $K$ .  $F_K$  induces transformations  $\mathbb{F}_K$  and  $\mathbb{F}_K^{\text{div}}$  used to map functions defined in  $\hat{K}$  to functions defined in  $K$ .

- (i) Scalar functions:  $p = \mathbb{F}_K \hat{p} = \hat{p} \circ F_K^{-1}$ ; for vector functions:  $\underline{v} = \mathbb{F}_K \hat{\underline{v}}$  by applying  $\mathbb{F}_K$  to the components of  $\hat{\underline{v}}$ ;
- (ii) Vector functions (Piola transformation):  $\underline{v} = \mathbb{F}_K^{\text{div}} \hat{\underline{v}} = \mathbb{F}_K \left[ \frac{1}{\mathbf{J}_K} \mathbf{D}F_K \hat{\underline{v}} \right]$ , where  $\mathbf{D}F_K$  is the Jacobian matrix of  $F_K$ , and  $\mathbf{J}_K = |\det(\mathbf{D}F_K)|$ .

In  $\hat{K}$ , scalar polynomials are usually of the form:  $\mathbb{P}_k(\hat{K}, \mathbb{R})$ , of total degree at most  $k$ , for the triangle;  $\mathbb{Q}_{k,t}(\hat{K}, \mathbb{R})$ , of maximum degree  $k$  in  $x$  and  $t$  in  $y$ , for the square.

### B.1. Poisson-compatible approximation spaces

Approximations spaces for flux  $\tilde{\mathcal{V}} \subset H(\text{div}, \Omega, \mathbb{R}^2)$  and pressure  $\tilde{\mathcal{P}} \subset L^2(\Omega, \mathbb{R})$ , for mixed formulation of Poisson problems, are generally piecewise defined as by local spaces  $V(K, \mathbb{R}^2) \subset H(\text{div}, K, \mathbb{R}^2)$  and  $P(K, \mathbb{R}) \subset L^2(K, \mathbb{R})$ . They are usually defined by  $P(K, \mathbb{R}) = \mathbb{F}_K \hat{P}$ , and  $V(K, \mathbb{R}^2) = \mathbb{F}_K^{\text{div}} \hat{\mathbf{V}}$ , mapping polynomial spaces  $\hat{\mathbf{V}}$  and  $\hat{P}$  defined on a reference element  $\hat{K}$ . We consider that  $\hat{\mathbf{V}}$  is spanned by a hierarchy of vector shape functions organized into two classes: the functions of interior type, with vanishing normal traces over all element edges,  $\hat{\mathbf{V}}^\circ$ , and the functions associated to the element edges  $\hat{\mathbf{V}}^\partial$ . Thus, the decomposition  $\hat{\mathbf{V}} = \hat{\mathbf{V}}^\partial \oplus \hat{\mathbf{V}}^\circ$  naturally holds. For stability (inf-sup condition), the divergence-compatibility condition  $\nabla \cdot \hat{\mathbf{V}} = \hat{P}$  is required. This property can be extended to the spaces  $\tilde{\mathcal{V}}$  and  $\tilde{\mathcal{P}}$  by the construction of a projection  $\boldsymbol{\pi}^D : H^1(\Omega, \mathbb{R}^2) \rightarrow \mathcal{V}$  such that  $(\nabla \cdot (\underline{\eta} - \boldsymbol{\pi}^D \underline{\eta}), \psi) = 0$ ,  $\forall \psi \in \tilde{\mathcal{P}}$ . There is an unified form to define  $\boldsymbol{\pi}^D$  by the so called projection-based operators (see Ref. 11). They are represented as  $\boldsymbol{\pi}^D \underline{\eta} = \boldsymbol{\pi}^{D, \partial} \underline{\eta} + \hat{\boldsymbol{\pi}}^D (\underline{\eta} - \boldsymbol{\pi}^{D, \partial} \underline{\eta})$  with edge and internal operators defined by

$$\begin{aligned} \langle \boldsymbol{\pi}^{D, \partial} \underline{\eta} \cdot \underline{\mathbf{n}}^K, \phi \rangle_{\partial K} &= \langle \underline{\eta} \cdot \underline{\mathbf{n}}^K, \phi \rangle_{\partial K}; \quad \forall \phi \in P(\partial K), \\ (\nabla \cdot \hat{\boldsymbol{\pi}}^D \underline{\eta}, \nabla \cdot \underline{\mathbf{w}})_K &= (\nabla \cdot \underline{\eta}, \nabla \cdot \underline{\mathbf{w}})_K, \quad \forall \underline{\mathbf{w}} \in \hat{\mathcal{V}}(K), \\ (\hat{\boldsymbol{\pi}}^D \underline{\eta}, \underline{\mathbf{w}})_K &= (\underline{\eta}, \underline{\mathbf{w}})_K, \quad \forall \underline{\mathbf{w}} \in \hat{\mathcal{V}}(K), \quad \nabla \cdot \underline{\mathbf{w}} = 0, \end{aligned}$$

where  $P(\partial K)$  represents the space of normal traces of vector functions in  $\hat{\mathcal{V}}(K)$ .

Two classical Poisson-compatible FE pairs shall be used in this paper:

$\mathcal{BDM}_k, k \geq 1$ <sup>5</sup>:  $\hat{V}_{\mathcal{BDM}_k}(\hat{K}, \mathbb{R}^2) = \mathbb{P}_k(\hat{K}, \mathbb{R}^2)$  and  $P_{\mathcal{BDM}_k}(\hat{K}, \mathbb{R}) = \mathbb{P}_{k-1}(\hat{K}, \mathbb{R})$ .  
 $\mathcal{RT}_{[k]}, k \geq 1$ <sup>28</sup>:  $\hat{\mathbf{V}}_{\mathcal{RT}_{[k]}} = \mathbb{Q}_{k+1, k}(\hat{K}, \mathbb{R}) \times \mathbb{Q}_{k, k+1}(\hat{K}, \mathbb{R})$  and  $\hat{P}_{\mathcal{RT}_{[k]}} = \mathbb{Q}_{k, k}(\hat{K}, \mathbb{R})$ .

### B.2. Stokes-compatible approximation spaces

Stokes-compatible finite element pairs  $\tilde{\mathcal{W}}, \tilde{\mathcal{Q}} \subset H^1(\Omega, \mathbb{R}^2) \times L^2(\Omega, \mathbb{R})$ , for velocity and pressure approximations in mixed Stokes formulations, are generally piecewise defined by local FE pairs  $W(K, \mathbb{R}^2), Q(K, \mathbb{R})$   $K \in \mathcal{T}$ . The following two classical Stokes-compatible FE pairs shall be used in this paper:

- Crouzeix-Raviart spaces ( $\mathcal{CR}_k$ ) for triangular elements, proposed in Ref. 10 for  $k = 2, 3$ , and extended to higher orders in Ref. 25:  $W_{\mathcal{CR}_k}(K, \mathbb{R}^2) = \mathbb{P}_k(K, \mathbb{R}^2) + b_K \mathbb{P}_{k-2}(K, \mathbb{R}^2)$ ,  $b_K = \lambda_1 \lambda_2 \lambda_3$  being the bubble function defined by the barycentric coordinates  $\lambda_i$  of the triangle  $K$ , and  $Q_{\mathcal{CR}_k}(K, \mathbb{R}) = \mathbb{P}_{k-1}(K, \mathbb{R})$ .
- Girault-Raviart spaces ( $\mathcal{GR}_{[k]}$ ) for quadrilaterals, considered in Ref. 18 or  $k \geq 2$ :  $W_{\mathcal{GR}_{[k]}}(K, \mathbb{R}^2) = \mathbb{F}_K(\mathbb{Q}_{k, k}(\hat{K}, \mathbb{R}^2))$  and  $Q_{\mathcal{GR}_{[k]}}(K, \mathbb{R}) = \mathbb{P}_{k-1}(K, \mathbb{R})$